**DOKUZ EYLÜL UNIVERSITY**

**GRADUATE SCHOOL OF NATURAL AND APPLIED SCIENCES**

# TEMPERATURE EFFECT ON IMPACT BEHAVIOR OF LAMINATED COMPOSITE PLATES

**by**

**Mehmet AKTAŞ**

**September, 2007**

**İZMİR**

# TEMPERATURE EFFECT ON IMPACT BEHAVIOR OF LAMINATED COMPOSITE PLATES

**A Thesis Submitted to the**
**Graduate School of Natural and Applied Sciences of Dokuz Eylül University**
**In Partial Fulfillment of the Requirements for the Degree of Doctor of Philosophy in Mechanical Engineering, Mechanics Program**

**by**

**Mehmet AKTAŞ**

**September, 2007**

**İZMİR**

**Ph.D. THESIS EXAMINATION RESULT FORM**

We have read the thesis entitled **"TEMPERATURE EFFECT ON IMPACT BEHAVIOR OF LAMINATED COMPOSITE PLATES"** completed by **MEHMET AKTAŞ** under supervision of **Prof. Dr. RAMAZAN KARAKUZU** and we certify that in our opinion it is fully adequate, in scope and in quality, as a thesis for the degree of Doctor of Philosophy.

Prof. Dr. Ramazan KARAKUZU

Supervisor

| Prof. Dr Onur SAYMAN | Assist. Prof. Dr. Mustafa TOPARLI |
|---|---|
| Thesis Committee Member | Thesis Committee Member |

| Prof. Dr. Muzaffer TOPCU | Prof. Dr. Sami AKSOY |
|---|---|
| Examining Committee Member | Examining Committee Member |

Prof.Dr. Cahit HELVACI
Director
Graduate School of Natural and Applied Sciences

## ACKNOWLEDGMENTS

From my heart, deep gratitude and appreciation goes to my supervisor, Professor Dr. Ramazan KARAKUZU, for his constant encouragement and invaluable guidance. His contribution to the achievements of this work is significant.

Special thanks also extend to my dissertation committee members, Professor Dr. Onur SAYMAN and Assistant Professor Dr. Mustafa TOPARLI, for their academic support and encouragement through my theses.

I would also like to express my appreciation for the financial support of The Scientific & Technological Research Council of Turkey (TÜBİTAK). Thanks to Izoreel firm for the manufacturing of the composite specimens.

I would like to thank all my coworkers in the Composite Research Laboratory and Mechanical Test and Research Laboratory. In particular, I would like to thank Assistant Professor Dr. Cesim ATAS, Dr. Bülent Murat İÇTEN and Research Assistant Yusuf ARMAN.

I am very grateful to my parents for their understanding, support and love. They worked very hard to support me all over past years.

Finally, I would like to thank my wife and my daughters. Without their help and love, the completion of this dissertation is impossible. For this reason, this dissertation is dedicated to them.

Mehmet AKTAŞ

**TEMPERATURE EFFECT ON IMPACT BEHAVIOR OF LAMINATED COMPOSITE PLATES**

## ABSTRACT

The main objective of this study is to investigate the thermal impact behavior of unidirectional laminated composite plates composed of glass fabrics and epoxy matrix under room (approx. 20°C) and high (40°C, 60°C, 80°C and 100°C) temperatures. In addition, mechanical properties of glass/epoxy composite plates are determined under mentioned temperature conditions. And also, compression after impact (CAI) strength of impacted plates is determined under room temperature.

Impact tests are performed by using Fractovis Plus impact test machine. Fourteen impact energies from 5 J to 70 J are selected for impact tests. The plate dimensions are of 100 mm x 100 mm for impact test and 150 mm x 150 mm for CAI tests. Two stacking sequences as $[0°/90°/0°/90°]_S$ and $[0°/90°/45°/-45°]_S$ are used to investigate the fiber orientation effects.

A numerical analysis is also carried out by using 3DIMPACT finite element code and compared with the experimental results in impact tests. The contact force between the impactor and the composite plate, and the maximum deflection at the center of the composite plate are plotted as function of time and damage area in interfaces is determined numerically.

Finally, the energy absorbed capability, mechanical properties and CAI strength of the composite plates based on polymer are decreased by increasing temperature. The contact force and contact time increases by increasing the temperature while the deflection of the plate and damage area in interfaces decrease.

**Keywords:** Thermal impact behavior, penetration and perforation thresholds, mechanical properties, Compression after impact strength

# SICAKLIĞIN TABAKALI KOMPOZİT PLAKLARIN DARBE DAVRANIŞINA ETKİSİ

## ÖZ

Bu çalışmanın temel amacı, cam lifi ve epoksi matriksten oluşmuş tek yönlü kompozit plakların termal darbe davranışlarını, oda sıcaklığı (yaklaşık 20°C) ve yüksek (40°C, 60°C, 80°C ve 100°C) sıcaklıklarda incelemektir. Ayrıca, cam lifi/epoksi kompozit plakların mekanik özellikleri bahsedilen sıcaklık koşullarında belirlenmiştir. Darbeye uğramış plakların darbe sonrası bası mukavemetleri de oda sıcaklığında belirlenmiştir.

Darbe testleri Fractovis Plus darbe test makinesi kullanılarak gerçekleştirilmiştir. Darbe testleri için 5 J' den 70 J' e kadar on dört adet darbe enerjisi seçilmiştir. Plaka boyutları darbe testleri için 100 mm x 100 mm ve CAI testleri için 150 mm x 150 mm dir. Fiber oryantasyon etkisini incelemek için $[0°/90°/0°/90°]_S$ ve $[0°/90°/45°/-45°]_S$ dizilimleri kullanılmıştır.

3DIMPACT sonlu elemanlar programı kullanılarak nümerik analiz gerçekleştirilmiş ve darbe testlerindeki deneysel sonuçlarla karşılaştırılmıştır. Vurucu ile kompozit plak arasındaki temas kuvveti ve kompozit plağın merkezindeki maksimum çökme zamanın fonksiyonu olarak çizilmiş ve ara yüzeydeki hasar alanları nümerik olarak belirlenmiştir.

Sonuç olarak; polimer esaslı kompozit plakların enerji absorbe etme kabiliyeti, mekanik özellikleri ve darbe sonrası bası mukavemetleri sıcaklık arttıkça azalmaktadır. Temas kuvveti ve temas zamanı sıcaklık arttıkça artarken, plağın çökmesi ve ara yüzeydeki hasar alanı azalmaktadır.

**Anahtar kelimeler:** Isıl darbe davranışı, nüfuziyet ve delme sınırı, mekanik özellikler, darbe sonrası bası mukavemeti

**CONTENTS**

# CHAPTER ONE
# INTRODUCTION

## 1.1 Introduction

Composite materials consist of two or more constituent materials. These constituent materials are a stiff phase called fiber implanted in a less stiff continuous phase called matrix. The most common fibers are glass, carbon, aramid, boron, alumina, polyolefin, and asbestos. The matrix material in a composite laminate is generally chosen polymers. Polymers are made up of thermosetting and thermoplastics resins. The most common thermosetting resins are epoxy, polyester, phenol-formaldehyde, melamine-formaldehyde, silicone, and furane. Thermoplastics include nylon, polyether-ether-ketone (PEEK), polyether sulphone, polyphenylene sulphide, polycarbonate, and polysulphone. The matrix and fiber together are used to form unidirectional (UD) laminae. These laminae can be bonded together, at different fiber orientations, to form a laminated composite. Laminated composites are generally classified into three different categories based on their matrix material as polymer matrix composites (PMCs), metal matrix composites (MMCs) and ceramic matrix composites (CMCs). In addition, laminated composites are classified by type of reinforcement as particulate, short fiber, long or continuous fiber, whisker and weave.

In recent years the use of composite materials has become increasingly common in a wide range of structural components, engineering applications, aerospace, automotive, defense, and sports industries. Composite materials have numerous advantages over more conventional materials because of their superior specific properties; such as high strength and stiffness to weight ratio, improved corrosion, and environmental resistance, design flexibility, improved fatigue life, and potential reduction of processing, fabrication and life cycle cost. Two thirds of laminated composites are used in aerospace applications, especially in many aircraft parts, such as vertical fins, ailerons, spoilers, rudders, elevators, flaps, overhead panels, and

engine nacelles, radar domes, wing to body fairings, wing skins, fuselage sections, space shuttle cargo doors, rocket motor castings and jet engine exit vanes.

In spite of having these advantages, laminated composites are also susceptible to damages under transverse impacts and the nature of damage induced due to such impacts are entirely different than that in case of conventional metallic materials. During the manufacturing process or during maintenance, tools can be dropped on the structure. In this case, impact velocities are small but the mass of the projectile is larger. If a composite laminate is subjected to normal low velocity impact of sufficient energy, impact could cause various damages, such as matrix cracks, delaminations, fiber fracture, fiber–matrix debonding and fiber pull-out. These damages cause considerable reduction in structural stiffness, leading to growth of the damage and final fracture. Therefore, the impact response of fiber reinforced laminated composites has been an important area of research for a long time. A large number of experimental, numerical and both of experimental and numerical or analytical studies have already been reported in literature in this direction. Some of the important studies are presented below.

### *1.1.1 Experimental Studies*

Composite materials are taken more ductile or more brittle according to under low and high temperature. As a result, laminate were absorbed more or less energy. Therefore, some investigators have investigated the low and high temperature effects on impact response of laminated composites. The low velocity impact on unidirectional and cross-ply glass/epoxy laminates were conducted by Li, Pang, Helms, & Ibekwe (2000), at temperatures from 50°C to 100°C and by Ibekwe, Mensah, Li, Pang, & Stubblefield (2006), at low temperatures as 0 C°, 10 C°, and 20 C°. The impact performances of glass/epoxy composites were investigated using charpy impact testing over a wide temperature range −196 °C, 20 °C, and 70 °C by Chang, Zhang, & Breidt, (2004). Salehi, Hassani, Haftchenari, & Hinton (2001), have done quasi static and dynamic tests to characterize glass/epoxy at low, room and high temperatures. Results showed that the temperature decreases the maximum

strength in quasi-static tests. Corte's & Cantwell (2006), have investigated the low and high velocity impact properties of carbon/PEEK and glass/PEI composites. They worked to develop a lightweight sandwich material for use in high temperature aerospace applications.

Rio, Zaera, Barbero, & Navarro (2005), have examined the response of unidirectional, cross-ply, quasi-isotropic and woven carbon/epoxy laminates at low temperature to investigate the effect of temperature on the threshold impact energy. The test temperature was chosen as ranged from 20°C down to -150°C. Im, Cha, Kim, & Yang (2001), have investigated the effect of low and high temperatures variations on impact damage in carbon/epoxy and carbon/PEEK composite laminates. Gao & Kim (2001), have investigated the effect of cooling rate on impact damage and compression after impact performance of carbon/PEEK composite. From the results obtained; initial impact energy and total damage area, damage initiation were shown higher in the order of fast-cooled carbon/PEEK, slow-cooled carbon/PEEK and carbon/epoxy laminates. Furthermore, the CAI strength reduction rate was lower for the fast-cooled specimen than the slow-cooled counterpart. Khojin, Bashirzadeh, Mahinfalah, & Jazar (2006), have investigated the effect of temperature on maximum energy, elastic energy, maximum deflection, maximum impact force, ductility, and compression after impact on the kevlar/glass laminated composite plates subjected to low velocity impact in the range of -50 °C to 120 °C. The energy levels are chosen in non-penetration, intermediate penetration, and full penetration of the composite plates at room temperature, respectively. Bonollo, Ceschini, & Garagnani (1997), have presented the impact behavior of commercially available aluminum matrix composites in a temperature range of 25 °C to 200 °C. The results of instrumented impact tests and fractographic observations were correlated with the tensile properties of these materials.

Halvorsen, Khojn, Mahinfalah, & Jazar (2006), have performed a series of impact tests to evaluate the maximum normal and shear stresses, maximum energy absorption and compression after impact strength of the sandwich composites with glass core and glass/kevlar face sheets in a range of −50 to 120 °C. Results showed

that the impact performance of these sandwich composites changed over the range of temperature considered and with the addition of a Kevlar layer. Erickson, Kallmeyer, & Kellogg (2005), have investigated the effect of temperature on the absorbed energy, maximum impact force, and damage mechanisms in composite sandwich panels at -25, 25, and 75 °C. Result showed that the temperature effects significantly on the energy absorbed and maximum force.

Some of the researchers have investigated the effects of impactor properties such as velocity (Corte's et al., 2006; Naik, Borade, Arya, Sailendra, & Prabhu, 2002; Sadasivam & Mallick, 2002; Uyaner & Kara, in press; Erickson et al., 2005; Mahfuz, Thomas, Rangari, & Jeelani, 2006; Kepler, 2004a, 2004b; Caprino, Spataro, & Luongo, 2004), mass (Naik et al., 2002; Caprino et al., 2004), energy (Habib, 2001; Naik et al., 2002; Caprino et al., 2004; Sadasivam, Cherng, & Mallick, 2000) and shapes (Mitrevski, Marshall, & Thomson, 2006; Mitrevski, Marshall, Thomson, & Jones, 2006; Naik et al., 2002; Kepler, 2004a, 2004b) on the impact response of various composite laminate. Target properties also affect the impact behavior. Therefore, effects of resin and fiber properties (Cartie & Irving, 2002; Abdullah & Cantwell, 2006; Kepler, 2004a, 2044b; Christopherson, Mahinfalah, Jazar, & Aagaah, 2005), of strain rates (Salehi et al., 2001; Vaidya & Hosur, 2003; Belingardi & Vadori, 2002; Naik, Ramasimha, Arya, Prabhu, & Rao, 2001; Mahfuz et al., 2006), of fiber volume fraction (Lee & Cheon, 2001; Ruhala & Engel, 2000), of thickness (Caprino, Langella, & Lopresto, 2003; Liu, Raju, & Dang, 1998), of stacking sequences (Lim, Tan, Ramakrishna, & Lee, 2002; Abdullah et al., 2006), and of in-plane dimensions (Liu et al., 1998; Moody, Harris, & Vizzini, 2002; Uyaner & Kara, in press) on the impact behavior of the various composite laminates were investigated. The effects of core material (Erickson et al., 2005), and different combinations of sandwich laminates (Hosur, Adbullah, & Jeelani, 2005; Naik et al., 2001) were examined. Temperature effects are the important impression on the composite laminates. Hence, Chang et al., (2004), Salehi et al., (2001), Corte's & Cantwell (2006), have studied the impact behavior of composite laminates under low and high temperature.

The impact response of woven carbon/epoxy (Mitrevski, Marshall, & Thomson, 2006), and of woven glass/epoxy laminates (Mitrevski, Marshall, Thomson, & Jones, 2006), were examined by using flat, hemispherical, ogival and conical impactor shapes. Result showed that, the conical impactor created the most energy and produced the largest penetration depth. The blunter hemispherical impactor produced the largest peak force and shortest contact duration. The damage threshold load was highest for the hemispherical impactor. Naik et al., (2002), have investigated the impact behaviors of glass/epoxy composites depends upon impactor parameters such as impactor mass, velocity, energy and impactor radius. Glass/epoxy composite material properties such as type of fiber, matrix, type of reinforcement, plate configuration and geometrical parameters such as stacking sequence and plate thickness were also examined. Caprino et al., (2004), have performed the effect of impact velocity, mass, and energy on glass/aluminum composite laminates. From the results obtained, the overall force–displacement curve only depends on the impact energy, rather than on the mass and speed separately. Sadasivam et al., (2000), investigated the effects of impact energy on the dynamic response of four random fiber reinforced composites that are commonly used for automotive body and chassis applications.

Kepler (2004a, 2004b), has investigated the effects of fiber-lay-ups, impactor tips, and velocities on sandwich panels. Results showed that the contributions from core compression and friction were not directly attributed to a measurable damage surface, but would be based on the core properties and the impactor geometry. Caprino et al., (2003), have carried out quasi-static tests on circular carbon fiber reinforced plastic plates of various thicknesses. The experimental results demonstrate that the penetration energy was substantially unaffected by the loading speed. Liu et al., (1998), have performed the thickness and in-plane dimensional effects on the impact response of glass/epoxy composite laminates. Experimental results showed that in-plane dimensional effect was not as significant as thickness effect. Abdullah & Cantwell (2006), have studied the influence of varying the stacking sequence on the perforation resistance of hybrid laminates. Lim et al., (2002), have reported the modes of damage, load-displacement response and the energy absorption

characteristics of kevlar fabric reinforced epoxy composites with three different stacking sequences.

Mahfuz et al., (2006), have investigated high strain rate and impact velocity effects on sandwich composites. Belingardi & Vadori (2002), have done low velocity impact tests to consider strain rate effect on the impact behavior of glass/epoxy composite plates. Vaidya & Hosur (2003), have examined the impact response of thick and thin high strain graphite/epoxy composite with polycarbonate facing. Impact tests were conducted both in the plane of the laminate, and through the thickness. Results showed that the use of polycarbonate was especially useful for thin laminates. Christopherson et al., (2005), have investigated the impact response of based on polymer honeycomb core and foam facesheet sandwich composites which have high strain rate.

Sadasivam & Mallick (2002), have studied the damage size, maximum deflection and force and impactor velocity dissipation of the glass fiber reinforced thermoplastic and thermosetting matrix composites. The residual tensile strength of the impact-damaged composites was also determined as a function of the impact energy. Lee & Cheon (2001), have investigated the impact energy absorption characteristics of glass/epoxy composites and glass/polyester composites with respect to fiber volume fraction by using Charpy impact test. Deng & Ye (2000), have carried out an experimental investigation on the graphite/epoxy composites to identify the effect of fiber- matrix adhesion for impact and dynamic mechanical properties. Results showed that the dynamic mechanical analysis was not very applicable for evaluating the fiber-matrix interfacial adhesion in practical applications. Whittingham, Marshall, Mitrevski, & Jones (2004), investigated the effect of an initial pre-stress on the impact response of carbon/epoxy plates for uniaxial and biaxial tension, pure shear and the zero pre-stress cases.

Atas & Liu (in press), have investigated the effects of the weaving angle on the peak force, contact duration, maximum deflection and absorbed energy on impact response of woven composites laminated plates. Result showed that the energy

absorption capability and perforation threshold of woven composites can be significantly improved by using a small weaving angle between interlacing yarns. Khondker, Leong, Herszberg, & Hamada (2005), have studied the effect of knit architectures and knit-structural parameters on the impact and compression-after-impact performance of weft-knitted composites. They have founded that both changes to the knit style and structural parameters affected the damage resistance and tolerance of composites.

Naik et al., (2001), have investigated the impact behavior and post impact compressive strength of three sandwich composites and only carbon and only glass composite plates with difference stacking sequences. From the results, glass-carbon/epoxy sandwich composites have lower notch sensitivity compared with only carbon or only glass composites. Hosur et al., (2005), have done impact tests to determine the response of four different combinations of woven sandwich laminates. Akimoto et al., (2000), have studied the behavior of woven glass fiber reinforced plastic and GFRP/stainless steel under low velocity impact test. Three types of woven GFRP specimens were used: chopped strand mat, biaxial or cross-ply type and quasi axial type. Result showed that the force at the initial peak and maximum force increase due to the presence of stainless steel in the composite. Hazizan & Cantwell (2003), have founded the indentation characteristic of two aluminum honeycomb sandwich structures using Meyer indentation law. Kang & Kim (2000), have investigated the impact behavior of the large deformable composites of Kevlar fiber reinforced composites, which have different preform structures.

Repeated impact is the serious phenomena for damage of composite laminate. Damage may be more critical due to repeated impact. For this reason, Datta, Krishna, & Rao (2004), have done repeated drop tests for glass/epoxy composite laminates to investigate the effects of variable impact energy and laminate thickness. Schrauwen & Peijs (2002), have determined the penetration energy, influence of laminate orientation and damage development on glass/epoxy laminates under repeated impact conditions. Kumar, Radhakrishna, & Rao (2005), have investigated the effects of different post cure applications on the impact resistance of glass/epoxy laminates

using an in-house drop weight impact tester. Sugun & Rao (2004), have carried out a series repeated impact tests on glass/epoxy, carbon/epoxy and kevlar/epoxy. Results showed that, with an increase in drop numbers, the peak load steadily decreased while the total energy increased, until failure. Baucom & Zikry (2005), Baucom, Zikry, & Rajendran (2006), have done an experimental study to consider the effects of reinforcement geometry on damage progression in 2D and 3D woven glass-fiber-reinforced composites under repeated impact loading. Results showed that the spread of damage was smallest for the 2D laminates and largest for the 3D woven composites. The 3D composites had the greatest resistance to penetration and dissipated more total energy than the 2D system. Morais, Monteiro, & d'Almeida (2005), surveyed the effect of repeated low energy impact on the performance of carbon–epoxy composites with three different stacking sequences.

Damage type such as delamination, matrix cracking, and fiber breakage may be occurring during the impact event. Damaged structures reduce its performance and using of them can be harmful for persons. Therefore, obtaining the damage type, size and shape in the laminated composite materials has been fairly interest. Park, Zhou, & Veazire (2000), have investigated the time-resolved characterization of the mechanical response and induced damage of fiber-reinforced composite laminates during impact. Margueres, Meraghni, & Benzeggagh (2000), worked to monitor the stiffness reduction and damage evaluation of composite glass/polyester manufactured by the resin transfer molding process. Chang et al., (2004), have studied the failure mechanisms at low and high temperature as −196 °C, 20 °C, and 70 °C. Cantwell (in press), has been investigated the damage–force maps of the glass/polyester circular and square composite plates at low and intermediate energies. Damage mechanisms and failure modes were also investigated for glass/polyester pultruded structures (Chotard & Benzeggagh, 1999; Chotard, Pasquiet, & Benzeggagh, 2000), for glass/epoxy laminated plates (Ruhala & Engel, 2000) and for thermoplastic sandwich structures (Kiratisaevee & Cantwell, 2005).

Delamination is one of the important damage modes during low velocity impact. Therefore, Kim & Sham (2000), have performed the fracture mechanisms of woven composite laminates in mode I and mode II delamination. Caprino, Lopresto,

Scarponi, & Briotti (1999), have evaluated the contact force and absorbed energy at the point of delamination initiation for carbon/epoxy composites, and penetration energy was also obtained for the same composites. Kim & Chung (2007), have investigated the impact force, the absorbed energy and the damaged area according to different energy levels and stacking sequences for woven composite laminates, which was used for a railway vehicle. They have obtained the highest absorbed energy and largest delamination area for $[fill]_8$ laminate. However, the lowest absorbed energy and smallest delamination area for $[fill_2/warp_2]_s$ laminate. Sutherland & Soares (2006), have studied the fiber damage of delaminated and undelaminated five marine laminates such as woven roving (WR) glass, chopped-strand mat (CSM) glass, WR/CSM glass, WR glass, and kevlar/WR. Results showed that the fiber damage was most severe for CSM and CSM/WR laminates. The WR and Kevlar/WR laminates were most resilient to fiber damage, but the Kevlar/WR did not perform better than the WR laminate

Stitching is the commonly used for increasing the energy absorbed capacity of laminated composites. Furthermore, through-thickness reinforcement of laminated composite can be increased by stitching. Thus, some authors have examined the impact behavior of the stitched laminated composite. Aymerich, Pani, & Priolo (2007), have improved the delamination resistance of cross-ply graphite/epoxy laminates by stitching. Results were showed that the delamination damage in unstitch laminate higher than the stitched laminate at the same energy level. Lopresto, Melito, Leone, & Caprino (2006), have studied the first failure load, penetration level, indentation and damage extent of stitched CFRP laminates, which have various thicknesses. The stitched laminates showed lower penetration energy compared to their 2D counterpart. Saito & Kimpara (in press), have carried out the damage progress for multi-axially stitching CFRP laminates by destructive and non-destructive evaluation. Furthermore, the residual compressive strength and fatigue property of impact-damaged CFRP laminates were determined by in-situ-damage growth using the thermo-elastic stress analyzer (TESA). Hosur, Adya, Alexander, Jeelani, Vaidya, & Mayer (2003), have discussed the response of stitched and unstitched plain and satin weave CFRP laminate at the range of 5–50 J. Results of

the study showed that the satin weave fabric composites display better impact resistance as compared to plain weave fabric composites.

Compression after impact tests used for obtaining the strength of composite materials after impact. Reis & Freitas (1997), investigated the limit loading capacity and the damage growth mechanisms of impacted carbon/epoxy composite laminates when subjected to compression after impact loading. Schubel, Luo, & Daniel (2007), have studied on the CAI strength of the damaged and undamaged sandwich structure composed of woven carbon/epoxy facesheet and a PVC foam core. Compression after impact strength were also obtained for sandwich composites with glass core and glass/kevlar face sheets in a range of −50 to 120 °C (Halvorsen et al., 2006) and for unidirectional and cross ply glass/epoxy laminated composite beams at low temperatures as 0 C°, 10 C°, and 20 C° (Ibekwe et al., 2006). Short, Guild, & Pavier (2002), have investigated the CAI strength of curved and flat glass/epoxy laminates. The same CAI strength for curved and flat laminates was founded.

The effects of specimen width and curvature on the residual compression strength of graphite/epoxy facesheet and nomex core sandwich panels were investigated by Moody et al., (2002). Results showed that the panel width and curvature not effect on the ultimate strength of the panel. But width and curvature increase the size of the damage. Cartie & Irving (2002), have studied the effect of resin and fiber properties on compression after impact in quasi-isotropic carbon/epoxy laminated plates.

Habib (2001), has proposed a new method to research the effects of impact damage on the initial buckling load and compression strength for impacted carbon/epoxy composite plates. Good correlations were obtained between the experimental and finite element values of the initial buckling load, within 9%. Naik et al., (2002), have carried out the compression after impact tests for impacted specimens using NASA fixture. Results observed that damage tolerance was higher for low mass and high velocity combination as compared to high mass and low velocity combination. Gustin, Joneson, Mahinfalah, & Stone (2005), have done compression after impact tests on carbon fiber and kevlar combination sandwich

composites to determine the reduction in compressive strength for impacted and non-impacted samples.

### *1.1.2 Numerical Studies*

A few of researchers have written an transient finite element codes to calculate stress and strain distributions through the laminate thickness (Wu & Chang, 1989), to investigate the damage initiation, the change of stiffness and damping for graphite/epoxy composite laminates (Guan &Yang, 2002) and to evaluate the in plane failure behavior of the woven composite (Naik, Sekher & Meduri, 2000). Some of them have done 3D dynamic finite elements analysis for a layered fiber-reinforced composite (Lee, Du & Liebowitz, 1984), for laminated composite beams (Lam & Sathiyamoorthy, 1999) and for composite sandwich laminates (Choi, 2006). In further, Hu, Sekine, Fukunaga & Yao (1999), have done a transient impact analysis on the composite laminates with multiple delaminations to calculate the impact force between the laminates and the rigid ball using a modified Lagrange multiplier technique and Hertzian indentation law. Breen, Guild & Pavier (2005), have simulated the dynamic and quasi-static impact on CFRP laminates to obtain the residual tensile strength using ABAQUS/EXPLICIT. The dynamically impacted specimen was found to have a 20% lower residual strength than the specimen with a simulated impact using quasi-static test.

A wide range of failure criteria and damage model have been used in the analysis of composite laminates. Hou, Petrinic, Ruiz & Hallett (2000), have implemented an improved failure criterion into LS-DYNA3D to obtaining the out-of-plane stresses. Ganapathy & Rao (1997, 1998), have predicted damage in the composite cylindrical/spherical shell using a Tsai-Wu quadratic failure criterion and maximum stress criteria. Interlaminar normal and shear stresses were also predicted by integrating the 3-D equations of equilibrium through the thickness. Zhao & Cho (2004, 2007), have investigated the impact-induced damage initiation and propagation in laminated composite shell by using the Tsai–Wu quadratic failure criterion. The impact energy threshold for the onset of damage and transient damage

areas were also predicted. Luo & DesJardin (2006), have developed a thermo-mechanical damage model for glass/phenolic composite materials subject to high temperature.

Damage resistance of laminated composite plates were investigated by Hosur, Karim & Jeelani (2003), for glass/epoxy composites subjected to repeated impact loading and by Dvorak & Suvorov (2006), for sandwich plates included thin and ductile interlayer (polyurethane or elastomeric foam) between the face sheet and the foam core. Results show that the polyurethane interlayer better supports the impacted face sheet than the elastomeric foam interlayer. The polyurethane layer also reduces the extent of permanent deformation of the foam core. Damage initiation and propagation were studied for carbon/epoxy composite plates by Luo, Green & Morrison (2001), and for sandwich panels by Xie & Vizzini (2005). Laurin, Carrere & Maire (2006), have predicted the failure behavior for various stacking sequences under a range of loading conditions.

When a foreign object impacts on a laminate; several damage modes such as delaminations, fiber breakage, and matrix cracks occur in the composite structure. Which damage mode is generally depends on the impact parameters of the impactor and the material properties of the composites. Pradhan & Kumar (2000), have predicted the initiation of matrix cracking, size and shape of the delamination in T300/976 graphite/epoxy composite laminates using 3D failure criteria. Roy & Chakraborty (2007), have evaluated the impact induced delamination of graphite/epoxy and combination of graphite/epoxy, kevlar/epoxy sandwich plates with hole. Naik, Meduri & Sekher (2000, 2001), have studied in plane failure of the layers in the form of matrix cracking, lamina splitting and delaminations. Chakraborty (2007), has performed a 3D finite element analysis for assessing delamination at the interfaces of graphite/epoxy composite plates subjected to low velocity impact of multiple cylindrical impactors. Potti & Sun (1997), have developed a model for different graphite/epoxy composite plates to predicted area of the target that was affected by delaminations during impact and penetration energy level. Parhi, Sinha & Bhattacharyya (2001), have studied the variations of contact

force, impactor and target displacement, and normal stress for multiple delaminated composite shells. Multiple delaminations modeling which was take care of whichever arbitrary number, size and placed at any location of the laminate were used.

For reinforcing laminated composites through the thickness, stitching has been commonly used. Sankar & Zhu (2000), have predicted the effects of stitching on the stitched delaminated beams. Hosur et al., (2003), have investigated the damage resistance of stitched/unstitched S2-glass/epoxy composites. Chen, Li, Kou & Gui (2004), have developed a 3D dynamic FEM to evaluate the impact damage characteristics of stitched carbon/epoxy laminates. Results showed that the transverse stitching can significantly improve the resistance of composite laminates. Furthermore, the area of delamination of stitched laminates is about 15% less than that of unstitched laminates.

Effects of some impact parameters; such as velocity (Breen et al., 2005; Khalili, Mittal & Panah, 2007; Khalili, Malekzadeh & Mittal, 2007; Changliang, Mingfa, Wei & Haoran, 2006; Her & Liang, 2004), mass (Khalili et al., 2007), energy (Khalili et al., 2007a, 2007b; Malekzadeh, Khalili & Mittal, 2006), shape (Sburlati, 2002a) and location of the impacted point (Khalili et al.,2007a; Malekzadeh et al., 2006), of the impactor, geometric and material nonlinearities (Changliang et al., 2006), length-to-thickness ratio (Khalili et al., 2007a; Cho & Zhao, 2002), out-of-plane stiffness, stacking sequence (Cho & Zhao, 2002), boundary conditions (Khalili et al., 2007a; Sburlati, 2002a; Her & Liang, 2004) of plates were investigated for various composite laminates. A few authors have also studied the thickness (Khalili et al., 2007a) and density of the core (Malekzadeh et al., 2006) effects on the impact behavior of sandwich composite plates.

The prediction impact response of cylindrical shells were investigated by Chandrashekhara & Schroeder, (1995); Krishnamurthy, Mahajan & Mittal, (2003); Gong, Lam & Reddy, (1999); Her & Liang, (2004). Zhang, Zhu & Lai (2006), have written and numerical code and implemented into ABAQUS/Explicit software to

predict the initiation and propagation of crack due to bending and delamination in carbon/epoxy composite plates. Li, Hu, Yin, Sekine & Fukunaga (2002), Li, Hu, Cheng, Fukunaga & Sekine (2002), have used a modified Newmark time integration algorithm for composite laminate which have various types of damages including delamination, matrix cracking and fiber breakage and their mutual influences on the impact behavior. Zhao & Cho (2004, 2007), have performed the influence of the stacking sequence, the thickness and the radius of curvature on damage behavior of composite shells. Naik, et al., (2000, 2001), have developed an in-house FEA code to investigate the effects of plate thickness, impactor mass and velocity on the damage initiation of woven E-glass/epoxy and T300/5208 carbon/epoxy composite plates.

Chakraborty (2007), Chakraborty & Kumar (2005), Khalili et al., (2007b), have investigated the impactor mass and velocity, uniaxial and biaxial tensile pre-stresses effects on the contact force, contact duration and deflection of the plate. Sankar & Sun (1985), have evaluated the effect of initial stresses on the contact duration, impact force, bending and shear stresses.

Roy & Chakraborty (2006), have investigated the effect of graphite/epoxy–kevlar/epoxy hybridization in improving the impact resistance of the laminated composites and also studying the chances of delamination at the interfaces of such laminates. Results are observed that the contact force magnitude was much less in the case of kevlar/epoxy laminates compared to that in graphite/epoxy laminates and they proposed the delamination extent was greater in the case of kevlar/epoxy laminates. Abatan & Hu (2002), have investigated the influence of cross-sectional material distribution and the number of layers on the impact response of metal/polymer sandwich laminate subjected to low and medium velocity impacts. Result showed that the number of layers was not affected while the relative material ratio significantly affects the impact response. Luo et al., (2001), have evaluated the static and dynamic threshold strength for carbon/epoxy composite plates. Results were shown that the threshold impact strength was much higher than the static strength.

Some authors have studied the compression after impact and buckling loads of various laminated composites. Moura, Goncalves, Marques & Castro (1997), developed a numerical model for predicting the compression failure of laminated composite containing delamination caused by low velocity impact. Puhui, Zhen & Junyang (2002), have modeled an impact damage zone as an equivalent hole to determine the CAI strength of composite laminates. Laurin et al., (2006), have investigated the effect of buckling on the final failure of laminates under compressive loadings.

A few researchers have investigated the effects of non-uniform load, boundary conditions, shear deformation, stacking sequence, through-the-width location of the delamination, delamination length, elliptical delamination and number of plies on the buckling loads of laminated composite plates (Li, Pang, Zhao & Ibekwe, 1999; Kalyan & Bhaskar, 2006; Wee & Boay, 2006; Kabir, Hamad, Duaij & John, 2007] and Aydogdu, (2006), have presented the effects of length-to-thickness ratio, plate aspect ratio and major-to-minor modulus of elasticity ratio and lay-ups on the thermal buckling loads of composite laminated plates. Shariat & Eslami, (2007), have done the thermal and mechanical buckling analysis of thick functionally graded plates under uniaxial and biaxial compression subjected to uniform and non-linear temperature through the thickness.

### *1.1.3 Both of Experimental and Numerical Study*

Choi & Chang (1992), Choi, Wu & Chang (1991), have developed a model based on the study of the line loading impact for graphite/epoxy laminated composites resulting from point-nose impact. Moura & Goncalves (2004), have predicted damage in carbon/epoxy laminates. They have observed that the impact-induced delamination and matrix cracks were the most harmful damage modes in laminated composites.

A quasi-static test may be a model for transient dynamic impact analysis. Therefore; Razi & Kobayashi (1993), have done quasi-static and impact tests to

perform the damage initiation and propagation in graphite/epoxy laminated beams and plates which have delamination. Huang & Lee (2005), have done quasi-static tests to investigate the impact behavior of carbon/epoxy composite shells with three different curvatures. Static experiments and simulations were obtained more effective than dynamic ones. In addition, this investigation proposed that the quasi-static method offers an economical way of estimating the maximum dynamic impact force.

Sharma, Murty & Krishna (2004), carried out low-velocity impact response of sandwich panels to investigate the maximum impact force, penetration time and depth of penetration for polyester/glass or epoxy/glass facesheet and polyurethane foam core sandwich composites. The results show that higher impact energy was required to crack initiation for epoxy/glass facesheet specimens than other types of specimens. Vaidya, Gautam, Hosur & Dutta (2006), have investigated the impact response of adhesively bonded lap joints in composite structures subjected to in-plane and out-of-plane loads. In this work, the response of a balanced, single-lap adhesively bonded joint was investigated by means of LS-DYNA software and supported experimentally.

Prediction of the damage may be preventing the person life. Therefore, a few authors have carried out the prediction of the damage initiation and propagation of the composite laminated plates (Moura & Marques, 2002; Cesari, Re, Minak & Zucchelli, 2007; Freitas, Silva & Reis, 2000). Iannnucci & Ankersen (2006), have developed a damage model and implemented into LS-DYNA3D software for unidirectional carbon/epoxy and woven/epoxy carbon shell elements to investigated the tensile, compressive and shear damage failure modes. Iannucci & Willows (2006), have written and implemented a damage model into DYNA3D/explicit software to correspond the maximum delamination envelope, the form of the stress–strain for woven carbon composites under high strain loading. Hosseinzadeh, Shokrieh & Lessard (2006), have investigated the damage behavior of thin and thick glass/epoxy, carbon/epoxy and carbon/glass/epoxy (sandwich) under different impact energies experimentally and by using ANSYS/LS DYNA. The thick plate of

glass/epoxy showed the best stability for all impact energies. Carbon/epoxy showed good structural resistance with compared to other materials. Carbon/glass/epoxy was proposed an optimized material like strength and weight reduction. Lee & Soutis (2005), predicted the impact-induced damage in circular composite plates under quasi-static and low velocity impact loading. In the study, a non-linear approximation method (Rayleigh–Ritz) and large deflection plate theory were used to predict the number of failed plies and damage area.

Shipsha & Zenkert (2007), have investigated the residual compressive strength and failure mechanisms of foam-cored sandwich panels. Kim, Kayır & Mousseau (2005), have characterized the modes of damage on adhesively bonded woven glass/epoxy composite joints due to impact in the overlap region. Finite element analysis was used to obtain the internal stress within the adhesive prior to failure.

The effects of stacking sequences (Roeder & Sun (2001), of target dimensions and thickness (Aslan & Karakuzu, 2002; Aslan, Karakuzu & Okutan, 2003; Aslan, Karakuzu & Sayman, 2002), and of impactor velocity and mass (Aslan & Karakuzu, 2002; Aslan et al., 2002, 2003; Lee & Huang, 2003) of impactor shape (Bull & Edgren, 2004; Meo, Morris, Vignjevic & Marengo, 2003) on the impact behavior of various composite laminates were investigated. Roeder & Sun (2001), have investigated the effects of stacking sequences and thermal residual stresses on impact resistance of thick and thin alumina/aluminum laminated structures experimentally and by using ABAQUS/Explicit software. Dynamic impact experiments showed that the thick layer laminates allowed less penetration than the thin layer laminates. Meo et al., (2003), have done a study to describe the impact and penetration damage of a sandwich panel by a solid, round-shaped impactor. Bull & Edgren (2004), have investigated the spherical and pyramid shaped impactors effects on impact damage and residual strength of sandwich panels with carbon/vinylester faces and PVC foam core. As a result the damages made from the pyramid shaped impactor were slightly different than the damages made from the spherical impactor with the same impact energy. Sutherland & Soares (2005), investigated the impact characterization of low

fiber-volume glass/polyester circular laminated plates for a range of diameter to thickness ratios.

Lee & Huang (2003), have obtained the impact force and strain histories using different impactor masses and velocities for carbon/epoxy laminated plates by user-defined material subroutine (UMAT) of the software ABAQUS. Kistler & Waas (1998), have performed the impact force and displacement histories of flat and curved laminated composite plates. Caprino, Lopresto & Iaccarino (2007), have carried out a serial impact tests on glass/aluminum and glass/epoxy laminates to calculate the force–time curve, dissipated energy, and contact duration. Gning, Tarfaoui, Collombet & Davies (2005), have investigated the influence damage initiation and propagation on the residual strength for glass/reinforced epoxy composite cylinders.

Sburlati (2002b), have investigated the relation between the impact force and the elastic indentation in sandwich plates which has graphite/epoxy facesheet and foam core. The test results were compared with those obtained from a finite element analysis. Results showed that the Hertzian contact pressure distribution appropriate to describe the response of sandwich panels with a high-density core, but not appropriate when the core has low-density. Li, Ma & Ye (2006), have proposed an elastic-plastic model to predict the dynamic response of a simply supported composite sandwich beam for different regimes such as elastic response regime, core crushing failure regime and final failure regime. Parameter studies were also carried out to investigate the influences of various non-dimensional variables. Kim & Donaldson (2006), have described the development of damage in the form of transverse ply crack and delamination within carbon/polymer composite laminates under combined thermal and mechanical loadings. The residual stresses due to difference in curing and test temperatures were calculated using classical laminated plate theory. The stress levels at the initiation of crack and delamination were determined by experimental study and compared with analytical predictions using the maximum stress criteria.

Many investigators have been curious about the parameters that effect the compression after impact strengths of laminated composites. Sala (1997), has investigated the impact energy, damage extent and residual strength on CAI strength of carbon/epoxy, carbon/high-temperature curing epoxy and carbon/epoxy-isocyanate. Zhang, Davies & Hitchings (1999), Zhang, Hounslow & Grassi (2006), have carried out the z-pinning through the thickness and preloading effects on the CAI strength of carbon/epoxy T300/914C. Results showed that the z-pinning increase the compression-after-impact (CAI) strength by about 45% and preloading raises the CAI strength. Xiaoquan, Mansour, Zhengneng & Chenghe (2005), have predicted the CAI strength on stitched laminates which have unnotched, with a hole, and with impact damage by experimentally and by using the MSC PATRAN software. Khondker, Herszberg & Hamad (2004), have proposed the linear regression analysis to establish the relationship between damage width and CAI strength of glass knitted textile composites with a circular hole. Shipsha & Zenkert (2005), have investigated the residual compressive strength of foam-cored sandwich panels. Tay & Shen (2002), have used to investigated the effects of thermal residual stresses on the buckling and post buckling in woven and non woven composite laminates. Result was founded the thermal residual stresses have a significant effect on the onset of buckling, but negligible influence on the distribution of the local strain energy release rate in the post buckled regime. Hwang and Liu (2002), have studied the buckling and post buckling behaviors of carbon/epoxy composite laminates with single and multiple delaminations under uniaxial compression tests. Experiments and numerical analysis have proven that the critical loads to delamination growth of single-delamination specimens were much higher than those of multiple-delamination specimens.

## 1.2 Objective of This Thesis

The primary objective of this work is to investigate the thermal effects on the impact behaviour of unidirectional glass/epoxy composite plates subjected to low velocity impact, both experimentally and numerically. Specific objectives of the dissertation research are also as follows:

- ✓ To obtain the thermal impact behavior of glass/epoxy laminated composites, all of samples were carried out under room 20 °C, and high temperatures (40 °C, 60 °C, 80 °C and 100 °C).
- ✓ To determination the stacking sequences effects on the impact behaviors under thermal condition, two types of plate orientation as $[0°/90°/0°/90°]_s$ and $[0°/90°/+45°/90°]_s$ were chosen.
- ✓ Overall damage patterns were determined by a non-destructive technique and also obtained by 3DIMPACT.
- ✓ Compression after impact strength of both orientations was obtained experimentally.
- ✓ Mechanical properties of glass/epoxy laminated composite plates were obtained experimentally under room and high temperature according to ASTM standards.
- ✓ Failure mechanisms of glass/epoxy plates subjected to a range of 5 J-40 J were analyzed by using 3DIMPACT commercial software.

### 1.3 Dissertation Outlines

This dissertation is organized into seven chapters. **Chapter 2** mainly provides a review of low and high velocities test systems. **Chapters 3** will talking about the damage characterization of laminated composite plates. Impact damage modes as matrix cracking, delamination, fiber breaking, and fiber-matrix debonding will be given in this chapter. **Chapter 4** will be present numerical procedure of contact mechanism and the failure criterion as matrix failure criteria and delamination failure criteria. **Chapter 5** consists of three sub-chapters; first sub-chapter presents the obtaining the mechanical properties at room and high temperatures, second sub-chapter perform the description of the impact test machine and impact characterization of glass/epoxy laminated composites at room and high temperatures, in this sub-chapter a numerical model will be also presented by using 3DIMPACT for predicting the force-time history, impact damage initiation and propagation in glass/epoxy laminated composites resulting from hemispherical impactor, and in the

last sub-chapter, compression after impact strength, which was obtained experimentally, were presented. **Chapter 6** contains conclusions of numerical and experimental results, and finally, **Chapter 7** includes recommendations for future researchs

### 1.4 Sponsorship

This thesis is sponsored by The Scientific and Technological Research Council of Turkey (TÜBİTAK), (Project Number: 104M426). Manufacturing of the laminated composites and preparation of the impact samples, CAI samples and specimens for determination of the mechanical properties were done by Izoreel firm, in Izmir-Turkey.

# CHAPTER TWO
# IMPACT TEST SYSTEMS

## 2.1 Introduction

A number of test systems have been proposed for simulating the actual impact by a foreign object. The selection of the appropriate test systems must be made very carefully to ensure that test conditions are similar to the impact conditions to be experienced by the actual structures. For example, during aircraft take off and landing, debris flying from the runway can cause damage. At this time, projectile has small mass and high velocity. So gas gun is the best simulation test systems for this case. Another case, an instrument such as a hammer is accidentally dropped on a structure. At this moment, projectile has larger mass and low velocity. Therefore, drop weight test systems must be used for this impact event (Abrate, 1998). Test systems classified by three main sections; low velocity, high velocity and hyper velocity. In this chapter, we will be discussing the low and high velocity test systems. Carrying out the hyper velocity test method is very difficult due to simulating the velocity, approximately 600 m/s and over, and test conditions. Therefore, hyper velocity will not be maintained in this chapter.

## 2.2 Low Velocity Impact Test Systems

The most common test systems for low velocity impact tests are Charpy and Izod test systems, dart or pendulum test method, cantilevered impact test method, and drop weight impact test method.

### *2.2.1 Charpy and Izod Test Systems*

The earliest test systems used for low velocity impact testing is Charpy and Izod test systems. Both systems were originally designed for the testing of metallic materials. For the Charpy test method; a beam is rested freely against two anvils and struck in the center by a pendulum. Charpy specimens may be machined with *U* and

*V* notches in the centre of the beam opposite the direction of strike, see Figure 2.1 (a). Charpy test method may be suitable for relative ranking of composite. However, it is unsuitable for glass/epoxy since this material is not sensitive to notches in either laminate direction (Amid, 2001; Reid & Zhou, 2000; Rydin, 1996).

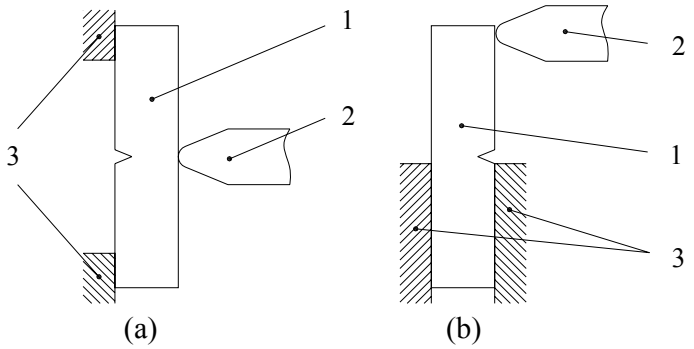


Figure 2.1 a) Charpy pendulum and b) Izod pendulum test system: (1) specimen, (2) striker, (3) anvil

The Izod test method is still commonly used for polymers. The Izod test method is similar to the Charpy test method except that the notch is near the fixed end of the specimen while the impactor strikes the free end of the specimen as shown in Figure 2.1(b). Potential energy is converted to kinetic strike energy during descent of the impactor. The energy absorbed by the specimen is measured by the height of the swinging pendulum. In either test, and with any material, the impact energy may be overestimated because energy is stored elastically in the specimen prior to failure. Impact energy can be expressed for a plastic or a composite as $U = E / b(d - c)$. Where *U* is the impact energy, *E* is the energy registered in the test, for a specimen of width *b*, and height *d*, containing a notch of depth *c* (Amid, 2001; Ellis, 1996; Reid & Zhou, 2000).

### *2.2.2 Dart or Pendulum Test Systems*

Falling dart test is a popular method, which is obtaining the impact energy. This test method was originally developed for rigid plastics. The test sample for falling dart test is 60 mm in diameter or 60x60 mm square and a range in 1-4 mm thickness.

Sample is clamped on a hollow steel cylinder with an inside diameter of 40 mm. The steel striker has a semi-circular head and is allowed to fall from height of up to 2 m onto the specimen. The maximum velocity in this test method is 6.3 m/s. An advance dart impact test has an accelerometer in the impactor tup for recording the load, target deflection and absorbed energy (Reid & Zhou, 2000; Rydin, 1996).

Pendulum-type test systems are also used to create low-velocity impacts. This test method consists of a steel impactor equipped with force transducers. The advantage of method is capable with measuring both impact and rebound velocity. The handicap of this test method; the acceleration of the tup at time that impact velocity was measured was not zero, in fact the acceleration was constant during the whole drop (Abrate, 1998; Herup, 1996).

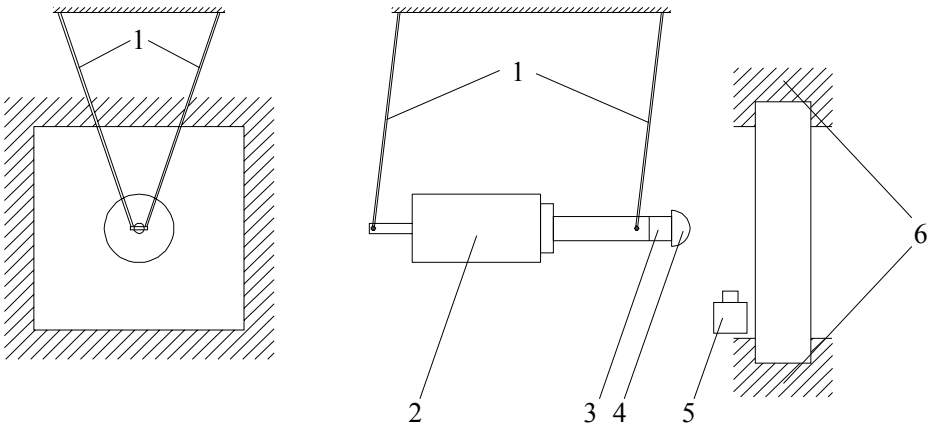


Figure 2.2 Illustration of pendulum test system

The test system is shown schematically in Figure 2.2. It has a few feature; 1) four kevlar strings to provide the effective impact point, 2) mass, 3) load cell which measures the force between the mass and the specimen, 4) a spherical hardened steel tup between the load cell and the specimen 5) a light gate to measure tup velocity just before and just after impact, 6) a stiff supported fixture to hold the specimen and a data acquisition system.

### *2.2.3 Cantilevered Impact Test System*

Literature overview considers the cantilever impact test system is not a commonly used test method. In this test system, impactor for which a 1-in. diameter steel ball is mounted at the end of a flexible beam which is pulled back and then released to be the cause of impact on the sample (Figure 2.3).

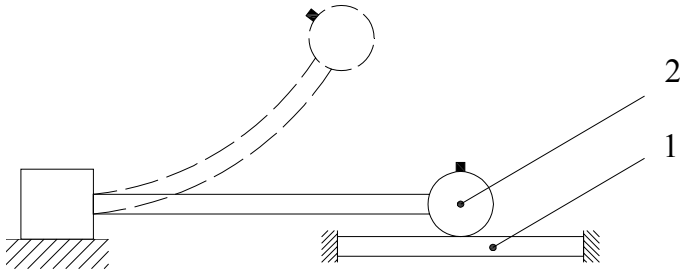


Figure 2.3 Cantilevered impact test system: (1) impactor, (2) specimen

### *2.2.4 Drop Weight Impact Test System*

In recent years, the drop-weight test system has become the preferred technique for impact testing of composites because a greater range of testing parameters is possible. A typical drop-weight testing apparatus is shown in Fig. 2.4. Drop weight test system is composed of three main components which are a dropping crosshead, two steel guide columns for movement of dropping crosshead, and a specimen supported fixture to provide boundary condition. Supported fixture is attached the T-grooved base plate by movement in T-channel for safety. A dropping crosshead also consists of adjustable weight, a rigid impactor which has generally 12.7 mm hemispherical nose, and a load cell mounted between the dropping crosshead and the rigid impactor. For provide rigidity and to increase productivity of obtaining data, each of guide columns and supported fixture which were fixed to solid base and then a concrete floor at four corners (Atas, 2004; Icten, 2006). Generally, the impactor was released from a chosen height and dropped freely on the specimen. To change the impact energy, the crosshead was increased or decreased. Crosshead can be filled by additional weight for a request energy level. However, for a highest impact

velocity the crosshead was raised to the highest point and springs can be used. When the specimen can not absorbed all of the energy, which is the impactor has, impactor strikes on the specimen more than one. At this time, a control system including brakes, namely called anti rebounding system, may be used to stop multiple hits (Dang, 2000; Herup, 1996).

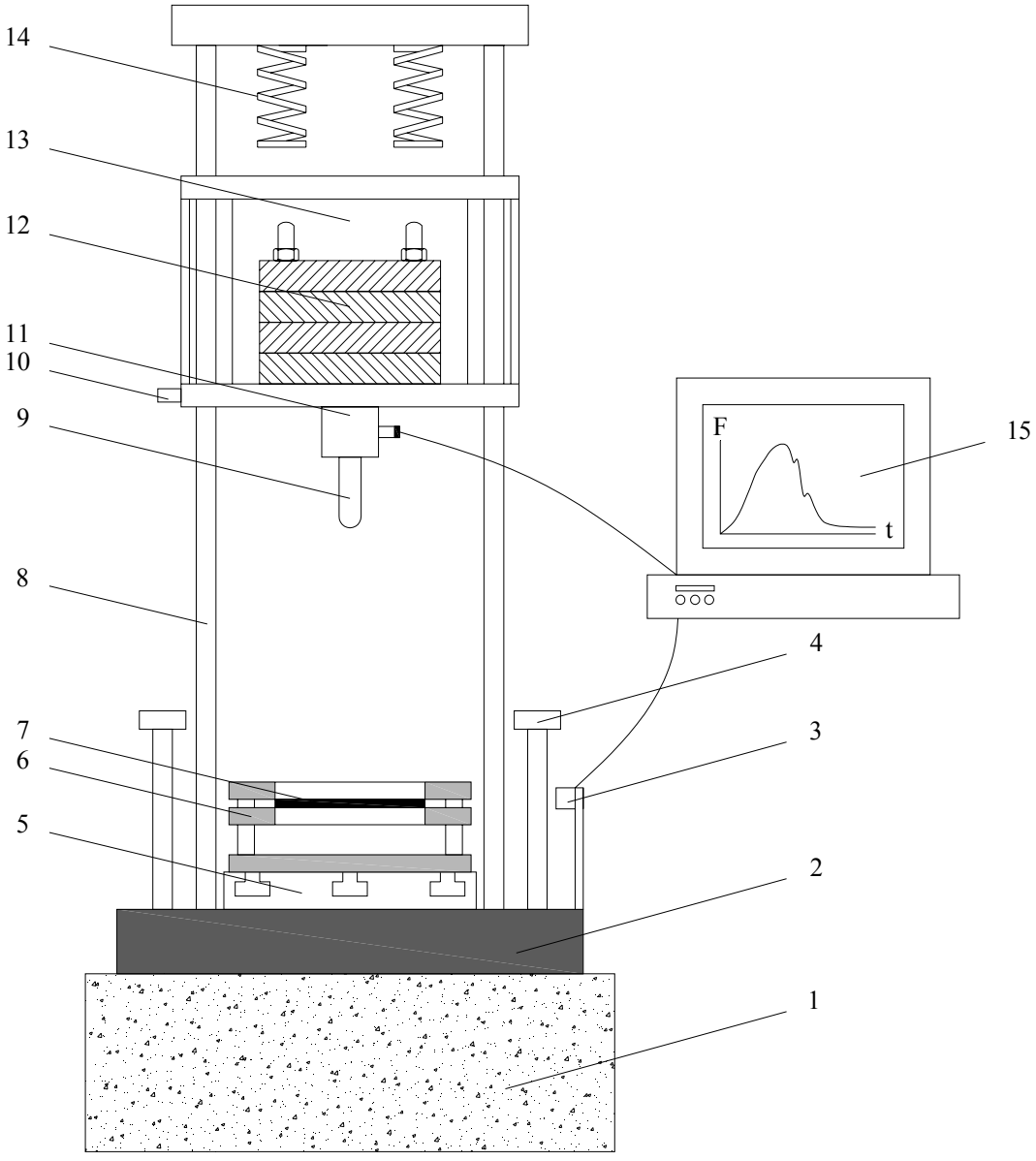


Figure 2.4 Schematic illustration of drop-weight test system: (1) concrete floor, (2) solid base, (3) emitter/detector, (4) anti rebounding system, (5) T-grooved base plate, (6) specimen, (7) support fixture, (8) guide columns, (9) impactor, (10) velocity flag, (11) load cell, (12) adjustable weight, (13) crosshead, (14) spring, (15) data acquisition system (Atas, 2004; Baker, 1994; Dang, 2000; Icten, 2006; Kowsika, 1997; Rydin, 1996).

Two independent transducers are combined in the test system during an impact event. The first device is a velocity flag to obtain the initial velocity of the crosshead and the others is an infrared emitter/detector to detect the impact velocity just prior to impact. The velocity flag also served as a switch to start the transferring the data from load cell to the data acquisition system (Icten, 2006; Majeed, 1995; Rydin, 1996).

Typically, a linear connection between the time and deflection is observed up to the point of failure However, after this point a slight non-linear relationship between the time and deflection is observed. The area under the load-deflection curve is computed at regular intervals of time/deflection to determine the energy absorbed. By the using data acquisition system; total contact force between the impactor nose and specimen and acceleration, velocity and displacement of the dropping crosshead versus time can be calculated (Kowsika, 1997).

## 2.3 High Velocity Impact Test Systems

The most commonly test systems for high and ballistic velocities are gas gun test system and split Hopkinson bar test system. These test systems will be maintained below.

### *2.3.1 Gas Gun Test System*

Gas gun test system is generally used for large structures and for high velocity ranging from 60 m/s to 240 m/s. The main features of a gas gun test system are shown in Figure 2.5. Generally, this test system has mainly four components as a pressure regulator, a tank, a solenoid valve and a speed sensing device. The cleared gas by a gas filter travel to pressure regulator. The pressure regulator with two high and low pressure gauge and a low pressure valve. The high and low pressure gauges read the pressure inside the tank and the supplied pressure, respectively. The low-pressure valve regulates the output pressure of the tank. The pressure inside the tank is released by opening a solenoid valve. After that, projectile travels through the gun

barrel and passes a speed-sensing device. This device is calculated the velocity of projectile just prior to impact. Sometimes a high speed camera may be used instead of speed sensing device to obtain the velocity of the projectile. When the gas has reached a pre-determined value the solenoid valve will be open and the accelerated impactor will be down the barrel to strike a specimen (Abrate, 1998; Amid, 2001).

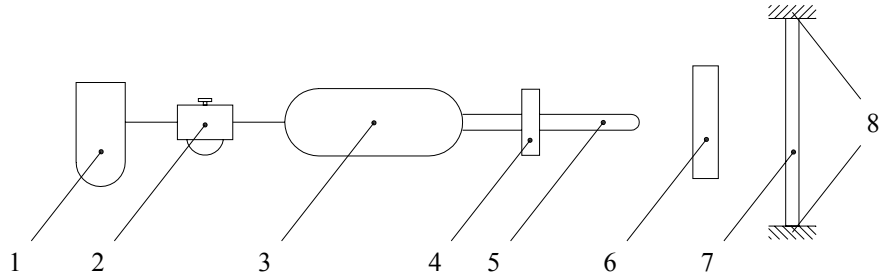


Figure 2.5 Representation of a gas gun test system: (1) gas filter, (2) pressure regulator, (3) tank, (4) solenoid valve, (5) tube, (6) speed sensing device, (7) specimen (Abrate, 1998).

### *2.3.2 Split Hopkinson Bar Test System*

The split Hopkinson bar test system (Figure 2.6) is a high velocity test system which is developed to simulate the transverse impacts on composite laminated plates. This test system is mainly composed of an air gun, an input bar, base plate for support condition and data acquisition system. In this test system; an impactor, accelerated by the air gun, hits the center of the input bar.

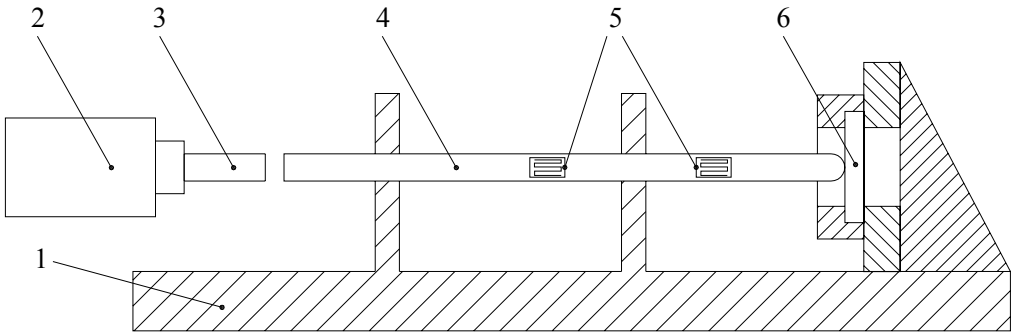


Figure 2.6 The split hopkinson bar system: (1) base plate, (2) air gun, (3) impactor, (4) input bar, (5) strain gauges, (6) specimen (Houde, 1990).

Generally, the end of the input bar is hemispherical and has a diameter of 12.7 mm. The velocity of the impactor before the impact was measured using the phototransistor. The signals from the strain gauges on the input bar were stored in a data recorder. The load acting on the specimen, the impactor velocity and the specimen displacement are obtained by using the recorded data which are stored from strain gauge (Houde, 1990).

# CHAPTER THREE
# DAMAGE CHARACTERISTICS IN LAMINATED COMPOSITES

## 3.1 Introduction

Composite materials are composed of two submaterials as matrix and fiber. Properties of these submaterials significantly influence the damage initiation and propagation due to affect the overall and contact stiffness of the composite structure. In addition to properties of the materials, a lot of parameters are considered in the literature. The thickness, size, and the stacking sequence of the laminate, the density, elastic properties, shape and initial velocity of the impactor, and also stitching, environmental condition such as temperature and humidity are all factors that influence the damage characteristic of the composite structures (Abrate, 1998).

The impact parameters that influence the damage characteristic of the composite structure will be considered in the preceding period of this chapter. Afterwards, different types of damage will be discussed and at the end of this chapter the damage criterion will be mentioned to understand the macro mechanics of the damage in the laminated composite materials.

## 3.2 Impact Damage Parameters

Damage generally results from locally high stress concentrations sufficient to cause localized failure of the material. Damage is reduced the stiffness, strength, and life of the composite structures. However, no damage occurs if the energy of the impactor is accommodated by the elastic strain energy in the material. A few important parameters that influence the damage type such as matrix cracking, delamination, and fiber breakage will be discussed as below:

**Laminate properties:** The *material properties* affect the damage characteristics of the composite structures directly. The elastic properties of the material ($E_1$, $E_2$, $\nu_{12}$ and $G_{12}$) are influence the rigidities of the laminate which greatly affects the contact

force history. The modulus in the fiber direction, $E_1$, and the modulus perpendicular to the fiber direction, $E_2$, has a major effect on the bending stiffness and the contact stiffness, respectively. In addition, increasing the difference between $E_1$ and $E_2$ modulus of the material leads to higher bending stiffness mismatching and therefore increased delamination. For composite materials, elastic modulus of the reinforcing fibers is usually much higher than that of the matrix. Therefore, fibers do not seem to affect the onset of matrix cracking and delamination. Delamination and the energy absorption capability reduce by increasing the fiber/matrix adhesion. Delamination can improve the impact resistance of the composite materials.

The stiffness of the laminate depends on the *thickness* which has a considerable effect on the maximum contact force which influences the extent of the damage. At low velocities, targets generally represent the bending behaviour. In this case, high tensile stress is placed in the lowest ply. Due to high stress concentration in the lowest ply, a matrix cracking occurs. Afterwards, delamination at the lowest interface follows the matrix cracking. In addition, when the thickness of laminate is increased, the impact energy threshold, which causes the damage, also increases. Thus, considering the damage size effect it appears that thick laminates are less susceptible to impact damages than are thin ones. Delamination increases by increasing the thickness of each layer, which has different fiber orientations (Abrate, 1998; Groves, 1986).

*Stitching* is one of the important methods that improve the delamination resistance of the laminate. During impact, stitching arrests the delaminations. Also, stitching improves the compression after impact strength of the laminate by prevents the growth of delamination.

The impact damage is more sensitive to the change of *stacking sequences* than of target thickness**.** In a unidirectional laminate, no delamination occurs due to the same orientation of fibers. If two adjacent plies have different orientation angle, the delamination occurs due to bending mismatching (Liu, 1988). The damage size

increases by increasing the bending mismatching. The peak load reached during impact is powerfully dependent on the stacking sequence.

**Impactor properties:** The higher *modulus of elasticity* of impactor gives a higher contact stiffness, which induces higher contact forces and a smaller contact area between the impactor and the target. Both of these factors cause the higher damage. The *mass* of the impactor affects the impact energy threshold and impact damage. The heavier impactors increase the contact force and contact time. A large mass with low initial velocity may not cause the same amount of damage as a smaller mass with higher velocity, even if the kinetic energies are exactly the same. Also, the *shape* of the impactors affects the damage in the laminate. For example, blunt impactors cause less damage than hemispherical tip impactors. Also, the extent of damage is caused by the smallest impactor which has a higher impact velocity when compared to any other impactor at constant impact energy (Abrate, 1998; Papanicolaou et all. 1998).

## 3.3 Impact Damage Modes

Damage characteristics of laminated composite material which are subjected to low velocity impact can be classified as fiber breakage, matrix cracking, fiber-matrix debonding and delamination. Delamination is the most important damage modes among these damage modes. Damage can be affects the reducing the stiffness, strength, and life of the composite. Experimental study shows that the damage starts after impact force reaches a critical value.

### *3.3.1 Matrix Cracking*

Matrix cracking is the most common damage in continuous fiber laminated composite materials. Matrix cracking occurs in a composite with a fairly brittle matrix; such as epoxy. Since, the epoxy is a more breakable sub material than the fibers in a composite structure; the epoxy fails at little strains than the fibers. So that when the structure is subjected to impact loads, cracks initially form in the matrix. The location of the initial matrix cracks is dependent on the stacking sequences of

the laminate. The cracks are oriented in directions parallel to the fiber direction of a damaged ply. Two kind of matrix cracking have been observed in the literature such as tensile cracks and shear cracks. These types of matrix cracks are observed in Figure 3.1.

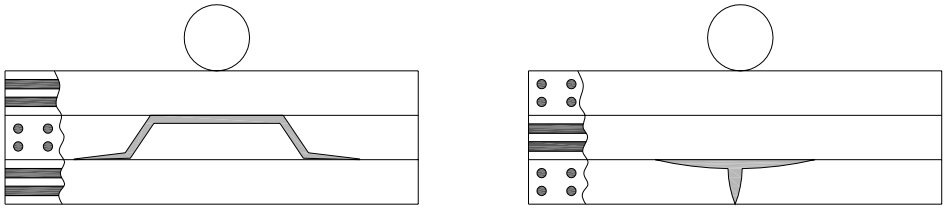


Figure 3.1 Two types of matrix cracking; (a) shear crack, (b) tensile crack (Abrate, 1998)

When in-plane normal stresses exceed the transverse tensile strength of the ply, tensile cracks occurs. Shear cracks are at an angle from the mid surface, which indicates that transverse shear stresses play a significant role in their formation. The overall stiffness of the composite structure is reduced by matrix cracking. For thick laminated plates, because of the high and localized contact stresses, matrix cracks are first produced in the first layer which is impacted by the impactor. In this case, damage progresses like a pine tree pattern from the top to down (Figure 3.2.a). For thin laminated plates, matrix cracks can be introduced in the lowest layer due to the bending stresses in the back side of the laminate (Figure 3.2.b). At this case, damage again starts with a pattern of matrix cracks and delaminations (Abrate, 1998).

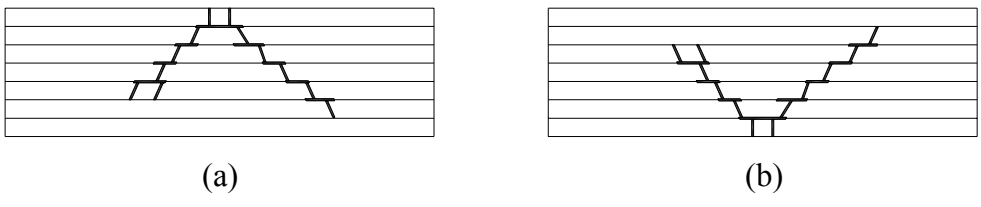


Figure 3.2 Pine tree pattern (a) for thick laminate (b) for thin laminate (Abrate, 1998)

### *3.3.2 Delamination*

Delamination occurs by debonding between adjacent laminas, i.e., delamination initiates at the intersection of a matrix crack with the ply interface. Delamination is fundamentally an interface failure, but can also be considered a matrix failure. Delamination is often attributed to the high interlaminar stresses occurring in the two adjacent laminas. Strength of the laminate can be reduced due to this damage mode. Residual compressive strength of laminated composite plates also reduces by occurring delaminations. Experimental studies showed that the delamination occurs only at interfaces between plies which have different fiber orientations. If two adjacent plies have the same fiber orientations, no delamination will be introduced at the interface between them (Abrate, 1998).

In a composite material, the material properties of the fibers are different than the matrix. According the stacking sequences of the different fiber orientations in a composite laminate, bending mismatches of these materials cause different nonuniform stress distributions in the laminate when it is subjected to impact loads. Liu (1988) explained that the delamination was a result of the bending stiffness mismatch between adjacent layers, which are in different fiber orientation. If the mismatch is higher, the delamination becomes larger. Delamination size and shapes are dependent on the mismatch properties of the layers. From the classical lamination theory, bending stiffness $D_{ij}$ is directly dependent on the stacking sequence, material constants and thickness of a composite plate. The difference in bending stiffness of two adjacent laminas can be defined by the bending stiffness mismatching coefficient, $M$ as

$$M = \frac{D_{ij}\left(\theta_b\right) - D_{ij}\left(\theta_t\right)}{D_{ij}\left(0^\circ\right) - D_{ij}\left(90^\circ\right)} \tag{3.1}$$

where $\theta_b$ and $\theta_t$ represent the fiber angles in the bottom and the top laminas of two adjacent laminas, respectively.

Depending on the stacking sequence of the laminate, delamination may be occurring in a wide range of shapes. The general characteristics of a delamination are shown in Figure 3.3. The delamination appears as an elongated ellipse. This elongated portion of the delamination is oriented in a direction which is directly aligned with the fiber direction of the bottom ply. The major delamination damage generally occurs at the back face of the laminate and progressively becomes smaller toward the impact face.

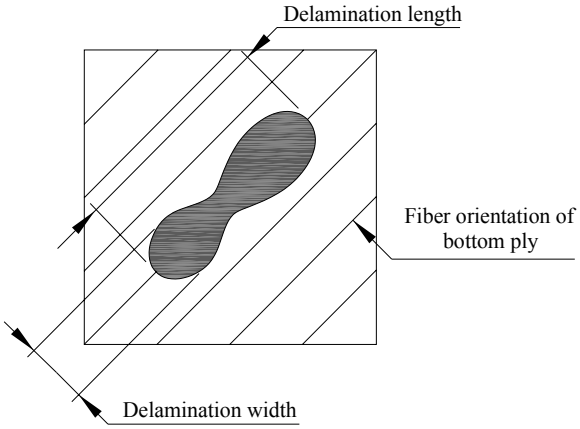


Figure 3.3 Typical delamination shape

### *3.3.3 Fiber Breaking*

*Fiber breaking* is the failure of the fibers of the composite laminate. Fiber breakage can be occur at the back face with visible outward deformation by high tensile forces due to bending in local regions of the laminate or by local shearing in the matrix. Until penetration of the specimen occurs, the outward deformation, which causes the internal plies being crushed, will continue with increasing the energy level. Fiber breaking increases by increasing the areas of fiber matrix debonding. Ultimate failure of the laminate occurs after all fibers have broken. The sharp impactor causes the bigger fiber breakage than the blunt one. Also, shaper impactor causes the larger degradation in tensile strength. When the fiber breakage starts, stiffness reductions can not be done completely. Because of the matrix is still bonded to the fibers in their laminas. If no bonding between the fiber and matrix in each of plies, stiffness reductions are expected (Groves, 1986; Fuoss, 1996).

### *3.3.4 Fiber-Matrix Debonding*

In the perpendicular to the fiber directions, the shrinkage creates tensile stresses which separate the matrix from the fiber at the fiber-matrix interface. It is commonly known as fiber-matrix debonding or pull-out. Along the fiber direction, the shrinkage creates shear stresses which can cause micro buckling for fiber at the fiber-matrix interface. Therefore, fiber-matrix debonding occurs due to this micro buckling. Fiber-matrix debonding is usually caused by a poor bond between the matrix and reinforcement, but can also obvious as shear failure in the matrix surrounding the reinforcement, as the matrix is unable to transfer the load sustained by the reinforcement. The illustration of the fibre-matrix debonding is given Figure 3.4. Fiber-matrix debonding can be completely, such that the reinforcement transfers no load to the matrix, or partial, where some load transfer still occur the interface (Floyd, 1994).

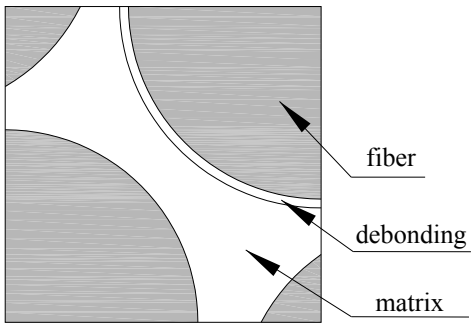


Figure 3.4 Illustration of the fiber-matrix debonding

## 3.4 Stress Field

To describe the stresses and mechanisms of the impact damage modes which are mentioned above Figure 3.5 is given. In this figure, a ply group containing a matrix crack and the two adjacent interfaces are represented. Each interface may be unrestrained or restrained. When the cracked ply group and the adjacent laminate are bonded perfectly, the interface will be restrained.

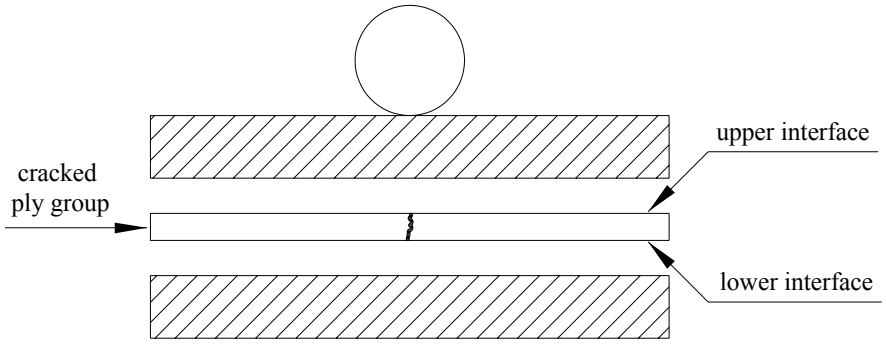


Figure 3.5 Representation of the cracked ply group with upper and lower interfaces (Finn, 1991).

The applied transverse load may result in *bending and twisting* of the plate. When a ply group is subjected to a transverse load, the curvature of the plies will be different due to their fiber orientation. This difference between curvatures causes delamination between the adjacent plies. According to the applied load, a plate may have a concave bend shape. In this case, if the lower interface of the cracked ply group is unrestrained and bending like a curvature in the normal directions to the fibers, the crack may be occur resulting in a difference in curvature between the cracked ply group and the adjacent laminas. As a result of this, delamination occurs along the upper interface, as illustrated in Figure 3.6.a. The stress in the cracked ply group connected with the bending just described is the in-plane normal tensile stress $\sigma_{yy}$. However, if the lower interface is restrained, bending does not open the matrix crack and thus delamination does not occur. Besides, bending may cause a curvature along the fiber direction of the cracked ply group (Figure 3.6.b). This type of bending causes a normal tensile stress in the fiber direction, $\sigma_{xx}$ in the cracked ply group. Nevertheless, bending in the fiber direction does not cause the delamination. Other cases, when the upper interface of the cracked ply group is unrestrained (Figure 3.6.c) and is restrained (Figure 3.6.d), the cracked ply group will be in compression form. In this case, the crack does not open and no delamination occurs. Hence, the transverse compressive stresses $\sigma_{yy}$ and $\sigma_{xx}$ will be appearing (Finn, 1991).

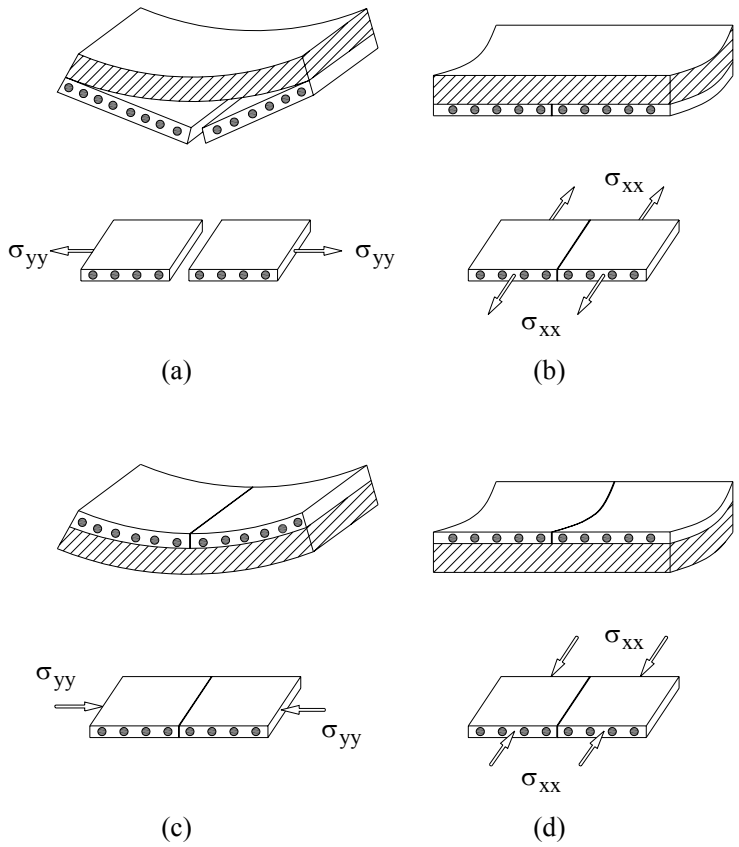


Figure 3.6 Bending of a plate (a), (c) curvature in the direction normal and (b), (d) curvature in the direction parallel to the fibers of the cracked ply group (Finn, 1991).

The transverse load may also cause a twisting of the plate. If the lower interface is unrestrained, the crack may open due to mismatch between the cracked ply group and the adjacent laminae. This mismatch causes a delamination to form along the upper interface (Figure 3.7.a). If the upper interface is unrestrained, the converse situation will be exists (Figure 3.7.b). For both case, in-plane shear stress $\sigma_{xy}$ will be occur in the cracked ply group. In addition, if both interfaces are restrained the delamination will not be existing.

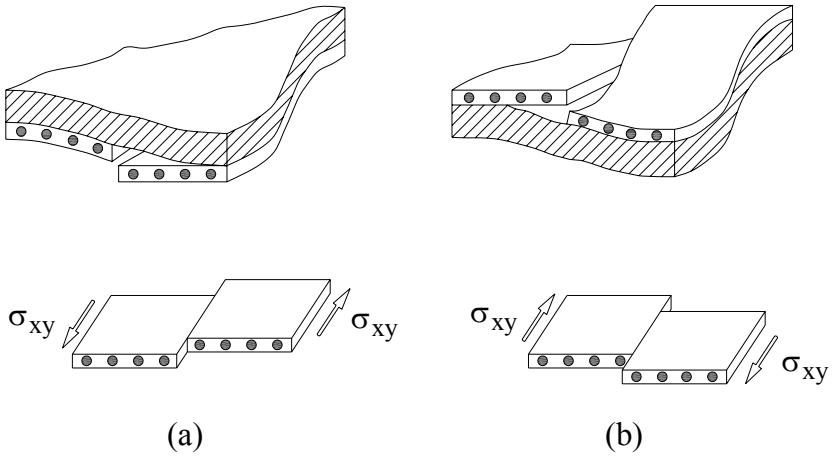


Figure 3.7 Twisting of a plate; (a) lower and (b) upper interface unrestrained (Finn, 1991).

The applied transverse load may also causes shearing of the plate. The adjacent plies may slide on each other by shearing. This sliding does not cause the delamination. But both of the transverse shear stresses $\sigma_{zx}$ and $\sigma_{zy}$ are occur (Figure 3.8.a, b).

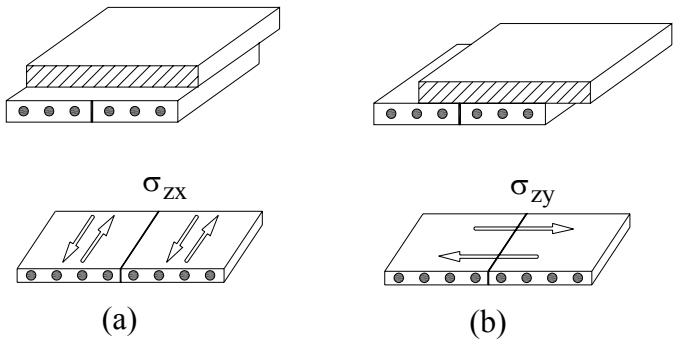


Figure 3.8 Interlaminar shearing (a) parallel and (b) normal to the fiber direction of the cracked ply group (Finn, 1991).

The transverse shear may also causes local curving in the directions normal and parallel to the fibers of the cracked ply group. When the curve exists in the direction normal to the fibers of the cracked ply group, the delaminations along both the upper and lower interfaces will be occurring due to local mismatch in curvature. The transverse shear stress $\sigma_{yz}$ in the cracked ply will introduce for this type of shearing (Figure 3.9.a). When the curve exists in parallel to the fibers of the cracked ply

group, the matrix cracking and delamination does not occur. The transverse shear stress $\sigma_{xz}$ will be introduced in the cracked ply group (Figure 3.9.b) (Finn, 1991).

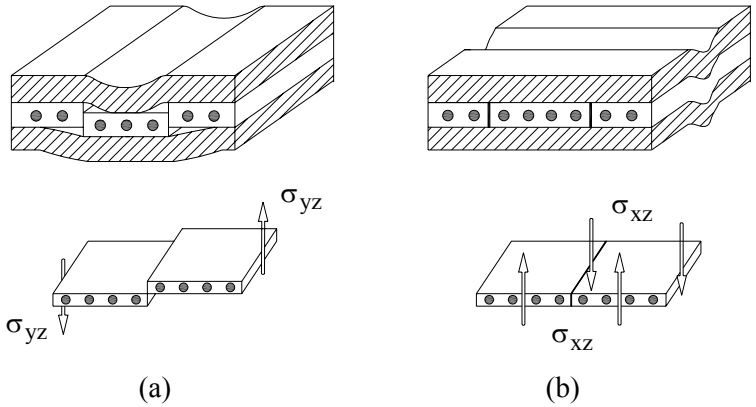


Figure 3.9 Shear-induced local curvatures; (a) normal and (b) parallel to the fibers of the cracked ply group (Finn, 1991).

In addition, transverse normal stress $\sigma_{zz}$ may stretch or compress the ply groups in the thickness direction (Figure 3.10). This deformation does not open the matrix crack and, thus, no delamination will be occurring.

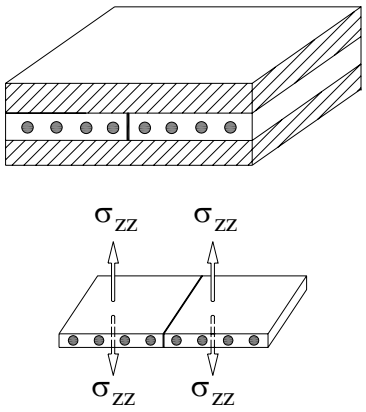


Figure 3.10 Normal stresses in the thickness of a cracked ply group

# CHAPTER FOURTH
# NUMERICAL PROCEDURE

## 4.1 Introduction

The numerical investigation is performed for predicting the impact damage in glass/epoxy laminated composites subjected to low velocity impact by a foreign object. In this current study; 3DIMPACT code is used for investigate the dynamic characteristics of glass/epoxy laminated composite in the view of the transient dynamic finite element analysis.

The numerical model has described to calculate the contact force between the impactor and composite plate, maximum deflection at the center of the plate and to show the impact damage in the interface of the two adjacent plies. The code allows us to change some impact parameters such as geometry and ply orientation of the composite plates, and the velocity and mass of the impactor. The code does not include the fiber fracture criterion. Therefore, only the energy levels up to 40J are analyzed during the numerical study to compare the results of the experimental study.

In the numerical study, eight node brick elements are used. To account the change in the material properties from layer to layer within the element, the direct Gauss quadrature integration scheme is used through the element thickness. The Newmark scheme is adopted to perform time integration from step to step. And, to calculate the contact force during impact, a contact law is incorporated with the Newton-Raphson method. In addition, an impact-induced delamination criterion and a matrix failure criterion are used for predicting the damage due to transverse impact.

## 4.2 Contact Force

Based on plane strain condition, the equilibrium equation at an instant *time=t* in a variational form can be expressed as (Wu & Chang, 1989)

$$0 = \int_{\Omega} w_i \rho u_{i,tt} dv + \int_{\Omega} e_{ij} E_{ijkl} \varepsilon_{kl} dv + \int_{\Gamma} w_i \sigma_{ij} n_j dA \tag{4.1}$$

where $\sigma_{ij}$ are the stresses, $\varepsilon_{kl}$ are the strains, $\rho$ is the density, $u_{i,tt}$ are the accelerations, $w_i$ are the arbitrary variational displacements, $eij$ are the strains from the arbitrary variational displacements, $\Omega$ is the plate volume, $\Gamma$ is the surface of the plate, $nj$ is the external unit normal vector on the plate surface, and $E_{ijkl}$ are the material properties of the laminates, which differ from layer to layer due to ply orientation of the laminate.

For solving the Equation (4.1), the contact force distribution between the impactor and the laminate must be known. The projectile is assumed as an elastic body with a spherical nose. In a force-deflection history curve, the portion of the curve up to the maximum contact force is called *loading*, and after this point other portion of the curve is named *unloading*. Therefore, the contact force distribution can be determined by the loading and unloading case.

According to the Hertzian contact law in the loading case, the contact force can be expressed as (Wu & Chang, 1989)

$$F = \kappa \alpha^{1.5} \tag{4.2}$$

where $\alpha$ and $\kappa$ are the indentation depth and the constant of the Hertz contact.

In the unloading case, the contact force can be determined as (Wu & Chang, 1989)

$$F = F_m \left[ \frac{\alpha - \alpha_0}{\alpha_m - \alpha_0} \right] \tag{4.3}$$

where $F_m$ is the maximum contact force just before unloading, $\alpha_m$ is the maximum indentation related to $F_m$, and $\alpha_0$ is the permanent indentation during loading/unloading process. The permanent indentation can be expressed as (Wu & Chang, 1989)

$$\alpha_0 = 0 \qquad \text{when } \alpha_m < \alpha_{cr}$$

$$\alpha_0 = \alpha_m \left[ 1 - \left( \frac{\alpha_{cr}}{\alpha_m} \right)^{2/5} \right] \qquad \text{when } \alpha_m \geq \alpha_{cr} \tag{4.4}$$

where $\alpha_{cr}$ is the critical indentation and is approximately 0.1 mm for glass/epoxy.

### 4.3 Governing Equation

By neglecting damping effect, the governing equation can be written as (Wu & Chang, 1989)

$$[M]\{\ddot{d}\} + [K]\{d\} = \{F\} \tag{4.5}$$

where $[M]$, and $[K]$ are the mass and stiffness matrices, and $\{F\}$, $\{d\}$ and $\{\ddot{d}\}$ are the force, displacement and acceleration vectors, respectively. At time $t + \Delta t$ governing equation can be written as below and for solving this equation the Newmark method is used.

$$[M]\{\ddot{d}\}^{t+\Delta t} + [K]\{d\}^{t+\Delta t} = \{F\}^{t+\Delta t} \tag{4.6}$$

Accordingly, the velocity and acceleration vectors at time $t + \Delta t$ are written as

$$\{\dot{d}\}^{t+\Delta t} = \{\dot{d}\}^{t} + (1-\lambda)\Delta t \{\ddot{d}\}^{t} + \lambda \Delta t \{\ddot{d}\}^{t+\Delta t} \tag{4.7}$$

$$\left\{\ddot{d}\right\}^{t+\Delta t}=\frac{1}{\beta\Delta t^{2}}\left\{d\right\}^{t+\Delta t}-\frac{1}{\beta\Delta t^{2}}\left\{d\right\}^{t}-\frac{1}{\beta\Delta t}\left\{\dot{d}\right\}^{t}-\left(\frac{1}{2\beta}-1\right)\left\{\ddot{d}\right\}^{t} \tag{4.8}$$

where $\beta$ and $\lambda$ are constants which are depend on the finite difference method. Accordingly to this method $\beta$ and $\lambda$ are $1/4$ and $1/2$, respectively. By substituting Eq. (4.8) into Eq. (4.6),

$$[\hat{K}]\left\{d\right\}^{t+\Delta t}=\left\{\hat{F}\right\}^{t+\Delta t} \tag{4.9}$$

where $[\hat{K}]$ is the effective stiffness matrix, and $\left\{\hat{F}\right\}^{t+\Delta t}$ is the effective force vector. These parameters are expressed as (Aslan, 2002)

$$[\hat{K}]=\frac{1}{\beta\Delta t^{2}}[M]+[K] \tag{4.10}$$

$$[\hat{F}]^{t+\Delta t}=\left\{H\right\}^{t}+\left\{F\right\}^{t+\Delta t} \tag{4.11}$$

where

$$\left\{H\right\}^{t}=[M]\left(\frac{1}{\beta\Delta^{2}}\left\{d\right\}^{t}+\frac{1}{\beta\Delta}\left\{\dot{d}\right\}^{t}+\frac{1-2\beta}{2\beta}\left\{\ddot{d}\right\}^{t}\right) \tag{4.12}$$

For solving equation (4.9) the displacement, velocity and acceleration at time *t* must be known at every point inside the plate. But, two components as displacement vector and the force vector are still unknown. For determining these unknown, an additional expression is needed.

By combining Eq. (4.9) and eq. (4.11)

$$[\hat{K}]\left\{d\right\}^{t+\Delta t}=\left\{H\right\}^{t}+\left\{F\right\}^{t+\Delta t} \tag{4.13}$$

The displacement vector $\{d\}$ is expressed as the sum of the displacement due to the force $\{H\}$, and the contact force $\{F\}$

$$\{d\}^{t+\Delta t} = \{d\}_H^{t+\Delta t} + f^{t+\Delta t}\{d\}_U^{t+\Delta t} \tag{4.14}$$

where $f^{t+\Delta t}$ is the contact force at time $t+\Delta t$ and it can be define depends on the loading and unloading case as

$$f^{t+\Delta t} = \kappa\left(\int_0^t\int_0^t \frac{f}{m}dtdt - \delta_{CH}^{t+\Delta t} - f^{t+\Delta t}\delta_{CU}^{t+\Delta t}\right)^{1.5} \quad \text{for loading case} \tag{4.15}$$

$$f^{t+\Delta t} = f_m\left(\frac{\int_0^t\int_0^t \frac{f}{m}dtdt - \delta_{CH}^{t+\Delta t} - f^{t+\Delta t}\delta_{CU}^{t+\Delta t} - \alpha_0}{\alpha_m - \alpha_0}\right)^{2.5} \quad \text{for unloading case} \tag{4.16}$$

where $\delta_{CH}^{t+\Delta t}$ and $\delta_{CU}^{t+\Delta t}$ are the magnitudes of the displacements at the center point of the mid-surface in the direction of impact at time $t+\Delta t$.

The contact force $f^{t+\Delta t}$ is calculated either by Eq. (4.15) for loading case and by Eq. (4.16) for unloading case by using Newton-Raphson method. At time $t+\Delta t$, the displacement vector $\{d\}$ can be calculated from Eq. (4.14), and the velocity and acceleration vectors can be calculated from Eq. (4.7) and Eq. (4.8). The above mentioned procedure is repeated at each timer step (Wu & Chang, 1989).

The 3DIMPACT code includes the Newmark method and implicit integration method for nonlinear dynamic response calculations. Therefore, these methods are used for comparing the experimental study.

## 4.4 Failure Mechanism

During the impact event, a transient compressive normal stress initiates and propagates through the panel. For a solid laminate, the compressive stress wave reflects from the back surface of the laminate as tension wave and may produce matrix cracking. Local transient bending waves are then initiated following several reflections of the transient normal waves. Interlaminar stresses associated with the local bending may cause the damage (Anderson, 1999).

In the numerical study, two failure criteria as critical matrix cracking criterion and impact-induced delamination criterion are used in the 3DIMPACT code which is proposed by Choi et al. (1991).

### *4.4.1 Matrix Cracking Criterion*

Base on transversely impact, there are only three stresses components that can contribute to initial matrix cracking in the 90° layers in the plane strain condition. These are the interlaminar shear stress $\sigma_{yz}$, in-plane tensile stress $\sigma_{yy}$ and out-of-plane normal stress $\sigma_{zz}$. However, the out-of-plane normal stress is very small in comparison with the other two stress components during the entire impact event. Hence, the matrix cracking criterion can be expressed as ($\sigma_{yy} \geq 0$) (Choi, 1990)

$$\left(\frac{{}^{n}\bar{\sigma}_{yy}}{{}^{n}Y_t}\right)^2 + \left(\frac{{}^{n}\bar{\sigma}_{yz}}{{}^{n}S_i}\right)^2 = e_M^2 \qquad \begin{cases} e_M \geq 1 & \textit{failure} \\ e_M < 1 & \textit{no failure} \end{cases} \tag{4.17}$$

where the subscripts of $x$ and $y$ are the local coordinates of the *n-th* layer parallel and normal to the fiber directions, respectively, and $z$ is the out-of-plane direction. ${}^{n}Y_t$ and ${}^{n}S_i$ are the in situ ply transverse tensile strength and interlaminar transverse shear strength within the *n-th* ply of laminate under consideration, respectively. ${}^{n}\bar{\sigma}_{yz}$ and ${}^{n}\bar{\sigma}_{yy}$ are the averaged interlaminar transverse shear stress and the averaged in-

plane transverse tensile stress, respectively. These stresses can be expressed as (Choi, 1990)

$$ {}^{n}\bar{\sigma}_{yz} = \frac{1}{h_n}\int_{t_{n-1}}^{t_n} \sigma_{yz}\, dz \tag{4.18} $$

$$ {}^{n}\bar{\sigma}_{yy} = \frac{1}{h_n}\int_{t_{n-1}}^{t_n} \sigma_{yy}\, dz \tag{4.19} $$

where $t_n$ and $t_{n-1}$ are the upper and lower interfaces of the *n-th* ply in the laminate and $h_n$ is the thickness of the ply.

For determining any additional matrix failure, the criterion must be applied to the other layers. If no additional matrix cracking is found during impact, then the impactor's velocity associated with the first matrix cracking is referred to as the impact velocity threshold, which is the velocity required to just cause the initial impact damage of the laminate.

### *4.4.2 Impact-Induced Delamination Criterion*

Delamination can be initiated from the matrix cracking in a ply within the laminate. To accurately simulate delamination propagation is very difficult and complicated. Basically two types of critical cracks initiating delamination resulting from impact as (Choi et al., 1991): one of them is shear crack and the other is bending crack. These types of crack are mentioned in the Chapter 3. Therefore, only mathematical approach is discussed here.

For the shear-crack, delamination can be occur due to the interlaminar longitudinal shear stress $\sigma_{xz}$ in the layer right below the interface and the interlaminar transverse shear stress $\sigma_{yz}$ in the layer right above the interface. A schematic illustration of the delamination propagation mechanisms induced by a

shear crack is shown in Figure 4.1. However, for the bending-crack, delamination can be occur due to the interlaminar longitudinal shear stress $\sigma_{xz}$ in the layer right below the interface and the in-plane bending stress $\sigma_{yy}$ in the layer right below the interface. An illustration of the delamination induced by a bending crack is shown in Figure 4.2.

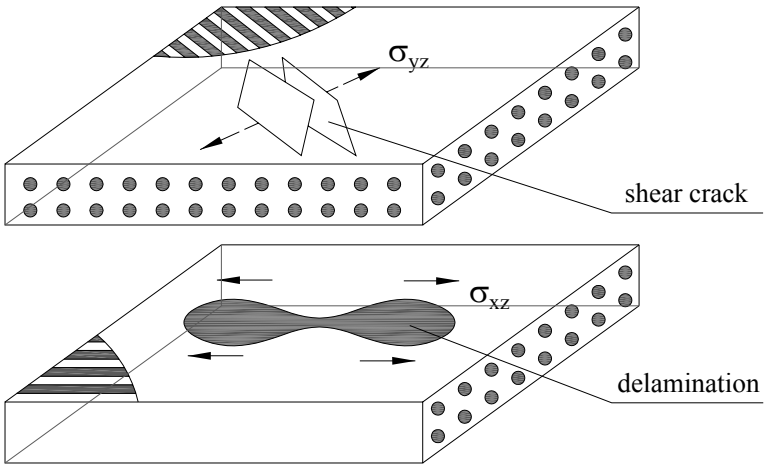


Figure 4.1 Delamination growth mechanism induced by a shear crack in laminated composite (Aslan, 2002).

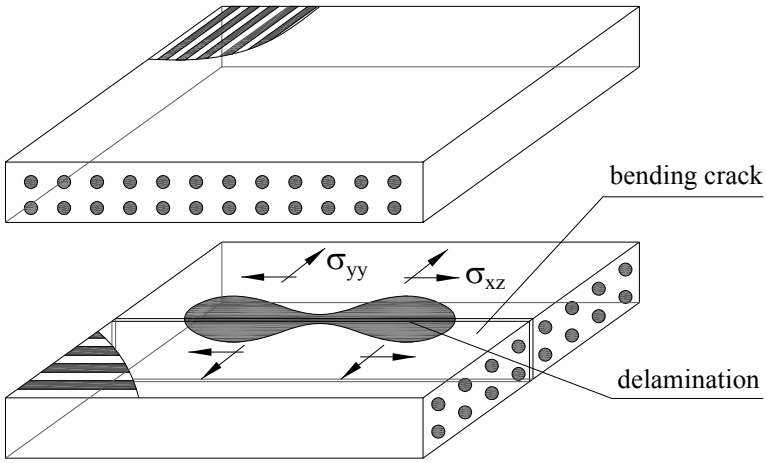


Figure 4.2 Delamination growth mechanism induced by a bending crack in laminated composite (Aslan, 2002).

By taking both failure mechanisms, delamination could occur only when the following two sequential conditions are met:

- One of the p1y groups intimately above or below the concerned interface has failed due to matrix cracking.
- The combined stresses governing the delamination growth mechanisms through the thicknesses of the upper and lower ply groups of the interface reaches a critical value.

Based on the above statement, impact-induced delamination criterion for low velocity impact proposed by Choi & Chang (1992) as

$$D_a\left[\left(\frac{{}^{n}\bar{\sigma}_{yz}}{{}^{n}S_i}\right)^2+\left(\frac{{}^{n+1}\bar{\sigma}_{xz}}{{}^{n+1}S_i}\right)^2+\left(\frac{{}^{n+1}\bar{\sigma}_{yy}}{{}^{n+1}Y}\right)^2\right]=e_D{}^2 \quad \begin{cases} e_D \geq 1 \quad failure \\ e_D < 1 \quad no\ failure \\ {}^{n+1}Y = {}^{n+1}Y_t \ \ if\ \bar{\sigma}_{yy} \geq 0 \\ {}^{n+1}Y = {}^{n+1}Y_c \ \ if\ \bar{\sigma}_{yy} < 0 \end{cases} \tag{4.20}$$

where $D_a$ is a constant which has to be determined from experiments. The superscripts *n* and *n+1* correspond to the upper and lower plies of the *n-th* interface, respectively. ${}^{n}\bar{\sigma}_{yz}$ and ${}^{n+1}\bar{\sigma}_{yy}$ are the averaged interlaminar and in-plane transverse stresses within the $n^{th}$ and $(n+1)^{th}$ ply, respectively. ${}^{n+1}\bar{\sigma}_{xz}$ is the averaged interlaminar longitudinal stress within the $(n+1)^{th}$ ply which can be expressed as

$${}^{n+1}\bar{\sigma}_{xz}=\frac{1}{h_{n+1}}\int_{t_n}^{t_{n+1}}\sigma_{xz}dz \tag{4.21}$$

where $t_{n+1}$ and $t_n$ are the upper and lower interfaces of the $(n+1)^{th}$ ply in the laminate and $h_{n+1}$ is the thickness of the ply.

# CHAPTER FIVE
# EXPERIMENTAL PROCEDURES

## 5.1 Introduction

This chapter deals with the experimental overview of the thesis. Experimental study will be presented in three subchapters. First subchapter is about the determination of the mechanical properties at room (approximately 20°C) and high temperatures (40°C, 60°C, 80°C and 100°C). Impact characterization at room and high temperatures is expressed in second subchapter. And, compression strengths after impact of the composite specimens, which are exposed to impact loads, are mentioned in the last sub chapter.

The fiber reinforced laminated composite materials used in the thesis are manufactured from unidirectional E-glass fabric having weight of 509 gr/$m^2$ and epoxy resin. The epoxy based on CY225 resin and HY225 hardener was used. Unidirectional glass/epoxy composite plate with eight plies is produced at Izoreel Firm by using hand lay-up technique. A hot lamination press was used for fabrication of composite plates. For curing process, laminated plates were retained at a constant pressure (15 MPa) and 120 °C during 2 hours. And then, composite plate is cooled to room temperature at the same pressure. The nominal thicknesses and fiber volume fraction of laminated composite plate are approximately obtained as 3 mm and 65%, respectively.

## 5.2 Determination of the Mechanical Properties

For determination of the mechanical properties of unidirectional glass/epoxy under static loading conditions, $[0]_8$ oriented composite laminated plates is produced. Nominal thickness of all tensile specimens is measured as 3 mm. To measuring the stiffness and strength of unidirectional plates under tension, compression and in-plane shear loading conditions, composite plates are trimmed according to the ASTM (American Society for Testing and Materials) standards. These basic properties of

the plates are necessary to use in input data for the 3DIMPACT programme. The mechanical properties of the composite lamina are measured in the Department of Mechanical Engineering of Atatürk University in Erzurum by using Shimadzu-AGIS Tensile Testing Machine of 100 kN load capacity at a ratio of 1 mm/min. This test machine has a thermostatically chamber is capacity from room temperature up to 350°C. To obtain the effect of the temperature on the mechanical properties of the unidirectional glass/epoxy laminated plates, room temperature, 40°C, 60°C, 80°C and 100°C are chosen. The temperature of the specimens is monitored by a thermocouple. It takes approximately 20 minutes to reach required temperature (for instance 100°C). All of the tests for the mechanical properties are done three times at each temperature.

The coordinate system used to describe the properties is shown in Figure 5.1. In the figure; 1, 2 and 3 are described the fibers direction, normal to the fibers direction in the laminate plane and out of plane direction, respectively. Direction 3 is also denoted through the laminate thickness. The mechanical properties of unidirectional laminated composite plates may be characterized as tension, compression, in-plane shear and interlaminar shear.

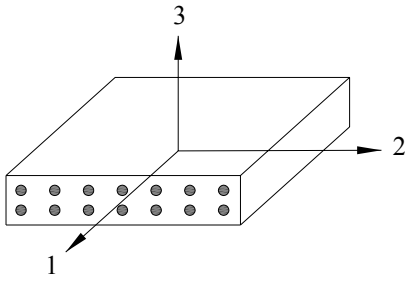


Figure 5.1 The coordinate system of the plates

### *5.2.1 Determination of the Tensile Properties*

According to the ASTM D3039–76 (ASTM D 3039–76, 1990) standard test method, longitudinal Young modulus $E_1$, poison's ratio $\nu_{12}$ and longitudinal tensile strengths $X_t$ are obtained by using longitudinal $[0]_8$ unidirectional specimens. The

dimensions of the specimens test have 12.7 mm wide and 229 mm long (Figure 5.2.a). Transverse Young modulus $E_2$ and transverse tensile strengths $Y_t$ are also obtained by using transverse $[0]_8$ unidirectional specimens. Test geometries of the specimens are 25.4 mm wide and 229 mm long (Figure 5.2.b). Tensile specimens are straight-sided coupons of constant cross section with adhesively bonded beveled glass/epoxy tabs.

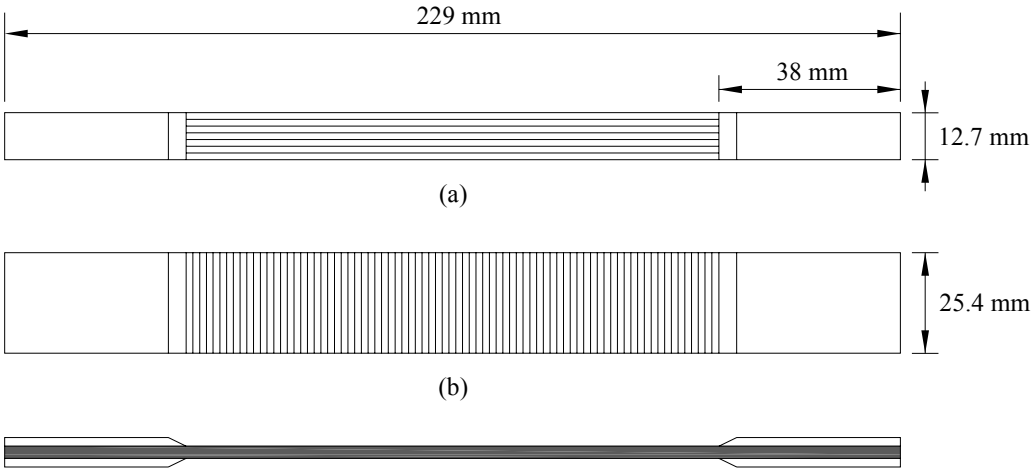


Figure 5.2 The dimensions of the specimens (a) for longitudinal ( $E_1$ , $\nu_{12}$ and $X_t$ ) and (b) for transverse ( $E_2$ and $Y_t$ ) properties (Daniel & Ishai, 1994).

To obtain the tensile properties, specimens are placed in the tensile testing machine. The specimens are loaded step by step up to failure loads in axial direction. The load-deflection curve is also drawn by the software which is work harmoniously with the test machine. While the tensile properties are measured at room and high temperatures, a biaxial video extensometer is used. Biaxial video extensometer does not loss its high measure capacity due to the high temperature in the thermostatically chamber. So, the values of $E_1$, $E_2$ and $\nu_{12}$ are determined. The tensile strength of the unidirectional composite plates ($X_t$ and $Y_t$) are determined by dividing the failure load to cross-section area of the longitudinal and transverse specimens, respectively (Table 4.1).

### *5.2.2 Determination of the Compressive Properties*

When fiber reinforced composites are loaded compressively in the fiber direction, the fiber may buckle or may failure due to locally large bending stresses. Because of this reason, compression testing is the most difficult test type. If the composite is compressively loaded in perpendicular to the fiber direction, matrix failure and fiber/matrix debonding will be occur (Carlsson & Pipes, 1997). Due to restrict mentioned above, compression test specimen must be specific long.

According to the ASTM D3410 (ASTM D 3410–87, 1990) standard test method specimens must be 140 mm long and specimens are trimmed 6.4 mm and 12.7 widths for longitudinal and transverse specimens, respectively. After bonded the tab at the side of both standard specimen, gage length of the specimen is remained as 12.7 mm (Figure 5.3). Then, compressive loads are recorded up to failure load for $[0]_8$ and $[90]_8$ orientated unidirectional glass/epoxy specimens by applying compression test. Longitudinal and transverse compressive strengths ($X_c$ and $Y_c$) are calculated by dividing the failure load to the cross-sectional area of the specimen a results are illustrated in (Table 4.1).

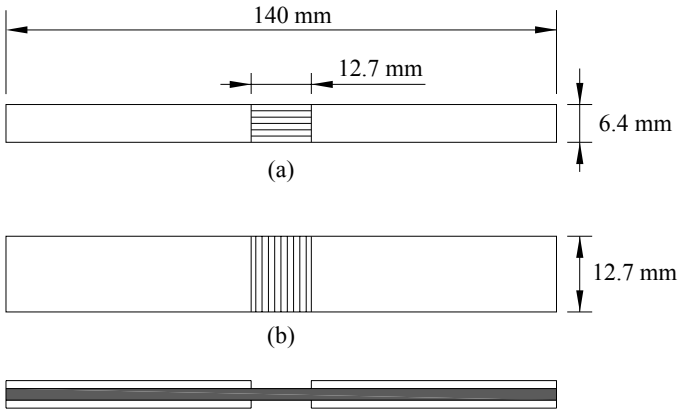


Figure 5.3 The dimensions of the compression test specimen (a) for longitudinal ($X_C$), and (b) for transverse ($Y_C$) strengths (Daniel & Ishai, 1994).

### *5.2.3 Determination of the Shear Properties*

To define the shear modulus, $G_{12}$, a specimen whose fiber direction is 45° from the loading direction (Figure 5.4.a). Firstly, $E_x$ modulus of the specimens is obtained by using biaxial video extensometer. After that, $G_{12}$ is calculated by using Eq. (5.1) (Jones, 1998).

$$G_{12} = \frac{1}{\left( \frac{4}{E_x} - \frac{1}{E_1} - \frac{1}{E_2} + \frac{2\nu_{12}}{E_1} \right)} \tag{5.1}$$

where, $E_1$ and $E_2$ denote the modulus of the fiber direction and the perpendicular of the fiber direction, respectively. $\nu_{12}$ is the poison ratio in plane of 1-2.

The $[\pm 45]_{2S}$ coupon test, which is accepted ASTM standard practice D3518, is used for determining the shear strength, $S_{12}$. Specimens are trimmed as the same geometry for the ASTM D3039 (Figure 5.4.b). End-tabs may not be required due to the balance orientation of the test specimen. And then, maximum loads are recorded up to failure load and shear strength are taken half of the failure stress which is calculated by dividing the failure load to the cross-sectional area of the specimen (as equation 5.2) (Carlsson & Pipes, 1997; Jones, 1998). Results for room and high temperatures are given in (Table 4.1).

$$S_{12} = \frac{\sigma_f}{2} \qquad \text{and} \qquad \sigma_f = \frac{P_{\max}}{A} \tag{5.2}$$

where, $\sigma_f$ and $P_{\max}$ denote the failure stress and the maximum load of the specimen, respectively.

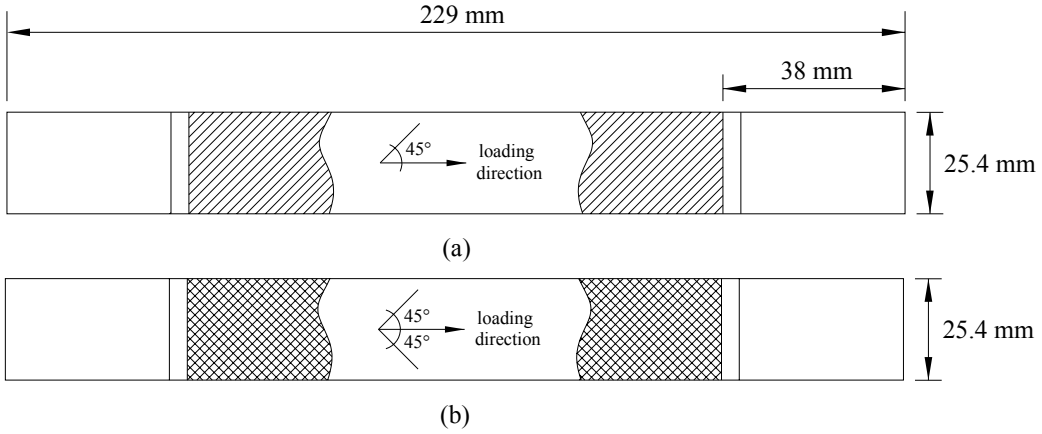


Figure 5.4 The shear specimen dimensions (a) for the shear modulus, $G_{12}$ and (b) for the shear strength, $S_{12}$ (Daniel & Ishai, 1994).

The other shear properties of the unidirectional laminated composites is interlaminar shear strength, $S_i$. This property is very important parameter to express the delamination damage of the laminated plates. To determine the interlaminar shear strength, double-notch shear test as described in ASTM specification D 3846–79 is used (ASTM D 3846–79, 1990). The dimension of the specimen for this test must be 79.5 mm long and 12.7 mm wide as shown in Figure 5.5. Two parallel notches or grooves are machined, one on each face of the specimen, 6.4 mm apart and of depth equal to half the specimen thickness. When this specimen is loaded in uniaxial tension, shear failure results along the mid plane of the specimen between the notches (Daniel & Ishai, 1994). The interlaminar shear strength is then calculated as Eq. (5.3). The variation of the interlaminar shear strength of the unidirectional glass/epoxy composite plates for room and high temperatures is given in (Table 4.1).

$$S_i = \frac{p}{wl} \tag{5.3}$$

where $P$, $l$ and $w$ denote the failure load, the distance between notches, and the width of the specimen, respectively.

In an impact analysis the mass of the structure has to be taken into consideration. Therefore, a density test is conducted in order to place the correct mass value in the

theoretical calculation. The density ρ of the composite laminates is derived by weighting the composite plates, measuring its volume and calculating their ratio.

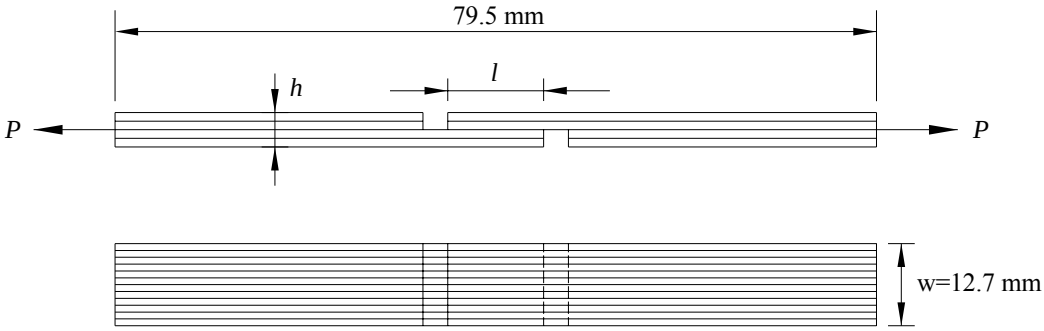


Figure 5.5 Double-notch specimen for determination of interlaminar shear strength (Daniel & Ishai, 1994).

Table 4.1 Mechanical properties of unidirectional glass/epoxy composites.

| | Temperature (°C) | | | | |
|---|---|---|---|---|---|
| Property | 20 | 40 | 60 | 80 | 100 |
| fiber volume fraction, $V_f$ [%] | 65.00 | 65.00 | 65.00 | 65.00 | 65.00 |
| density, $\rho$ $[gr/cm^3]$ | 1.83 | 1.83 | 1.83 | 1.83 | 1.83 |
| longitudinal modulus, $E_1$ $[GPa]$ | 40.51 | 39.82 | 39.72 | 28.27 | 19.45 |
| transverse modulus, $E_2$ $[GPa]$ | 13.96 | 11.54 | 11.09 | 6.11 | 5.70 |
| in-plane shear modulus, $G_{12}$ $[GPa]$ | 3.10 | 2.63 | 2.56 | 2.05 | 0.81 |
| poison's ratio, $\nu_{12}$ | 0.22 | 0.22 | 0.21 | 0.21 | 0.20 |
| long. tensile strength, $X_t$ $[MPa]$ | 783.30 | 726.20 | 706.40 | 658.50 | 509.20 |
| trans. tensile strength, $Y_t$ $[MPa]$ | 64.00 | 65.20 | 65.50 | 67.40 | 68.60 |
| long. comp. strength, $X_c$ $[MPa]$ | 298.00 | 279.00 | 272.50 | 256.50 | 206.30 |
| trans. comp. strength, $Y_c$ $[MPa]$ | 124.00 | 115.00 | 112.00 | 104.50 | 80.80 |
| interlaminar shear strength, $S_i$ $[MPa]$ | 38.00 | 34.50 | 33.00 | 22.50 | 15.90 |
| in-plane shear strength, $S_{12}$ $[MPa]$ | 69.00 | 57.20 | 51.80 | 44.70 | 37.80 |

The mechanical properties of the unidirectional glass/epoxy composites for room (app. 20°C) and for high temperatures (40°C, 60°C, 80°C and 100°C) are shown as bars in Figure 5.6–5.9. It is clear from the figures that all of the mechanical properties except tensile strength in transverse direction losses their rigidity and their strength by increasing temperature.

The elastic constants of a unidirectional composite are dependent on the elastic properties of the constituent fiber and matrix phases. As the temperature of the composite increases, the polymer matrix becomes more compliant, therefore the composite elastic stiffness constants such as shear modulus and transverse modulus (Odegard & Kumosa, 2000). The longitudinal, transverse and shear modulus of the unidirectional glass/epoxy as functions of temperature are shown in Fig. 5.6. Fig. 5.6 clearly shows that longitudinal modulus is nearly same up to 60°C. After this temperature it is suddenly decreased. The longitudinal modulus has dropped by approximately 52% from 20°C to 100°C. And also transverse modulus has dropped by approximately 59% from 20°C to 100°C. The change in the shear modulus due to temperature increase is approximately 74% 20°C to 100°C. From the results; the properties of glass fiber and epoxy matrix are reduced less than the fiber-matrix debonding properties by the change in temperature.. And also, the shear modulus of unidirectional glass/epoxy is fairly influenced by the temperature. The demonstration of the variation of $\nu_{12}$ for unidirectional glass/epoxy is shown in Fig. 5.7. From this figure, the temperature is not significantly effect on $\nu_{12}$.

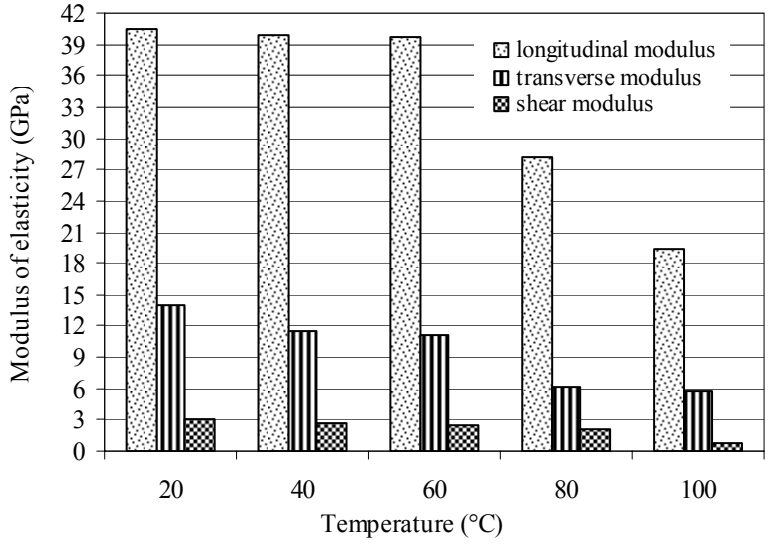


Figure 5.6 Variation of the longitudinal, transverse and shear modulus according to temperature for unidirectional glass/epoxy

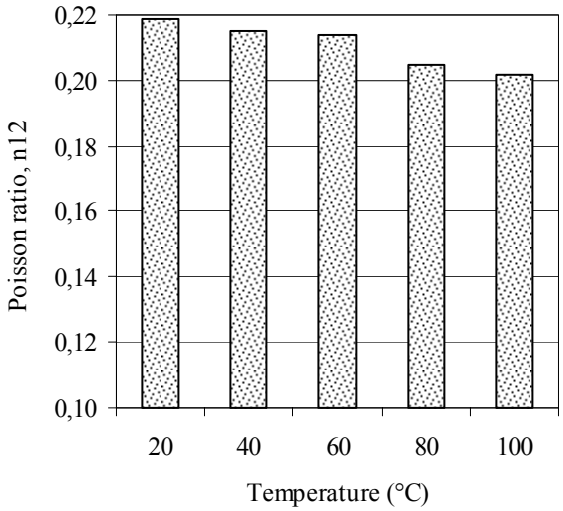


Figure 5.7 Variation of the Poisson's ratio according to temperature for unidirectional glass/epoxy

Composites tend to exhibit lower shear and transverse tensile strength values as the temperature is increased. Polymer matrix may losses its strength due to result in more ductile at higher temperatures (Odegard & Kumosa, 2000). Failure initiation depends also on material imperfections, such as voids, resin rich regions and fiber misalignment. Variation of the tensile and compressive strength with temperature for unidirectional glass/epoxy composite is shown in Fig. 5.8. It is clear that the compressive and tensile strength in fiber direction and in transverse fiber direction decrease by increasing the temperature from 20°C to 100°C.

The compressive failure of unidirectional glass/epoxy laminates occurs due to fibre micro buckling regardless of temperature. However, matrix will be more ductile with the increasing in temperature. Therefore, compressive strength of glass/epoxy composite will be decreased with the temperature. In general, the tensile strength of a composite depends more on its fiber reinforcement, but compressive strength relies more upon its matrix material (Soutis & Turkmen, 1993)**.** The longitudinal strength of unidirectional glass/epoxy composite is weaker in compression than in tension due to fibre micro buckling. For example, the longitudinal tensile strength is 66% more than the longitudinal compressive strength at 20°C. However, the transverse strength is stronger in compression than in tension. Because transverse failure results matrix

failure and brittle material as epoxy matrix have higher strength in compression than in tension. For instance, the transverse tensile strength is 94% less than the transverse compressive strength at 20°C (Fig.5.8).

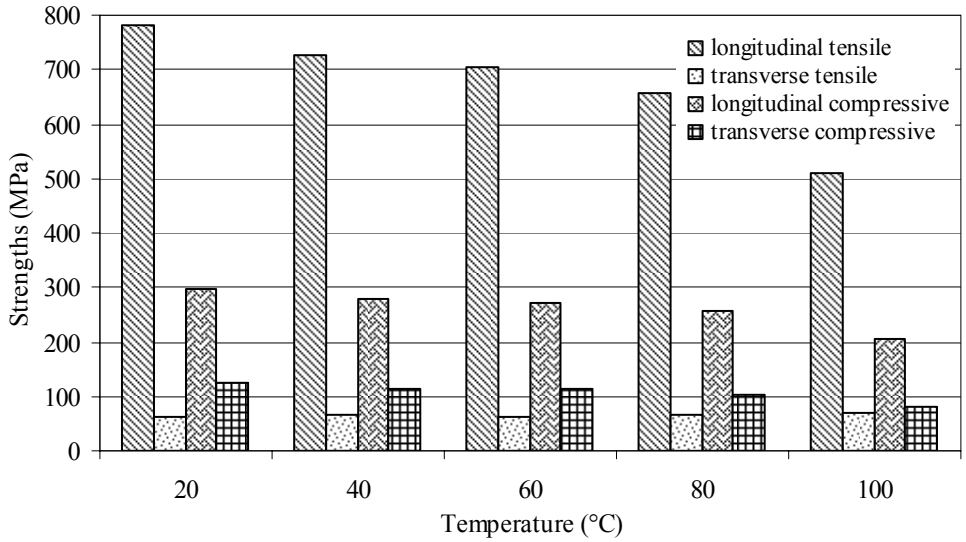


Figure 5.8 Variation of the tensile and compressive strength according to temperature for unidirectional glass/epoxy

The variation temperature versus shear strengths of the unidirectional glass/epoxy is shown in Figure 5.9. Both of the shear strength decrease by increasing the temperature. Matrix is the dominant phase when obtaining the interlaminar shear strength. Therefore, interlaminar shear strength is lower than the in-plane shear strength of the composite. The in-plane shear strength decreased from 69 MPa at room temperature (20°C) to 37.8 MPa at 100°C (approx. 45% reduction). And, also interlaminar shear strength decreased from 38 MPa at room temperature to 15.9 MPa at 100°C (approx. 32% reduction).

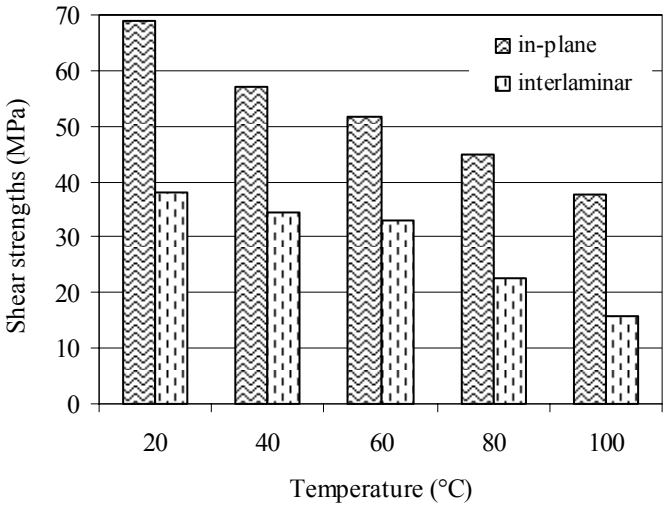


Figure 5.9 Variation of the in-plane and interlaminar shear strength according to temperature for unidirectional glass/epoxy

## 5.3 Impact Behavior of Glass/Epoxy

### *5.3.1 Impact Test Machine*

In this thesis, a Fractovis Plus impact test machine as shown in Figure 5.10 is used to investigate the impact behavior of the composite laminated plates. Test instrument consists of three main parts as following:

***Upper part of the instrument:*** *Automatic impactor recovery/releasing system* is used to moves the impactor at the correct height and to release it for impact test on the specimen. *Additional energy system* is used to increase the speed of the impactor up to 24 m/s (with falling mass 2 kg) or 7 m/s (with falling mass 70 kg). The test instrument has capable the 1800 J maximum potential energy with the additional mass. The *impactor holder* joints mechanically the impactor to the recovery/releasing system. Moreover it can contains one or more weights used to increase the impact mass. Up to 70 kg mass can be put into the impactor holder.

The *impactor* is used to strike the specimen surface when the impact test is carried out. It provide full details of the impact event from initial contact to final breaking of the specimen by recording the force/time curve of the entire impact event through a

data acquisition system connected to a PC. *Data acquisition system*, which the instrumented impactor is connected, can be take 16000 data during the impact event.

An *anti-rebounding system* is included in the test instrument to stops the impactor after impact to avoid the repeated impact on the specimen. The residual *energy absorbers* are used to damp the impactor residual energy after impact.

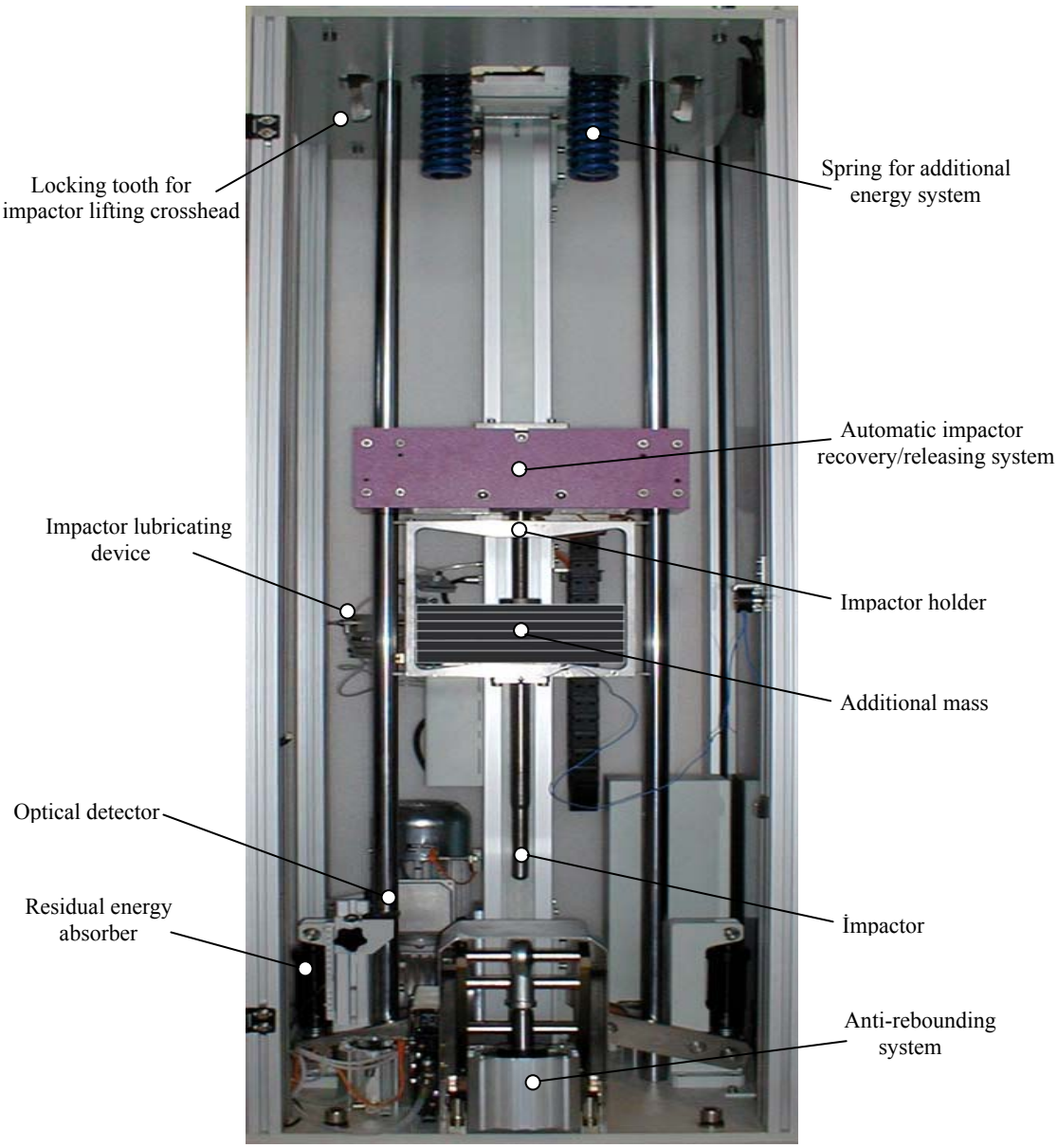


Figure 5.10 Photograph of upper part of the Fractovis Plus impact test machine

An *impactor lubricating device* used to lubricate the head of the impactor before the test. It consists of a pneumatic cylinder equipped with a sprinkler (a device that sprays oil) on its end and a small oil tank. When the test cycle starts the cylinder automatically moves forward until the sprinkler is positioned under the impactor head, at this point the sprinkler squirts the lubricating oil on the impactor head and the cylinder returns to the rest position.

*The impact and rebound velocity optical detector* is used to measure the velocity of the impactor just *before* the impact and to activate the impactor anti-rebound system in case of impactor rebound. It consists of a photocell fixed with a bracket to the structure and a flag fixed to the impactor holder. When the impactor holder is released for test, the flag pass through the photocell interrupting the light-ray two times consecutively.

The *additional optical detector* measures the velocity of the impactor just *after* the impact and it is used to calculate the energy lost for the impact. It consists of a second photocell fixed below the first one through which pass the flag.

***Lower part of the instrument:*** The Fractovis Plus impact test machine is equipped with an *environmental chamber* for specimens conditioning at temperatures range from -100°C to 150°C. The environmental chamber is cooled through the expansion of liquid nitrogen taken from an external tank. The nitrogen flows inside the chamber through pipes endowed with capillary holes. The chamber is heated by means of heating resistances. The uniformity of the temperature is assured through an electric fan which circulates air and nitrogen inside the chamber. The temperature set is automatically controlled by a temperature regulator. This device receives the signal from a temperature probe located inside the chamber and, depending on whether the requirement is for cold or hot, it enables a solenoid valve to open the nitrogen inlet or the electric heating resistance. Environmental chamber is equipped with *automatic clamping device*. It clamps the specimen on the support before the impact.

#### *5.3.1.1 Data Calculation by Software*

The software program that called VisualIMPACT is used to calculate the absorbed energy, velocity and deflection. The impact force value at each time step, $F(t)$, are recorded by data acquisition system (DAS). The specimen deflection is calculated in main points. Deflection derives from a double integration of force curve as

$$\delta_i = \int_i \int \frac{F(t) - gM_{total}}{M_{total}} dt^2 \tag{5.4}$$

where $\delta_i$ is deflection of the specimen up to point *i*, $F(t)$ is force acquired by data acquisition system, $g$ is gravity acceleration and $M_{total}$ is total impact mass.

The absorbed energy up to point *i* is calculated as the area described under force-deflection $F(\delta)$ curve,

$$E_i = \int_i F(\delta) d\delta \tag{5.5}$$

The velocity up to point *i*, derives from a single integration of force-time curve $F(t)$,

$$v_i = \int_i \frac{F(t) - gM_{total}}{M_{total}} dt \tag{5.6}$$

### *5.3.2 Preparation of the Impact Test Specimens*

The fiber reinforced laminated composite materials used in the thesis are manufactured from unidirectional E-glass fabric having weight of 509 gr/m$^2$ and epoxy resin at Izoreel Firm. For matrix materials, epoxy CY225 and hardener HY225 are mixed. A hand lay-up method is used to construct the composite plate. This

method consisted of laying down the fabric layer by layer and pouring the epoxy over the fabric and then consecutively spreading the epoxy over the surface with a squeegee. Then another layer of fabric is placed on top of the previous layer and the process is repeated until the desired number of layers is obtained.

The curing is carried out by using a hot lamination press at 120 °C for 2 hours under a pressure of 15 MPa. Then, it is cooled to room temperature at the same pressure. To investigate the stacking sequences effects on the impact behavior of the glass/epoxy composites, two different stacking sequences are chosen as $[0°/90°/0°/90°]_S$ and $[[0°/90°/+45°/-45°]_S$. After manufacturing process, the impact specimens are trimmed from the laminated plates by using a diamond saw as dimensions 100 x 100 $mm^2$. The nominal thicknesses of the each specimen are measured as 3 mm.

### *5.3.3 Impact Tests*

The impact tests are performed using Fractovis Plus impact test machine in the Composite Research Laboratory of Dokuz Eylül University. The impact energy is gradually increased from 5 J up to 70 J for examination of the impact energy level. To investigate the temperature effects on the impact behavior of the glass/epoxy laminated composites, each of the impact tests are done at 20°C, 40°C, 60°C, 80°C and 100°C. And, also for investigate the effects of the stacking sequences on the impact characteristic of the laminated composite plate, two different orientation are selected as $[0°/90°/0°/90°]_S$ and $[0°/90°/45°/-45°]_S$.

The Fractovis Plus impact test system is a test system suitable for a wide variety of applications requiring low to high impact energies under various temperatures. The impactor with a hemispherical nose of 12.7 mm in diameter is used. The testing machine has a force transducer with capacity of 22.24 kN. The total mass of the impactor used is 5.02 kg (included impactor mass and crosshead mass). The impact specimens with dimensions of 100 mm by 100 mm are clamped by using a

pneumatic fixture. Four specimens are tested at each of the impact energy and temperature condition.

The developed VisualIMPACT software for Fractovis Plus impact test machine gives us the time versus load, velocity, deflection and energy histories. Three special tests results including *rebounding*, *penetration*, and *perforation* are given in Figure 5.11.

The contact force-time curve for the three cases is shown in Figure 5.11.a. It is seen from this figure that contact force increases by increasing the impact energy. At the rebounding case, the contact force reaches the zero and the curve look like a mountain shape. When the impact energy is high enough, perforation will be occurring. At this time, contact force is expected to be zero. But it does not ever zero due to the friction at the interface of the hemispherical impactor and specimen.

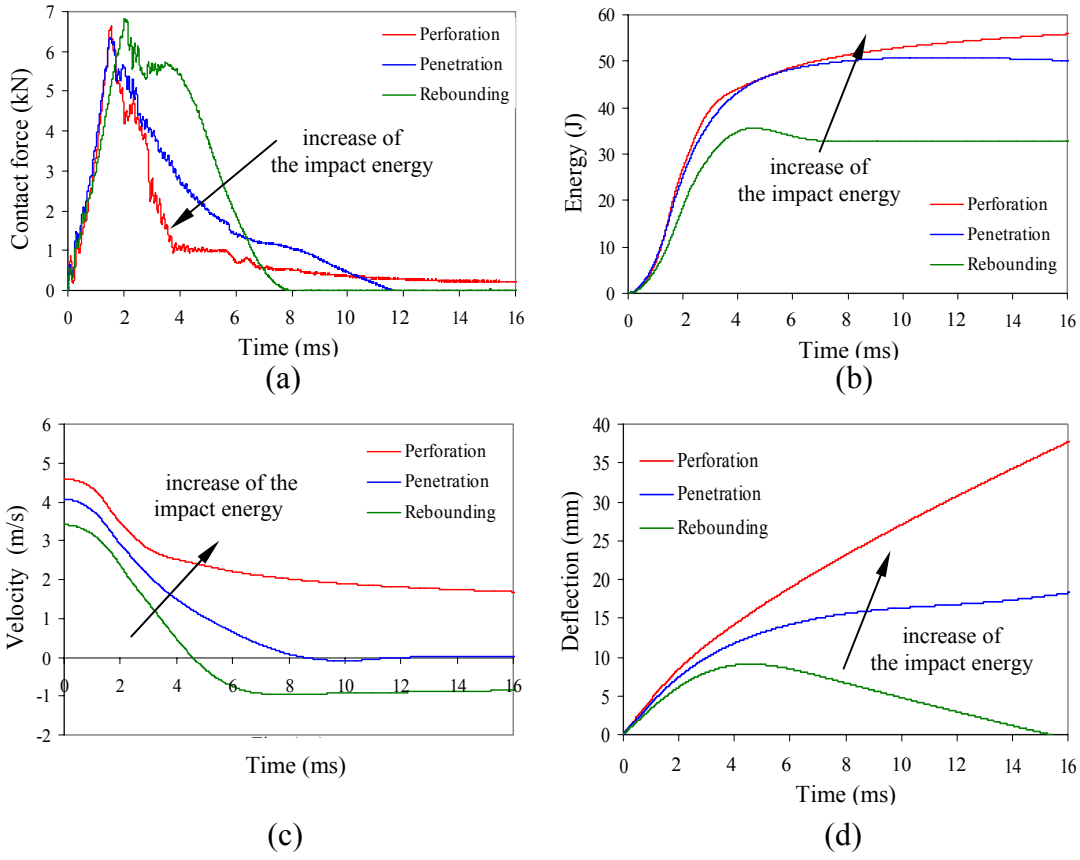


Figure 5.11 Time versus (a) contact force, (b) energy, (c) velocity and (d) deflection

Variation of the energy, which is calculated from force-deflection curves, is shown in Figure 5.11.b. At the rebounding case, impact energy is higher than the absorbed energy. So specimen can not absorb the impact energy that the impactor has. For the penetration case, specimen absorbs all of the impact energy. However, absorbed energy lowers than the impact energy that the impactor has.

The velocity-time history of impact event is given in Figure 5.11.c. The velocity of the impactor decreases after first contact event. For the rebounding case the impactor velocity has negative value indicating the reverse impact direction after impact event. At the maximum deflection of the midpoint of the specimen the velocity reaches zero for the penetration case. However, for the perforation case, the impactor moves after impact event due to the all of the impact energy not absorbed by specimen. The deflection-time curve for the perforation, penetration and rebounding cases are shown in Figure 5.11.d. When the contact force reaches the maximum value, the maximum deflection of the midpoint of the specimen will be occurring. The maximum deflection increases by increasing the impact energy. For the perforation case, after impact event have done the impactor will be continue to move due to not any object try to stop.

#### *5.3.3.1 Energy Level Effects*

In order to investigate the energy level effects on the impact behavior of the composite plates, fourteen impact energies from 5 J to 70 J are selected. For better consideration, only seven energies levels (10 J, 20 J, 30 J, 40 J, 50 J, 60 J and 70 J) are given in the curve of the contact force versus time and deflection. Figure 5.12.a-b is given for an example of the contact force-time and contact force-deflection curves, respectively.

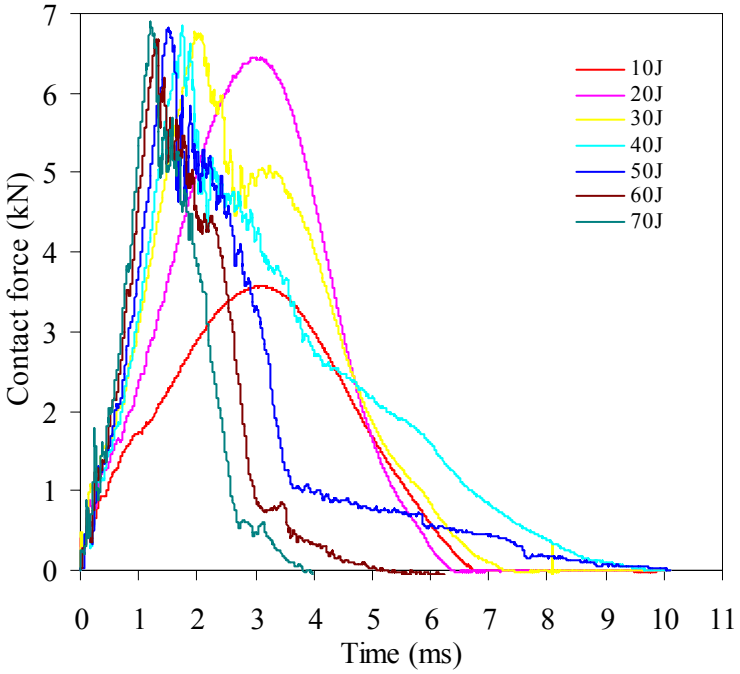


(a)

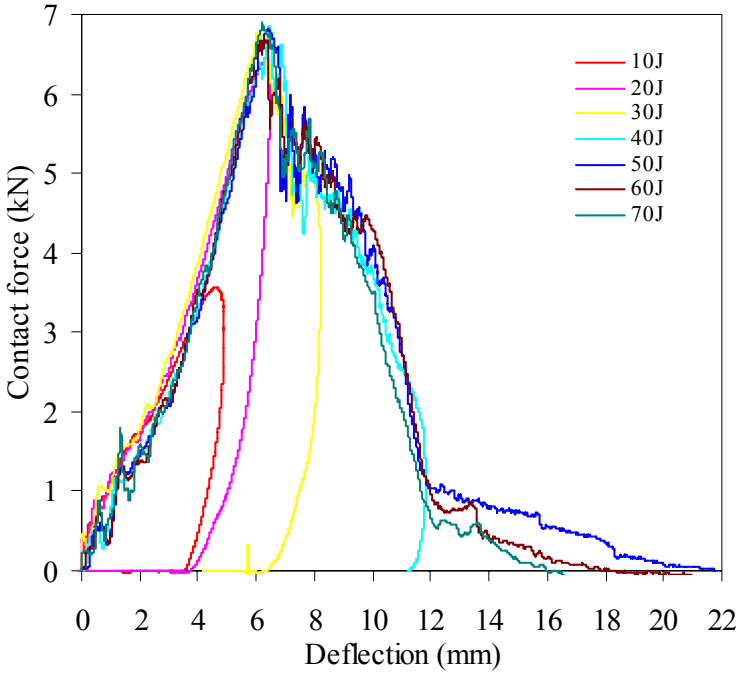


(b)

Figure 5.12 (a) The contact force-time and (b) the contact force-deflection history for $[0°/90°/0°/90°]_S$ at 20°C.

From the result of the Figure 5.12.a-b, it can be seen that the contact force increases by increasing the impact energy level. This is an expected result of the equation (5.5). Nevertheless, impact time decreases by increasing the impact energy level. 30J energy level is the initial of the rebounding-penetration transition energy.

The contact forces do not change significantly by increasing energy level from 30 J to 50 J. But the peak time, which is occurred at the peak contact force, changes by increasing energy level. Also, by increasing energy level, the deflection of the specimen increases.

The absorbed energy can be calculated from the area under the contact force-deflection curve. The absorbed energy represents the difference between the total impact energy transferred from the impactor to the specimen and the amount of energy returned to the impactor from the specimen due to elastic restitution. In the penetration and perforation cases, there is no elastic energy returning to the impactor.

The loading portion of the curve for all energy levels is the same. But the unloading portion of all differs from each other due to different damage mechanisms. So, deflection value and the impact time of the plates which are subjected to different energy levels are different (Figure 5.12.a-b).

The deflection of the plate can be expressing the rebounding, penetration and perforation thresholds. In the rebounding case, unloading portion of the contact force-time curve must be return, after peak contact force, in the parallel to the loading portion of the curve (10 J, 20 J and 30 J). In the penetration (40 J) and perforation (50 J, 60 J and 70 J) cases, unloading portion of the curve do not return parallel to the loading portion of the curve.

#### *5.3.3.2 Temperature Effects*

In order to investigate the temperature effects on the impact characterization of the laminated composite plates, impact tests are done at room temperature (approx.

20°C) and at four high temperatures (40°C, 60°C, 80°C and 100°C ). Before all impact tests, thermostatic chamber is heated for require temperature. Then, chamber is kept at require temperature about 20 min to stabilize the specimen.

To understand the thermal impact behavior in the rebounding, penetration and perforation thresholds, for $[0°/90°/0°/90°]_S$ and $[0°/90°/45°/-45°]_S$ fiber orientation, Figure 5.13-15 are given. In these figures; 20 J, 40 J and 60 J energies are selected for representing the rebounding, penetration and perforation cases, respectively.

The contact force-deflection history of glass/epoxy composite plates for $[0°/90°/0°/90°]_S$ and $[0°/90°/45°/-45°]_S$ orientation in the case of rebounding (Figure 5.13.a-d), penetration (Figure 5.13.b-e), and perforation (Figure 5.13.c-f) are illustrated. It is clear from these figures that the contact force increases and permanent deflection decreases by increasing the temperature due to composite specimens which behave more brittle. The loading portion of the curve is nearly same. But unloading case differs from each other for all temperature due to different damage characterization.

The contact force in the rebounding case for $[0°/90°/0°/90°]_S$ orientation is smaller than the orientation of $[0°/90°/45°/-45°]_S$. The slope of the curve decreases from rebounding case to perforation case for both stacking sequences (Figure 5.13). As a result of this behavior, the deflection value corresponding to maximum contact force increases from rebounding case to perforation case. At 40 J energy level; specimen is penetrated by impactor at all temperatures for $[0°/90°/0°/90°]_S$ orientation while it is perforated at 40°C and 80°C for $[0°/90°/45°/-45°]_S$ orientation.

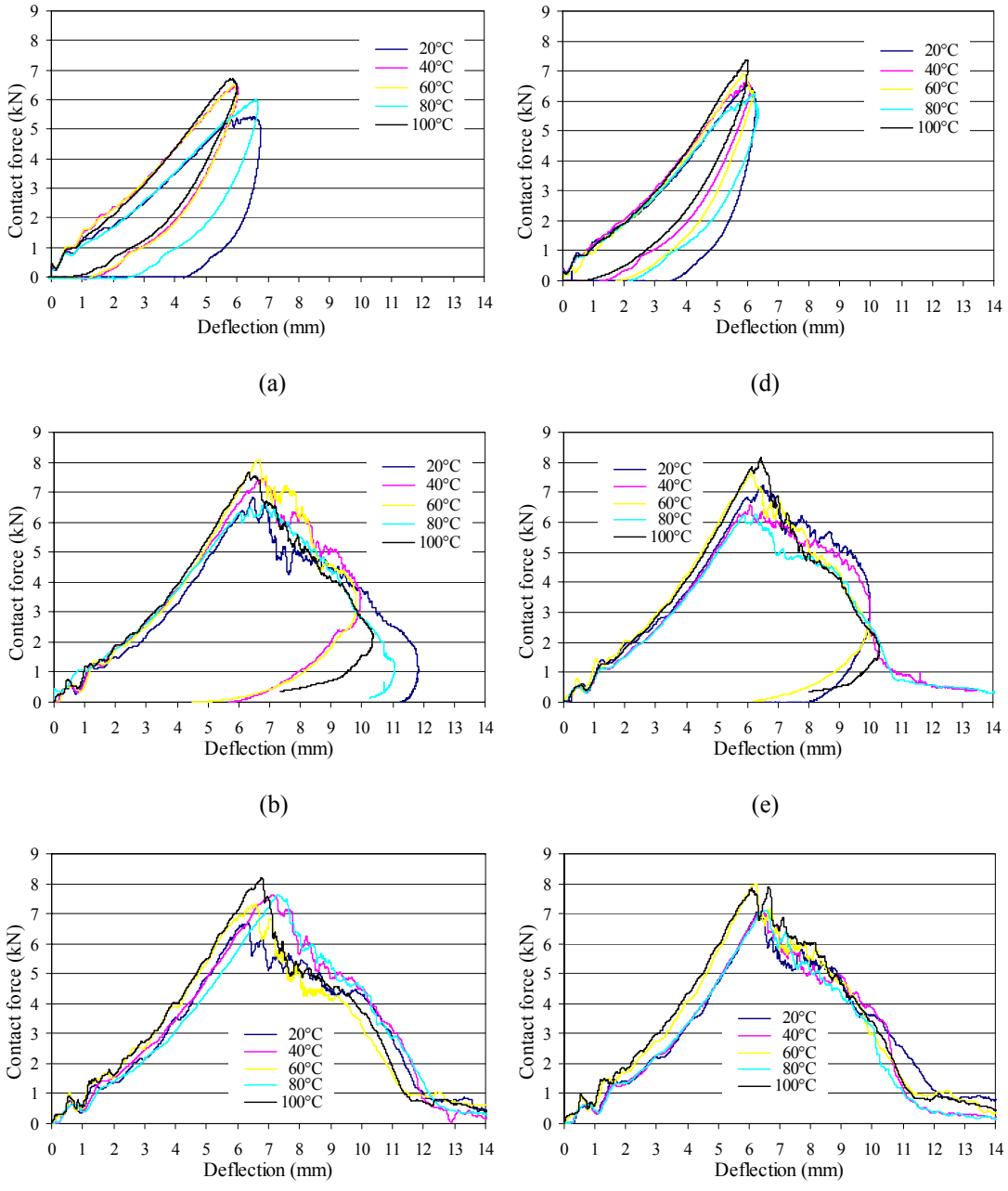


Figure 5.13 The contact force-deflection history for (a) rebounding (20 J), (b) penetration (40 J) and (c) perforation (60 J) cases for $[0°/90°/0°/90°]_S$, and (d) rebounding (20 J), (e) penetration (40 J) and (f) perforation (60 J) cases for $[0°/90°/45°/-45°]_S$.

Figure 5.14 represents the contact force-time history for $[0°/90°/0°/90°]_S$ and $[0°/90°/45°/-45°]_S$ orientation in the case of rebounding penetration, and perforation case. It can be said from these figures that contact time increases by increasing of

temperature for both configurations. The maximum and minimum contact times occur in the case of penetration (40 J) and perforation (60 J), respectively.

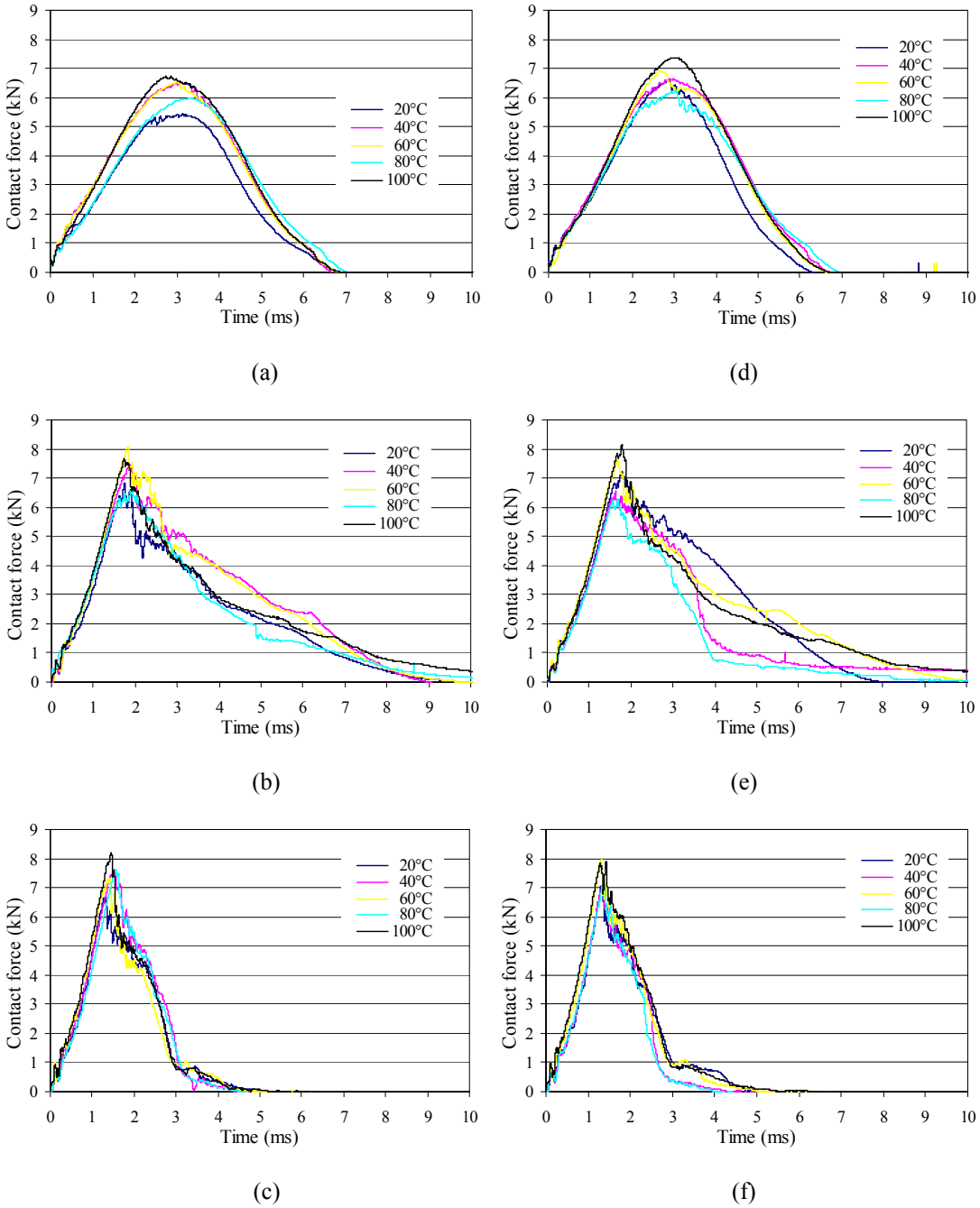


Figure 5.14 The contact force-time history for (a) rebounding (20 J), (b) penetration (40 J) and (c) perforation (60 J) cases for $[0°/90°/0°/90°]_S$, and (d) rebounding (20 J), (e) penetration (40 J) and (f) perforation (60 J) cases for $[0°/90°/45°/-45°]_S$.

The deflection-time history for $[0°/90°/0°/90°]_S$ and $[0°/90°/45°/-45°]_S$ orientation in the cases of rebounding, penetration, and perforation is shown in Figure 5.15.

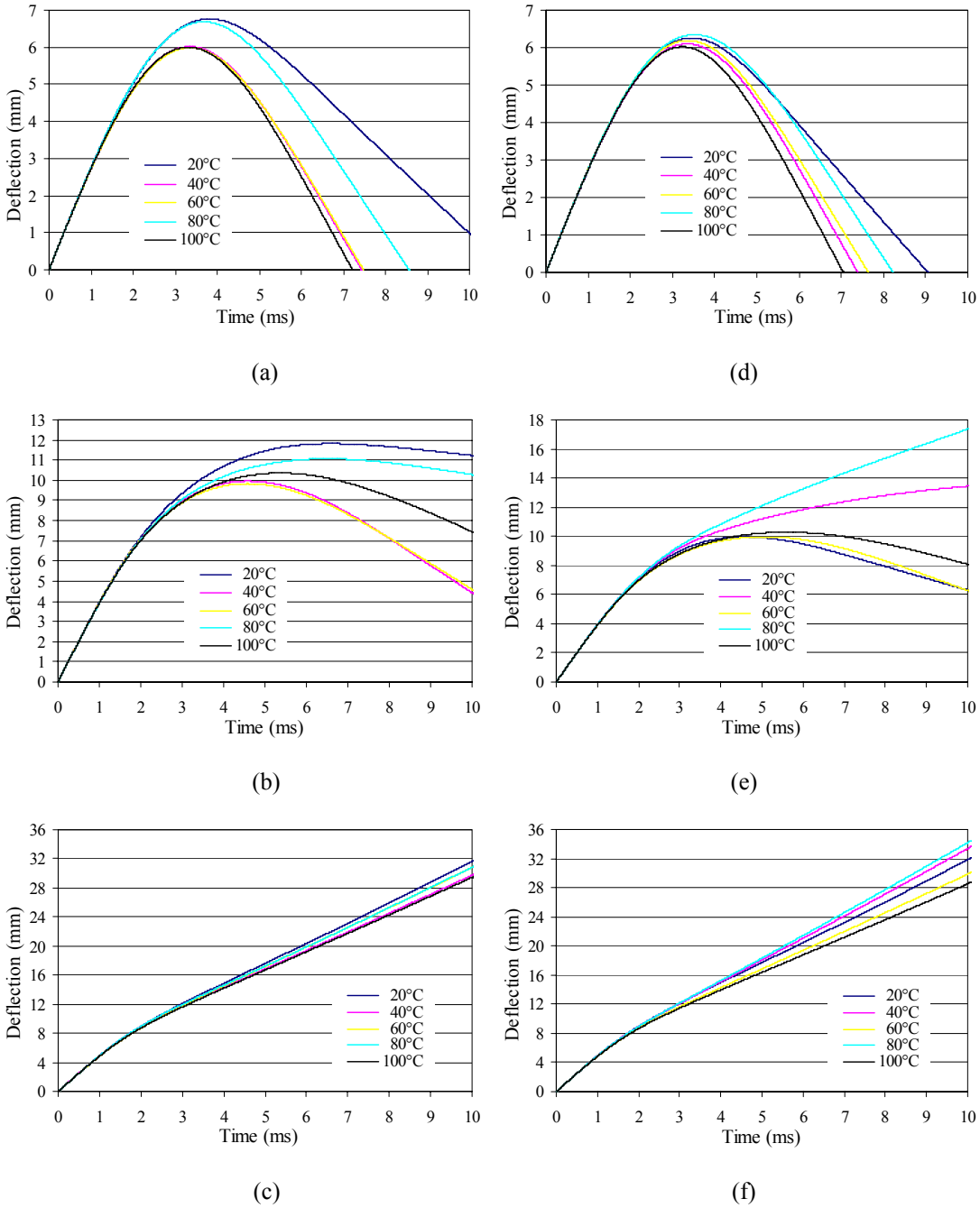


Figure 5.15 The deflection-time history for (a) rebounding (20 J), (b) penetration (40 J) and (c) perforation (60 J) cases for $[0°/90°/0°/90°]_S$, and (d) rebounding (20 J), (e) penetration (40 J) and (f) perforation (60 J) cases for $[0°/90°/45°/-45°]_S$.

It is clear from these figures that the deflection decreases by increasing temperature for both configurations.

In the rebounding case (Figure 5.15.a-5.15.d), permanent deflection is nearly zero for all temperature and for both configuration except for $[0°/90°/0°/90°]_S$ at 20°C. The permanent deflection at this temperature occurs approximately 1 mm (Figure 5.15.a).

The deflection versus time curve helps us to obtain the perforation threshold of the composite plates. When the deflection changing with time is linear, the perforation threshold starts. The perforation threshold at 60 J energy level for $[0°/90°/0°/90°]_S$ and $[0°/90°/45°/-45°]_S$ occurs at 8 mm deflection and 2 ms at all temperatures (Figure 5.15.c-f). In addition to this, perforation threshold exists at 10 mm deflection and 3,5 ms for $[0°/90°/45°/-45°]_S$ orientation at 80°C and at 40°C and 40 J, while the penetration occurs for $[0°/90°/0°/90°]_S$ orientation in the same conditions (Figure 5.15.b-e).

Figure 5.16 and Figure 5.17 are given for $[0°/90°/0°/90°]_S$ and $[0°/90°/45°/-45°]_S$ orientation to show the changing of penetration level by the temperature at 40 J and 45 J, respectively. It is clear from Figure 5.16 that the perforation do not occur for $[0°/90°/0°/90°]_S$ orientation at 40 J while it occurs for $[0°/90°/45°/-45°]_S$ orientation at the same energy and at 40°C and 80°C temperatures.

In Figure 5.17, the perforation occurs for all temperatures of $[0°/90°/45°/-45°]_S$ orientation at 45 J impact energy while the penetration exists at 40°C temperature for $[0°/90°/0°/90°]_S$ orientation as different from $[0°/90°/45°/-45°]_S$ orientation.

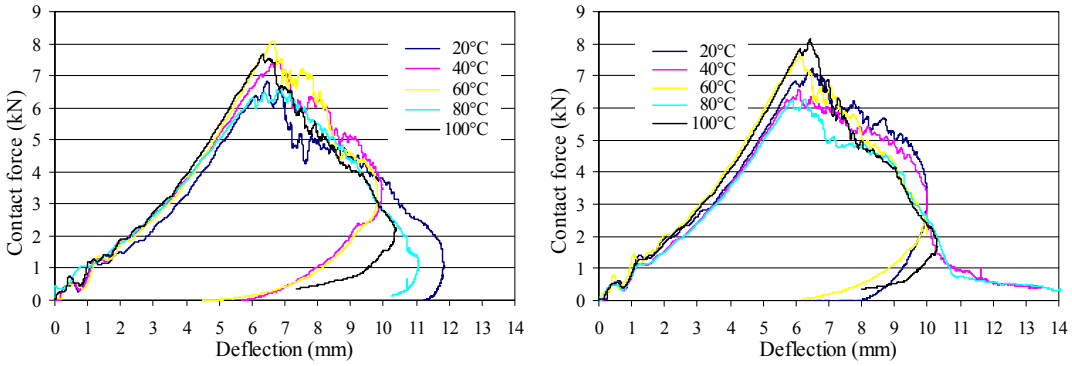


(a) (b)

Figure 5.16 The contact force versus deflection diagrams at 40 J (a) for $[0°/90°/0°/90°]_S$ orientation and (b) for $[0°/90°/45°/-45°]_S$ orientation.

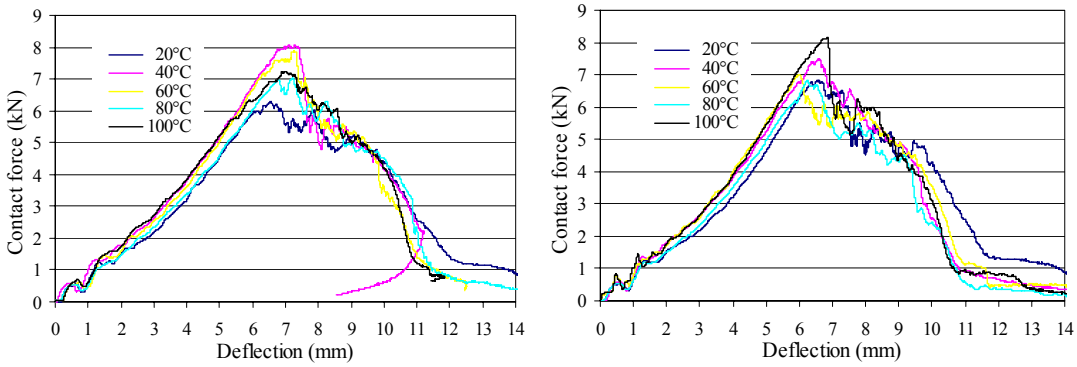


(a) (b)

Figure 5.17 The contact force versus deflection diagrams at 45 J (a) for $[0°/90°/0°/90°]_S$ orientation and (b) for $[0°/90°/45°/-45°]_S$ orientation.

To simplify understanding the temperature effects on the glass/epoxy laminated composite plate; only peak value of the contact force, contact time, deflection of the specimen, and permanent deflection are given in Figure 5.18-25 according to the impact energy at different temperatures. Figure 5.18 and Figure 5.19 show the maximum contact force-impact energy diagram for $[0°/90°/0°/90°]_S$ and $[0°/90°/45°/-45°]_S$ stacking sequences, respectively. The maximum contact force increases rapidly from 5 J to approximately 20 J for both orientations and for all temperature conditions except for $[0°/90°/0°/90°]_S$ at 20°C. After this energy level, the maximum contact force increases with small increments by increasing energy, because matrix and delamination failures exist up to 20 J. In addition these failures, fiber breakage occurs from 20 J to 50 J. So the contact force shows alternating

behavior. The minimum value of the maximum contact force occurs at 20°C for both plate configurations.

The value of maximum contact force increases by increasing the temperature. This is a result of the composite laminated plate that behaves more brittle by increasing temperature. The contact force for $[0°/90°/45°/-45°]_S$ orientation is generally greater than for $[0°/90°/0°/90°]_S$ orientation because of the higher bending stiffness. The contact force for $[0°/90°/0°/90°]_S$ orientation increases linearly up to 25 J at 20°C temperature while it changes linearly up to 20 J for $[0°/90°/45°/-45°]_S$ orientation. This situation can be explained by bending stiffness.

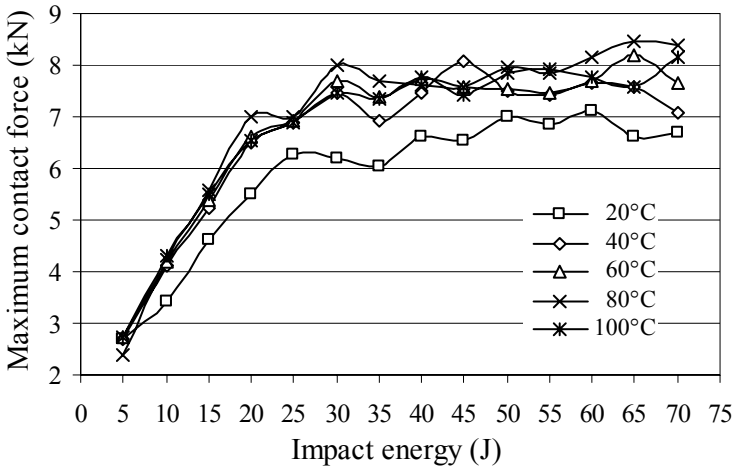


Figure 5.18 The maximum contact force-impact energy diagram depending on the temperature for $[0°/90°/0°/90°]_S$.

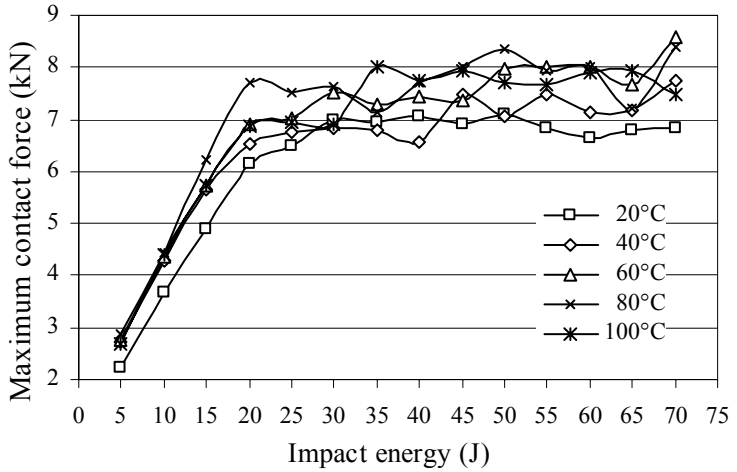


Figure 5.19 The maximum contact force-impact energy diagram depending on the temperature for $[0°/90°/45°/-45°]_S$.

Figure 5.20 and Figure 5.21 represent the contact time-impact energy diagram depending on the temperature for $[0°/90°/0°/90°]_S$ and $[0°/90°/45°/-45°]_S$, respectively. The contact time very few changes in the range of 5 J-20 J for all temperature cases. This energy range represents the rebounding energy level. The effective damage mode is delamination in the rebounding energy level. Therefore, it can be said that the delamination decreases the contact time. In the energy range from 20 J to approximately 45 J, contact time is gradually increased by increasing energy level. This range of energy may be representing the rebounding-perforation range. This range generally depends on the thickness of the composite plate. For the thick laminate this range will be more extensive than the thin laminate (Abrate, 1998).

The maximum contact time is obtained for 45 J at all temperature. This peak contact time value corresponds to the perforation threshold. After this level contact time rapidly decreases by impact energy and so on. The characterization of the contact time-impact energy curve for $[0°/90°/45°/-45°]_S$ orientation is as same as $[0°/90°/0°/90°]_S$ orientation. However, the perforation threshold of $[0°/90°/45°/-45°]_S$ exists at 40 J for 60°C, 80°C and 100°C.

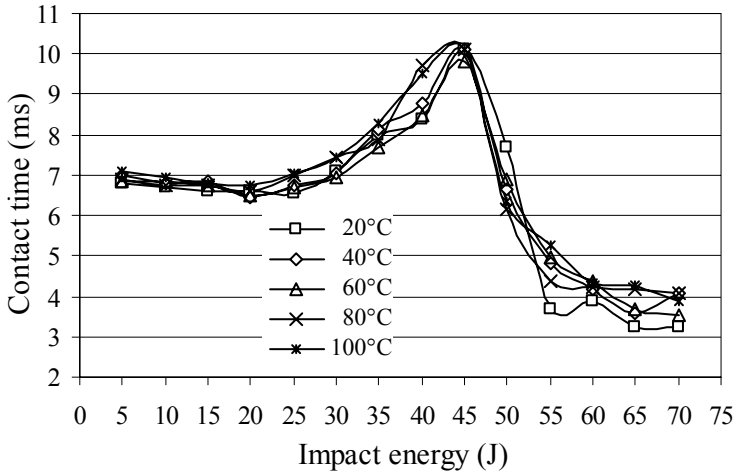


Figure 5.20 The contact time-impact energy diagram depending on the temperature for $[0°/90°/0°/90°]_S$.

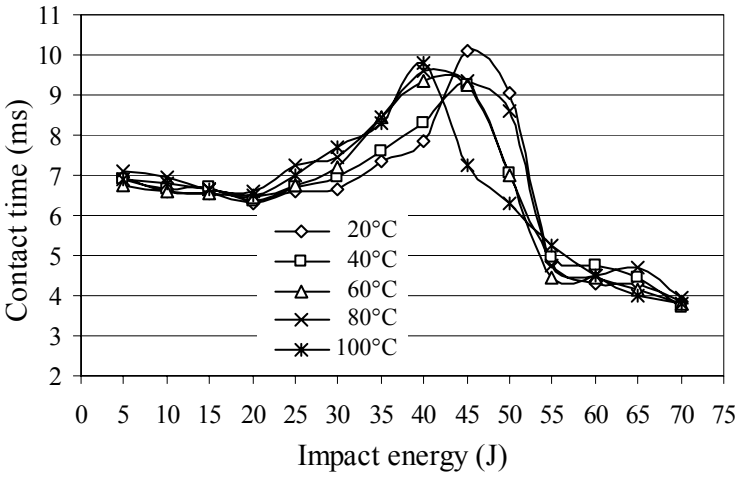


Figure 5.21 The contact time-impact energy diagram depending on the temperature for $[0°/90°/45°/-45°]_S$.

Figure 5.22 and Figure 5.23 illustrate the maximum deflection-impact energy diagram depending on the temperature for $[0°/90°/0°/90°]_S$ and $[0°/90°/45°/-45°]_S$, respectively. The maximum deflection of the plate changes linearly in the range of 5 J-20 J for both orientation and for all temperature. After 20 J, it does not change significantly by changing energy level for all temperature. The maximum deflection value for $[0°/90°/0°/90°]_S$ orientation is higher than $[0°/90°/45°/-45°]_S$ orientation for all energy levels and all temperature cases.

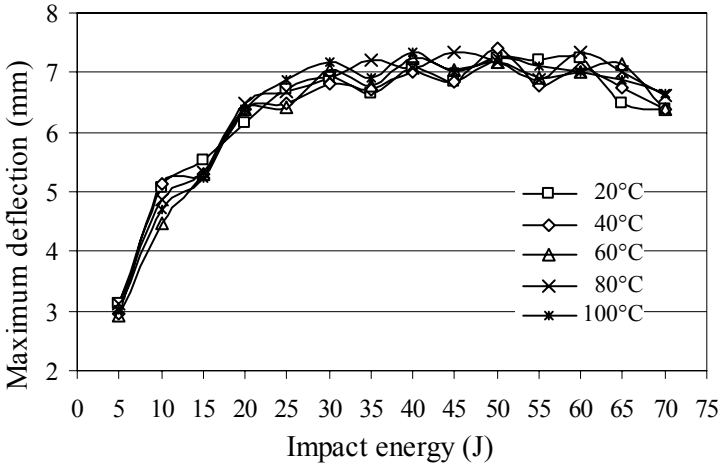


Figure 5.22 The maximum deflection-impact energy diagram depending on the temperature for $[0°/90°/0°/90°]_S$.

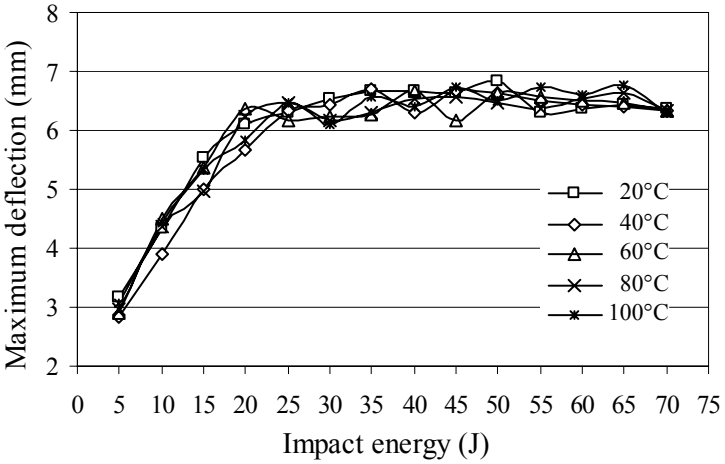


Figure 5.23 The maximum deflection-impact energy diagram depending on the temperature for $[0°/90°/45°/-45°]_S$.

Figure 5.24 and Figure 5.25 show the permanent deflection-impact energy diagram depend on temperature for $[0°/90°/0°/90°]_S$ and $[0°/90°/45°/-45°]_S$, respectively. The permanent deflection of the composite plate increases by changing energy level. In the rebounding cases having the range of 5 J-20 J, the permanent deflection of the plate is nearly constant by changing energy level. In the range of 20 J-40 J, the permanent deflection quickly increases for all temperature because of the fiber breakage. The maximum value of the permanent deflection occurs at 20°C from 5 J to 40 J for both stacking sequences. After penetration (40 J), impactor passes through out the thickness of the composite specimen. So perforation cases are not shown in the figures.

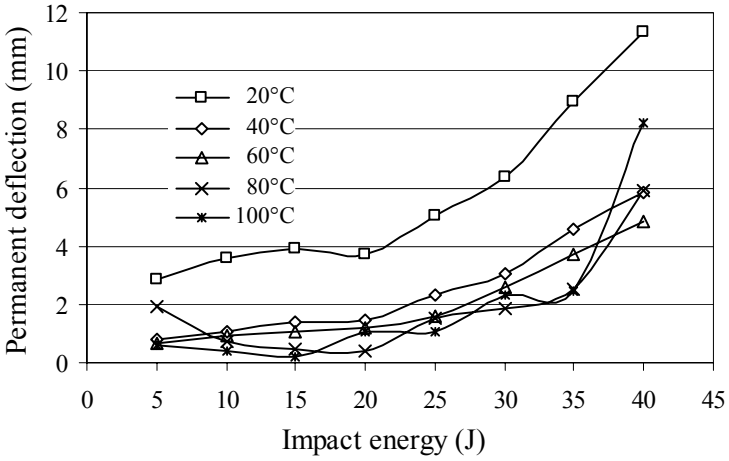


Figure 5.24 The permanent deflection-impact energy diagram depending on the temperature for $[0°/90°/0°/90°]_S$.

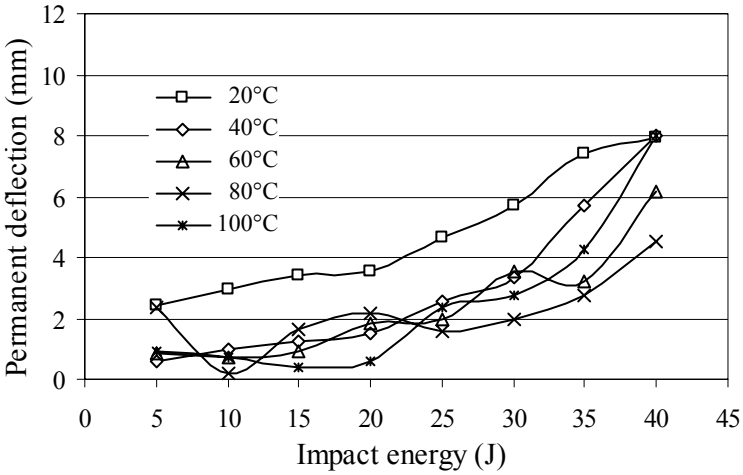


Figure 5.25 The permanent deflection-impact energy diagram depending on the temperature for $[0°/90°/45°/-45°]_S$.

The damage areas at the impacted and back faces of the specimen with $[0°/90°/0°/90°]_S$ and $[0°/90°/45°/-45°]_S$ stacking sequences for different impact energies are given in Figure 5.26 and Figure 5.27, individually. From the figures it can be said that the damage area of back face is much bigger than the impacted face due to tensile crack by bending and delamination of back part of the plate.

The damage area in the impacted face and back face increases by changing impact energy for all temperatures and both configurations. The damage areas of impacted and back faces for $[0°/90°/0°/90°]_S$ orientation are bigger than the $[0°/90°/45°/-45°]_S$ orientation. The plate with $[0°/90°/0°/90°]_S$ orientation has low bending stiffness. So it absorbs more energy and more delamination occurs.

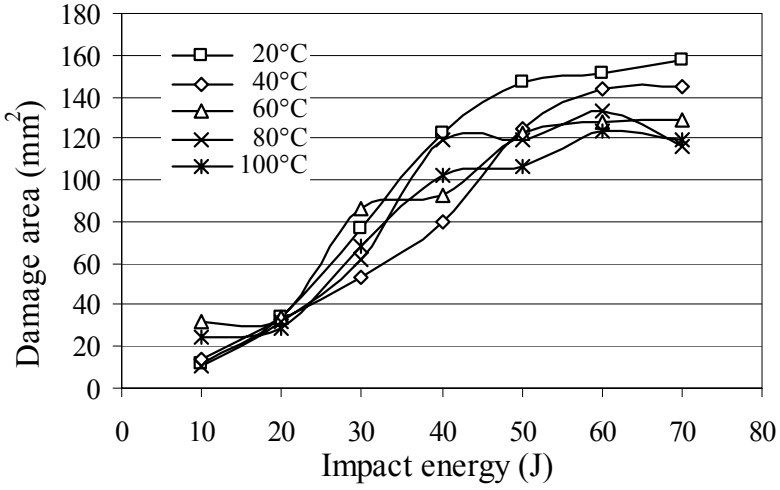


(a)

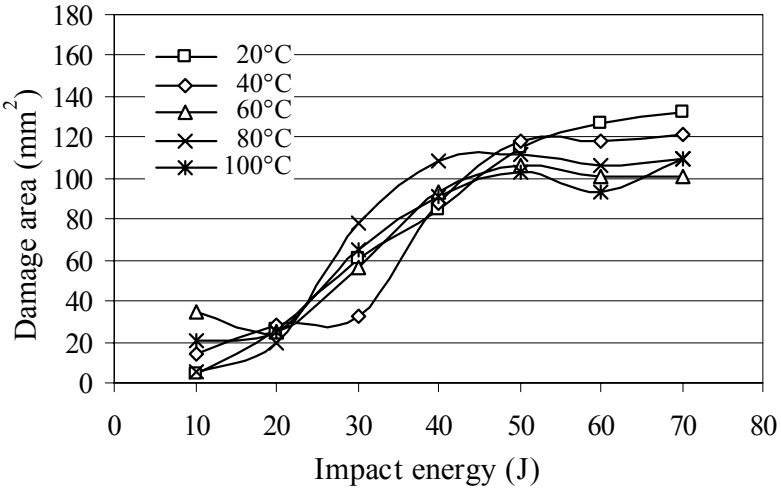


(b)

Figure 5.26 The impacted face damage area of the specimen with orientation of (a) $[0°/90°/0°/90°]_S$ and (b) $[0°/90°/45°/-45°]_S$.

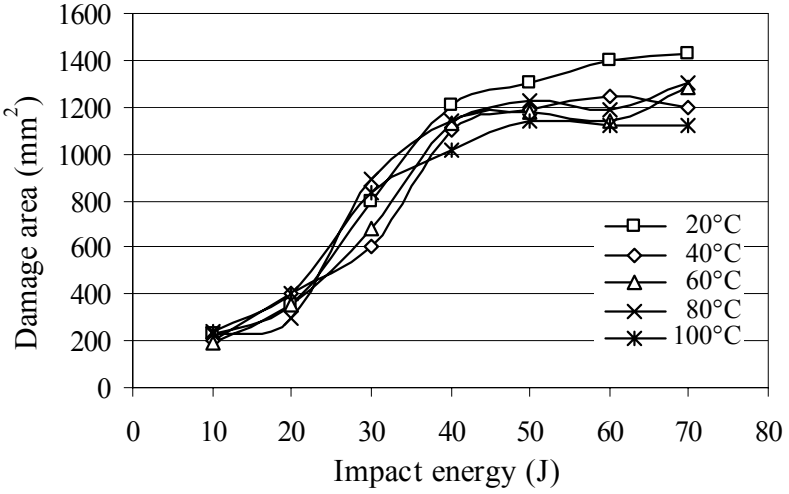


(a)

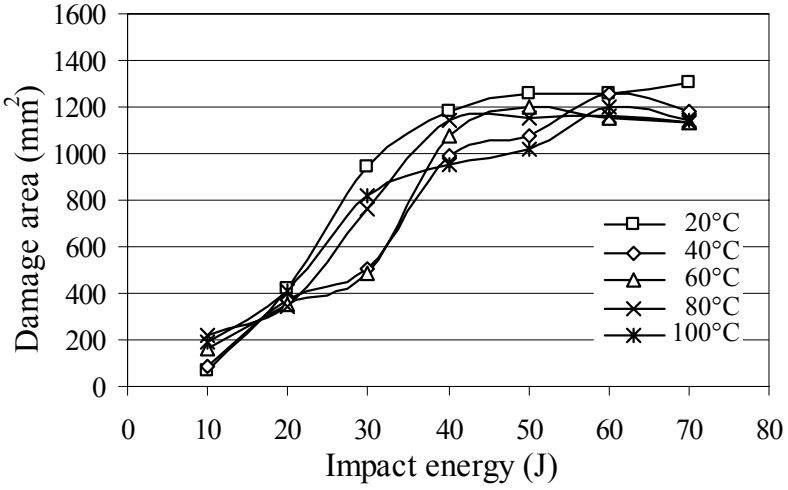


(b)

Figure 5.27 The back face damage area of the specimen with orientation of (a) $[0°/90°/0°/90°]_S$ and (b) $[0°/90°/45°/-45°]_S$.

### *5.3.3.3 Energy Profiling Method (EPM)*

Impact energy ($E_i$) and absorbed energy ($E_a$) are two important parameters to assess impact response of composite structures. The impact energy is defined as the total amount of energy introduced to a composite specimen. The absorbed energy is the energy absorbed by the composite specimen through the impact event by formation of damage inside specimen. The diagram showing relationship between

impact energy and absorbed energy is called as “energy profile”. The energy profiling method becomes possible to characterize some impact properties such as pure elastic limit, penetration ($P_n$) and perforation ($P_r$) thresholds.

The shape of an energy profile diagram, in general, may be influenced by a number of factors associated with both the impactor and target. As examples; geometry of fibers, thickness and stacking sequence of target, and shape of the impactor can be given. A general schematic illustration for energy profile diagram is illustrated in Figure 5.28.

The energy profile diagram consists of three regions; AB, BC and CD. Here, AB represents a region in which specimens remain non-penetrated (rebounding case). As expected, the extent of damage in specimens is dependent on the impact energy, i.e. overall damage area increases by increase of impact energy. In this region, the curve is below the equal energy line, implying that there is excessive impact energy (the difference between the curve and the equal energy line). The excessive energy ($E_e$) is retained in the impactor and used to rebound the impactor from the specimen at the end of an impact event (Liu, 1988).

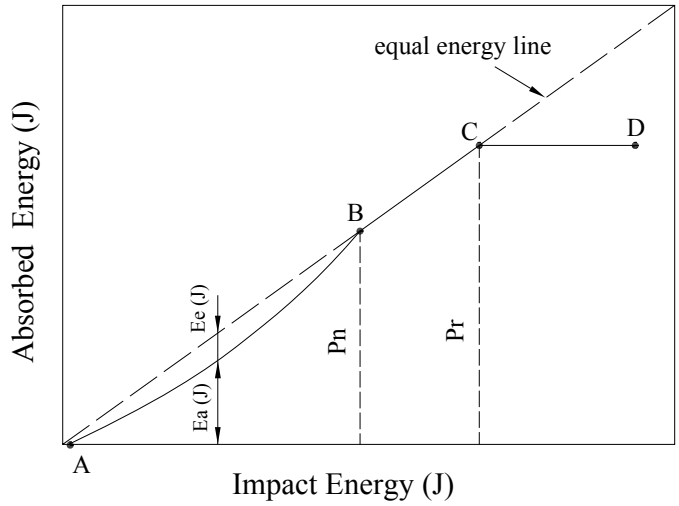


Figure 5.28 Typical energy profile diagram of a composite plate

Region BC is expressed as the penetration range where the total impact energy is probably absorbed by specimens. And, region CD stands for specimens perforated. In addition, point B and C represent the penetration and perforation thresholds, respectively. The penetration threshold can be defined as the point where the absorbed energy equals the impact energy for the first time. That is to say, at penetration threshold, the impactor sticks into specimens and does not rebound any more. From the perforation threshold, the energy absorbed by specimens remains nearly constant. It implies that the impactor does not result in further damage in specimens even if the impact energy increases. The dashed diagonal line in the diagram represents the equal energy line between the impact energy and the absorbed energy.

In order to drawing the energy profile diagram of the $[0°/90°/0°/90°]_S$ and $[0°/90°/+45°/-45°]_S$ stacking sequences at room (20°C) and high temperatures (40°C, 60°C, 80°C and 100°C), a number of tests are performed under various impact energies ranging from 5 J to 70 J.

Figure 5.29 and Figure 5.30 show energy profile diagrams of $[0°/90°/0°/90°]_S$ and $[0°/90°/+45°/-45°]_S$ fiber configurations, respectively. As seen in these figures, the minimum excessive energy is obtained at 20°C for both fiber configurations. The excessive energy increases by increasing the temperature from 20°C to 100°C up to penetration level, i.e., energy absorbed capability of the specimen reduces. The first penetration level is obtained for $[0°/90°/0°/90°]_S$ at 20°C and in 35 J energy level (Figure 5.29). 45 J is penetration threshold for $[0°/90°/0°/90°]_S$ orientation at 40°C, 60°C, 80°C and 100°C, and it is also penetration threshold for $[0°/90°/45°/-45°]_S$ configuration at 20°C and 100°C. In addition, penetration is obtained at 40 J in $[0°/90°/45°/-45°]_S$ sequences and at 40°C, while it does not never exist at 60°C and 80°C (Figure 5.34). The absorbed energy is nearly constant after first perforation level for all temperatures and for both fiber configurations.

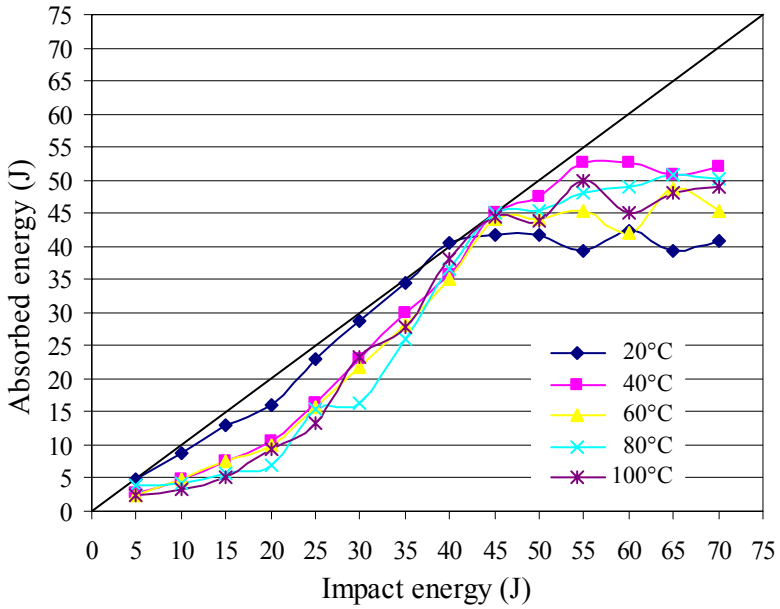


Figure 5.29 The energy profile for $[0°/90°/0°/90°]_S$ orientation.

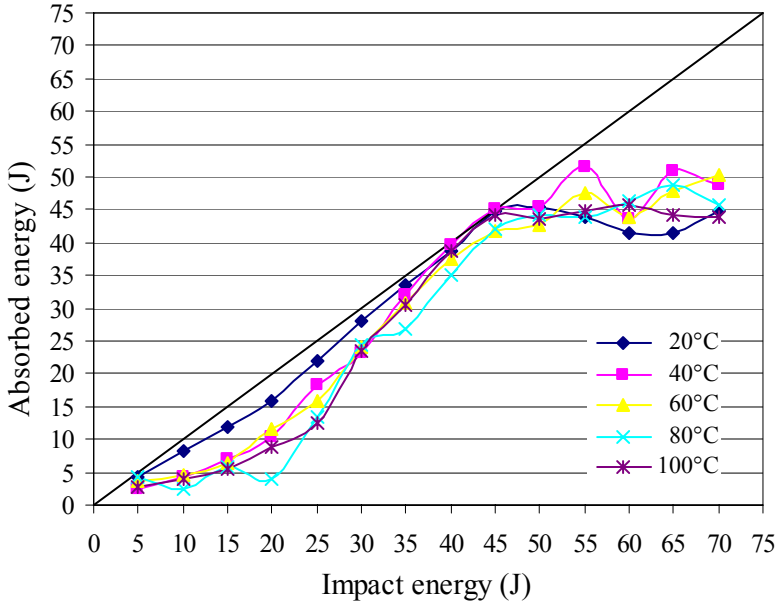


Figure 5.30 The energy profile for $[0°/90°/45°/-45°]_S$ orientation.

### *5.3.3.4 Damage Mechanism*

When a foreign object impacts on a composite laminate; several damage modes such as delaminations, fiber breakage, and matrix cracks occur in the composite structure. Which damage mode is dominant depends on, in general, the impact

parameters of the impactor and the material properties of the composites. In this study, the primary damage mode is observed as fiber breakage accompanied by delaminations and matrix cracks.

For lower impact energies (less than approx. 25 J), the main damage mode is detected as delamination and matrix cracks rather than fiber fracture. However, for the higher impact energies, splitting between fiber and matrix and fiber fractures are dominant damage modes around point of impact. In addition, a kind of delamination (debonding) which resulted from the local deformation of the fibers rather than the difference between rigidities of two bottom plies at point of impact is also observed. A schematic illustration representing these damage modes is given in Figure 5.31.

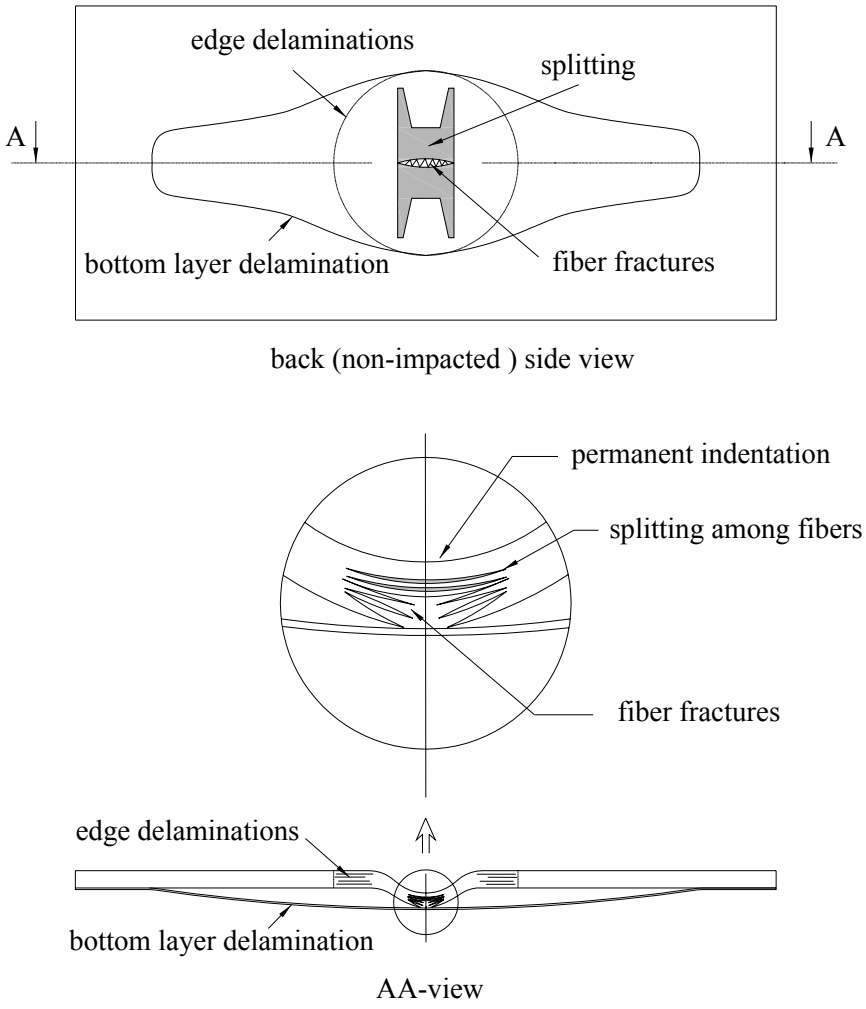


Figure 5.31 Schematic illustrations for different damage modes.

In view of the Figure 5.31, the damage mechanisms in the unidirectional glass/epoxy laminates, in this study, can be summarized as:

- Permanent *indentations* having semi-spherical shapes under the impactor, along with interlayer and intralayer matrix cracks.
- *Delamination* at interior interfaces due to different fiber orientations of adjacent plies, for impact energies lower than approx. 25 J.
- *Splitting* among undamaged fibers due to deformation around impact point.
- *Fiber fracture* resulting from bending and/or stretching of fibers. Except for very bottom layer, it starts to take place in the layers at non-impacted side and extends towards interior layers with the increase of impact energy.
- *Edge delaminations* occurred around the point of impact.
- *Delamination* at the bottom layer, resulting from vertical displacement of the fibers broken and unbroken.

To explain the main damage mode of the glass/epoxy composites, images of perforated and non-perforated specimens for $[0°/90°/45°/-45°]_S$ are given in Figure 5.32 and Figure 5.33, respectively. As seen in Figure 5.32.a, the delamination seems to have a larger area. However, as the bottom layer is removed, it seems that there is no further delamination in interior layers (Figure 5.32.b). So, the result of this appearance is bending of the bottom layer due to the fiber fracture. Figure 5.33.a is given for a perforated sample. After removing delaminated area, splitting of fibers (Figure 32.b) and fracture of fibers (Figure 5.33.b) depending on the impact energy become more visible.

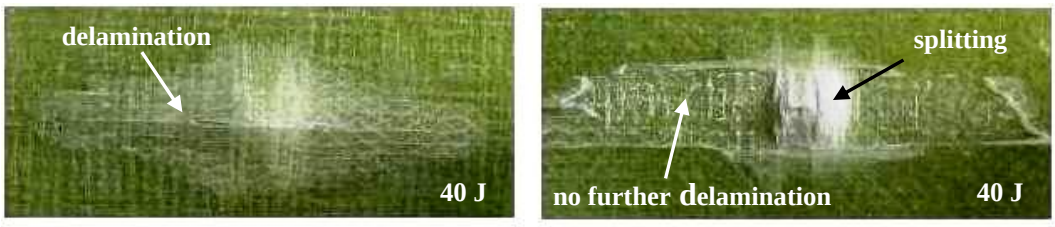


(a) (b)

Figure 5.32 The impact damage of non-perforated specimen

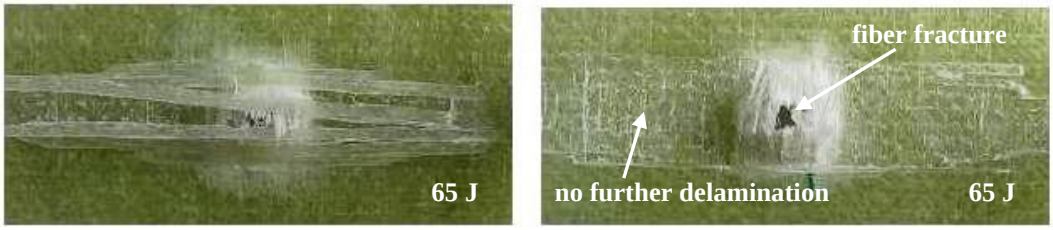


(a) (b)

Figure 5.33 The impact damage of perforated specimen

In order to show other damage modes, some representative photographs of damaged specimens for impacted and back faces taken with high intensity backlighting are given in Figure 5.34. Likewise Figure 5.32-5.33, the images are given only for one stacking sequence, $[0°/90°/+45°/-45°]_S$. Before taking photographs, delaminated parts of the bottom layer are removed. The damage characterizations of 25 J, 40 J and 65 J impact energies for the specimens are given in Figures 5.34.a, 5.34.b and 5.34.c, respectively.


(a)

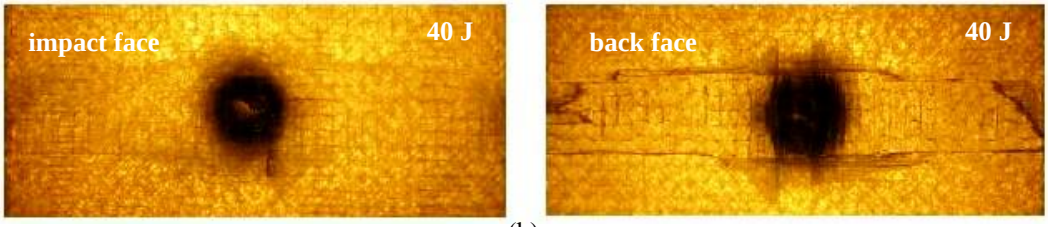


(b)

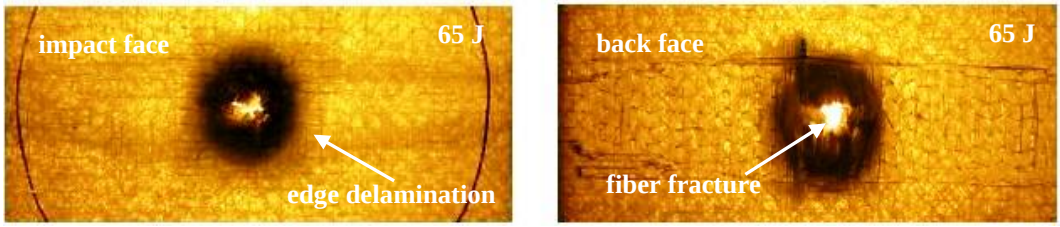


(c)

Figure 5.34 Some representative photographs of damaged samples taken with high intensity backlighting

As seen in Figure 5.34, delamination at the interior layers becomes visible after backlighting. From the figures, it is also seen that the amount of fibers damaged and the overall damage area gets larger. And, it is also believed that, for higher impact energies, the delaminations around impact point occur as a result of the free edge effect rather than the difference between rigidities of adjacent plies.

### *5.3.4 Numerical Analysis*

The 3DIMPACT finite element code is used to compare the experimental study with numerical results. It can be used for determining the deflection of the composite plates, the contact force between impactor and the composite plate and delamination shape in the interfaces. The code does not include the fiber fracture criterion. So impact analysis is carried out up to 40 J in the composite plates.

In the numerical analysis, the impact specimen is modeled with the three dimensional mesh. An eight point brick element is used for meshing. The laminate is divided four elements through the thickness and the other dimensions are divided twelve elements. Total number of element is 576. For right simulation, numerical model is clamped at all edges (Figure 5.35).

The numerical results for $[0°/90°/0°/90°]_S$ and $[0°/90°/45°/-45°]_S$ stacking sequences do not change considerably. Therefore, only $[0°/90°/0°/90°]_S$ results are given in the figures.

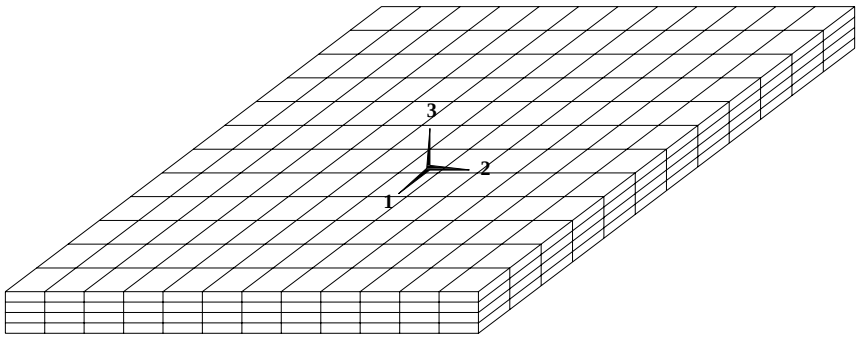


Figure 5.35 Finite element mesh of the simulated plate

To consider the energy effects on the contact force and deflection, the results of specimen which is impacted at 20°C and has $[0°/90°/0°/90°]_S$ fiber orientation is given in Figure 5.36 and Figure 5.37, respectively. It is seen from figures that the contact force and deflection increase by increasing the energy. However, energy level does not significantly affect on the contact time. In Figure 5.36, unloading portion of the contact force-time curves has some zigzag.

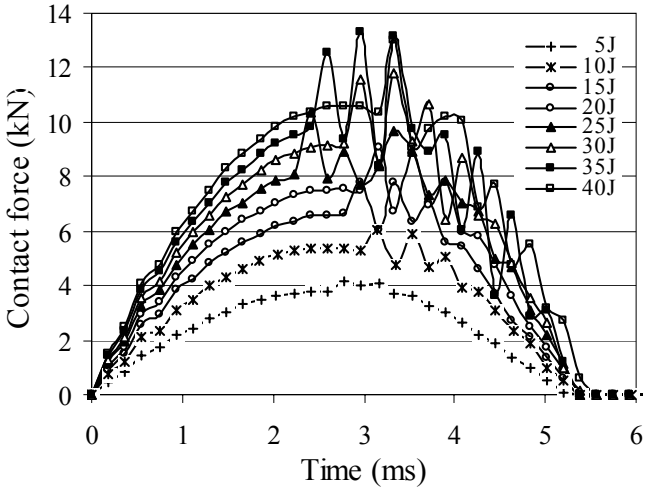


Figure 5.36 The numerical contact force-time diagrams depending on the energy for $[0°/90°/0°/90°]_S$ at 20°C.

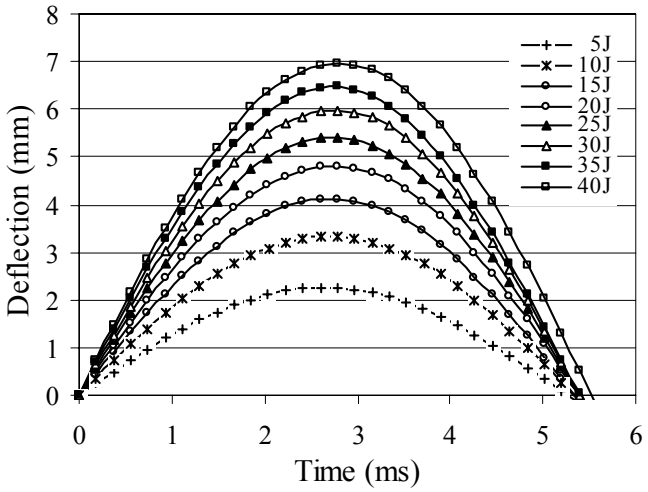


Figure 5.37 The numerical deflection-time diagrams depending on the energy for $[0°/90°/0°/90°]_S$ at 20°C.

To show the delamination in interfaces of the laminated plates with $[0°/90°/0°/90°]_S$ and $[0°/90°/45°/-45°]_S$ orientation Figure 5.38 and 5.39 are given, respectively. It is seen from figures that delamination is orientated in the direction of bottom layer of two adjacent layers except (45°/90°) interface of $[0°/90°/45°/-45°]_S$ fiber orientation. The maximum and minimum delamination areas occur at lower and top interfaces, respectively.

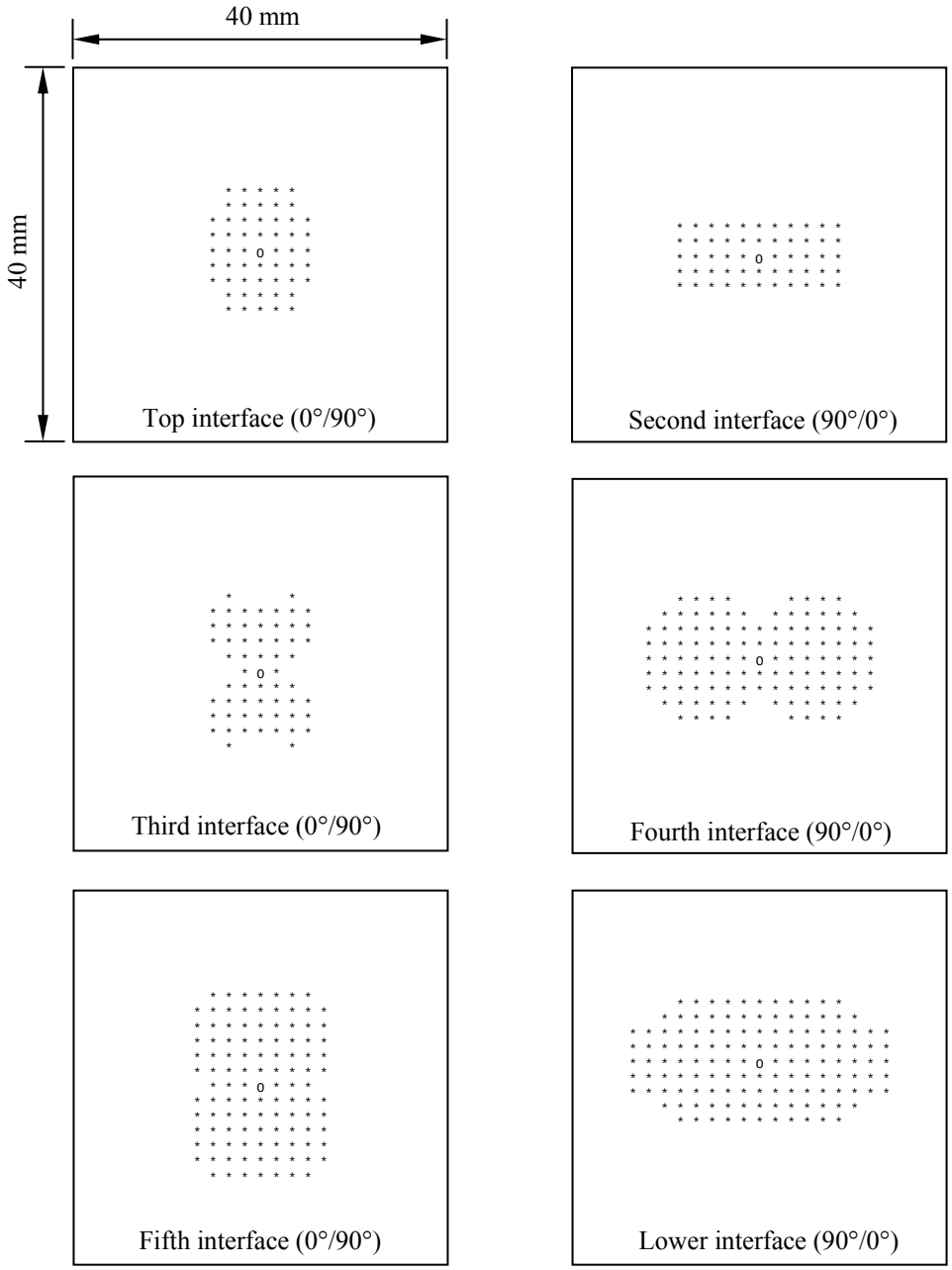


Figure 5.38 Delamination damage for $[0°/90°/0°/90°]_S$ orientated plates subjected to 20 J impact energy for 20°C.

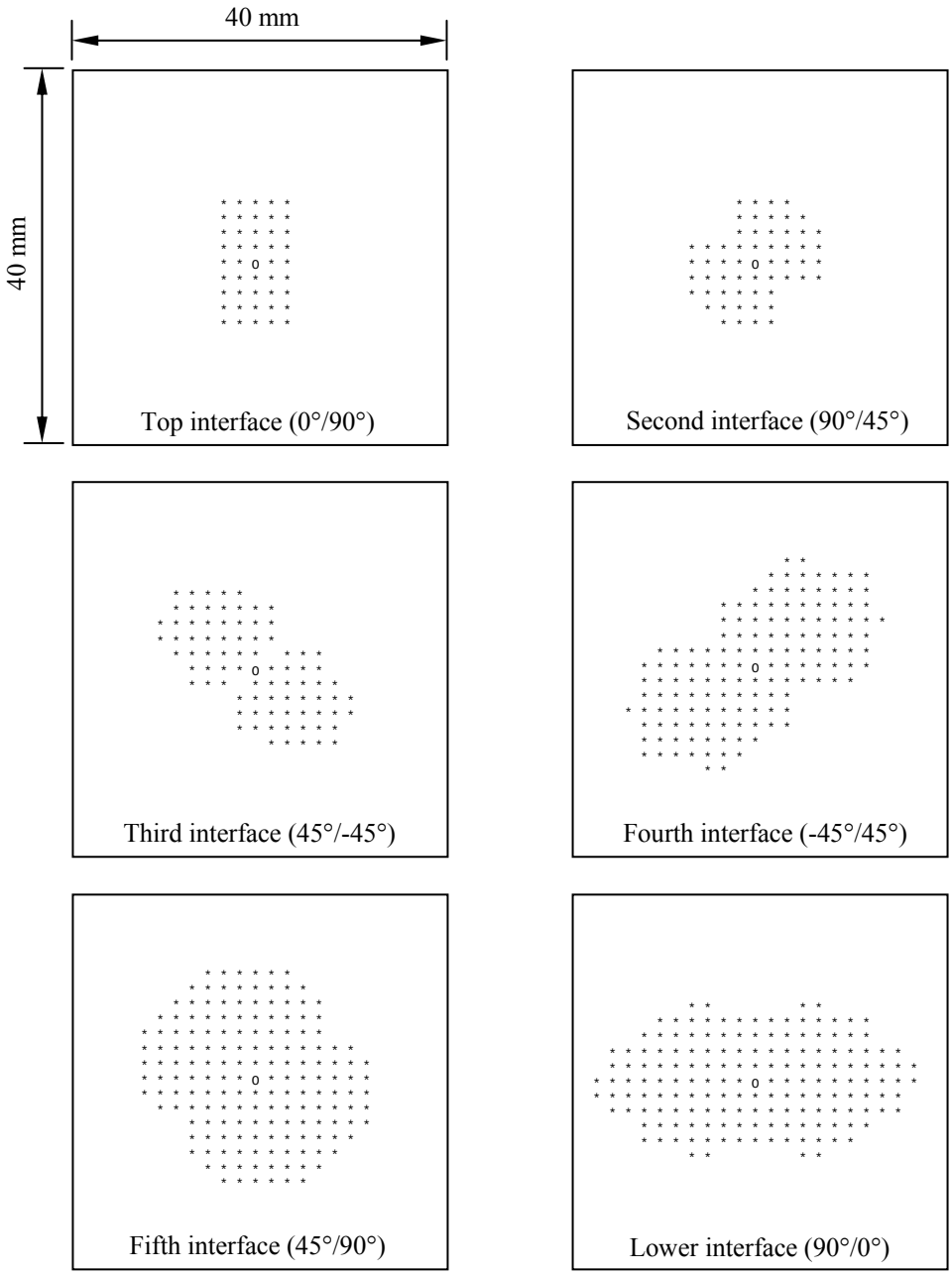


Figure 5.39 Delamination damage for $[0°/90°/45°/-45°]_S$ orientated plates subjected to 20J impact energy for 20°C.

Figures 5.40-44 are given for considering the overall delamination for 20°C, 40°C, 60°C, 80°C and 100°C, respectively. For an example overall delaminations in which obtain at 20 J impact energy is only given in figures. It is seen from figures that the overall delamination depends on the laminate configuration. The delamination areas increase by changing temperature from 20°C to 100°C.

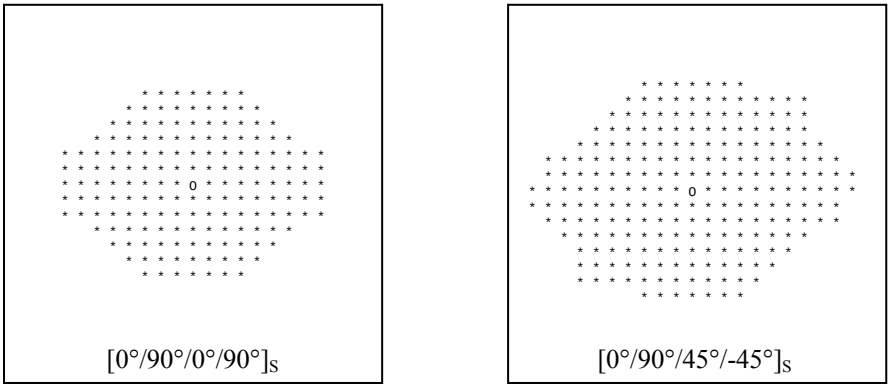


Figure 5.40 Overall delamination for 20 J impact energy at 20°C

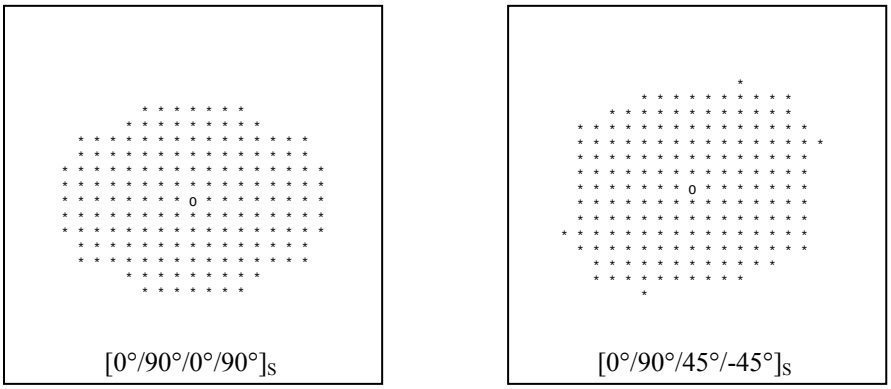


Figure 5.41 Overall delamination for 20 J impact energy at 40°C

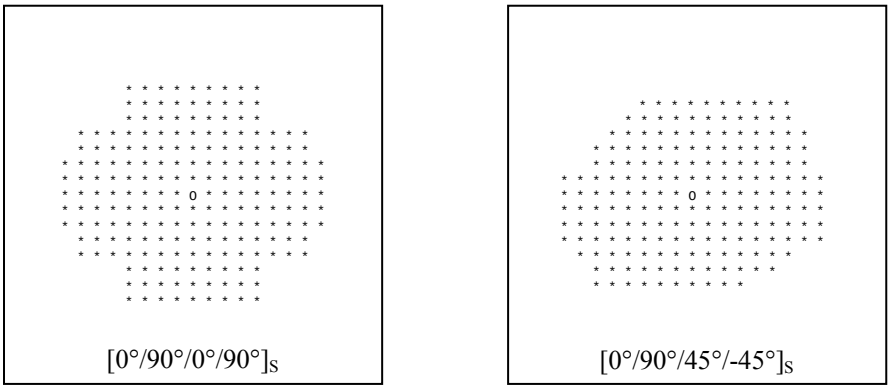


Figure 5.42 Overall delamination for 20 J impact energy at 60°C

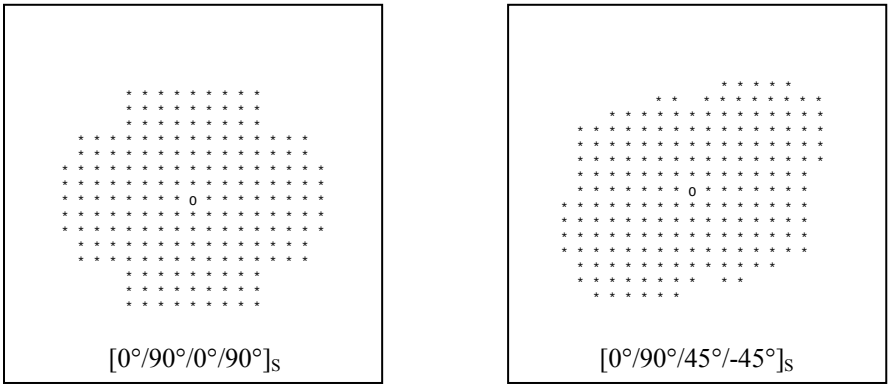


Figure 5.43 Overall delamination for 20 J impact energy at 80°C

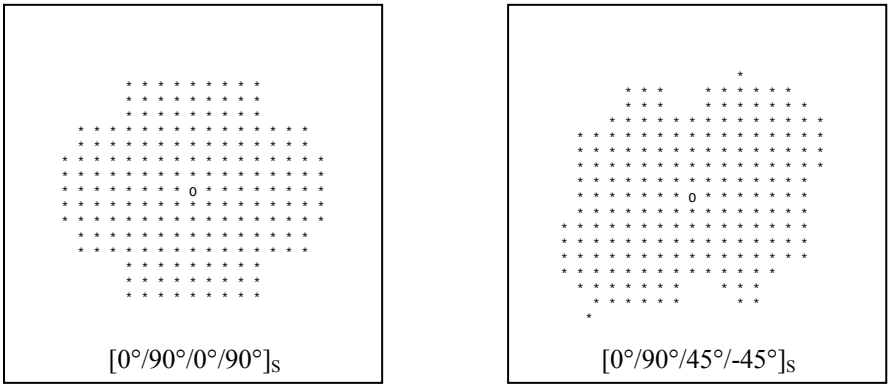


Figure 5.44 Overall delamination for 20 J impact energy at 100°C

### *5.3.5 Comparing the Experimental and Numerical Studies*

The comparison of the numerical and experimental contact force-time curves are given in Figure 5.45. It is clearly seen from figure that the experimental peak contact force is smaller than the numerical one. In spite of this, contact time for experimental study is larger than the numerical study. However, the absorbed energy obtained from both study are approximately same. A reason of the difference between the both studies is the fiber fracture criterion which code does not include. Therefore, in the numerical study, only energies up to 40 J are analyzed and compare with the experimental results.

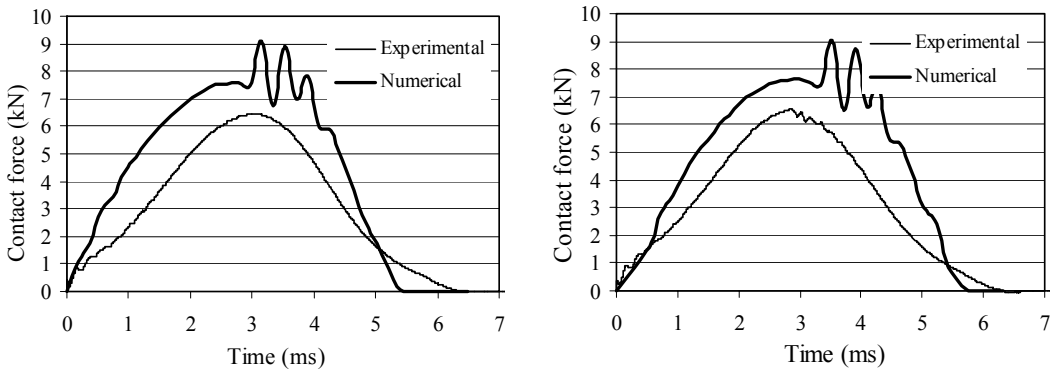


Figure 5.45 Experimental and numerical contact force-time diagram for (a) $[0°/90°/0°/90°]_S$ and (b) $[0°/90°/45°/-45°]_S$ at 20 J and 20°C temperature condition.

The unloading portion of the numerical study behaves a zigzag. This behavior may be because of the matrix cracking and delamination. For this reason, only first peak contact force is taken.

To compare maximum contact force in experimental study with the numerical one depending on the temperature for both configurations Figure 5.46 is given. The maximum contact force increases by increasing energy and it decreases by changing temperature. But, in the experimental work the maximum contact forces do not change significantly from 20 J to 40 J because of the fiber breakage in the composite laminates. However, numerical analysis for the energies from 20 J to 40 J is done to see how the fiber breakage effects on the contact force and deflection. And, the gap between experimental and numerical study is opened by the changing energy after 20 J.

The numerical results for both configurations at same energy are overlapped. However, each of the experimental results differs from each other. In addition, the numerical results are higher than the experimental results for both orientation under 20°C, 40°C and 60°C temperatures. The maximum contact force in the specimen which is analyzed under 80°C and 100°C is smaller than the experimental ones.

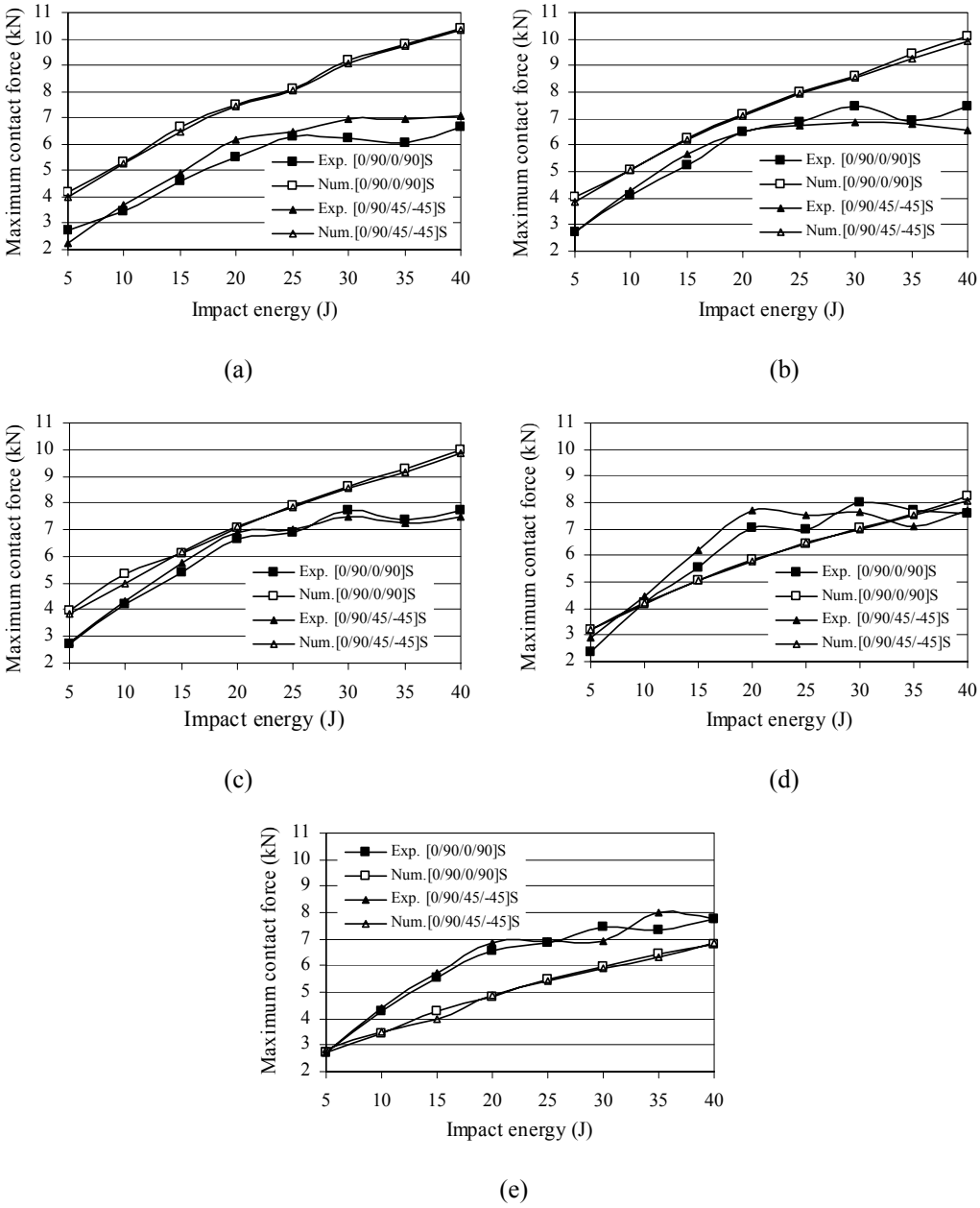


Figure 5.46 Variation of the maximum contact force versus impact energy at (a) 20°C, (b) 40°C, (c) 60°C, (d) 80°C and (e) 100°C.

Figure 5.47 is given for comparing deflection of the specimen in experimental study with the numerical one. It is seen from figure that deflection increases by increasing energy and it does not change significantly by increasing temperature in experimental study. However, it clearly changes by temperature in the numerical study for both specimen orientations. At same energy level, the deflection is

overlapped in the numerical results for both configurations. The numerical results are good agreement with the experimental one except 100°C.

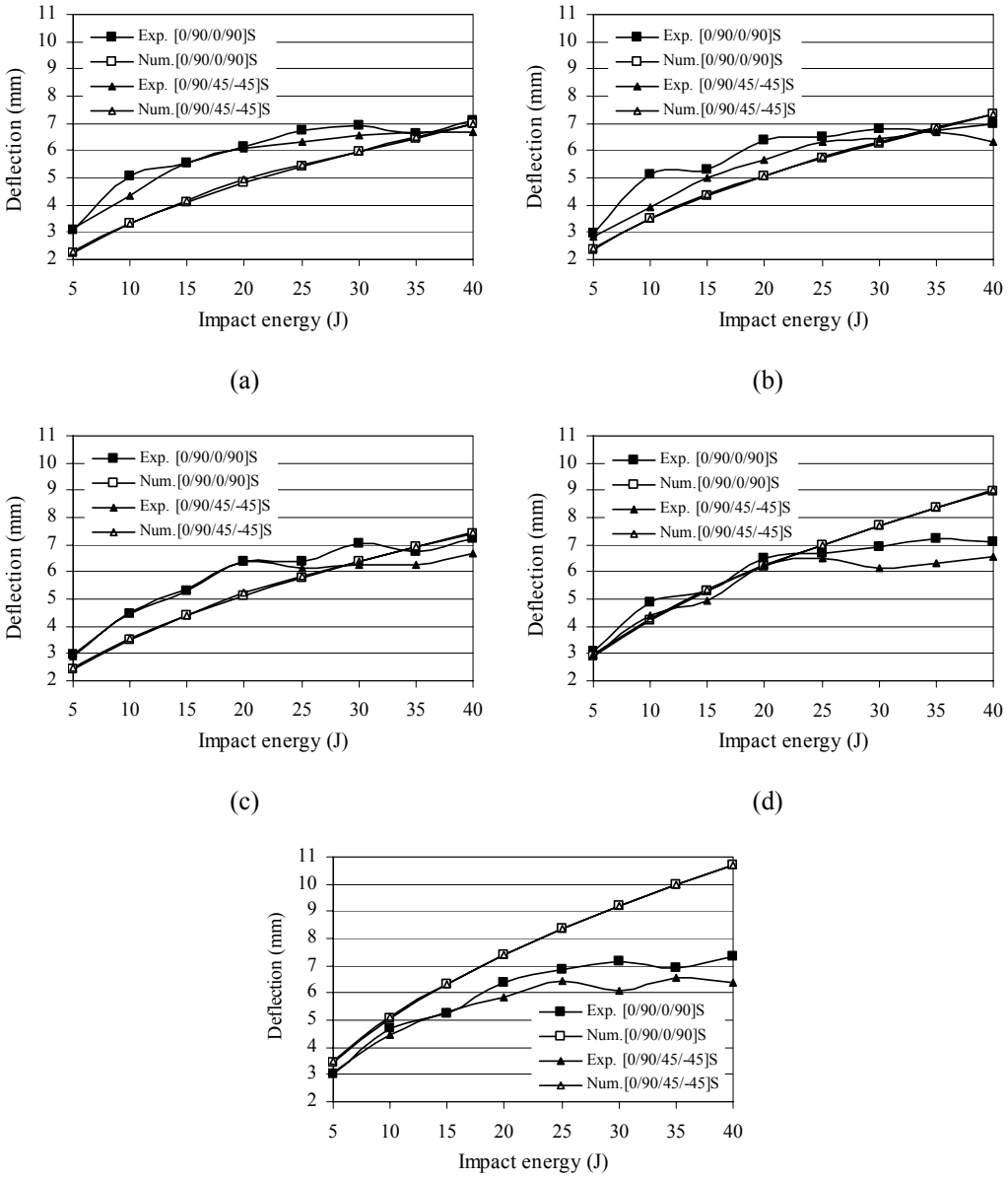


Figure 5.47 Variation of the deflection of the specimen versus impact energy at (a) 20°C, (b) 40°C, (c) 60°C, (d) 80°C and (e) 100°C

For comparing the delamination area of the specimen in experimental study with the numerical one Figure 5.48 and Figure 5.49 are given for $[0°/90°/0°/90°]_S$ and

$[0°/90°/45°/-45°]_S$ stacking sequences, respectively. It is seen from figures that the numerical damage area shows good agreement with the experimental damage zone.

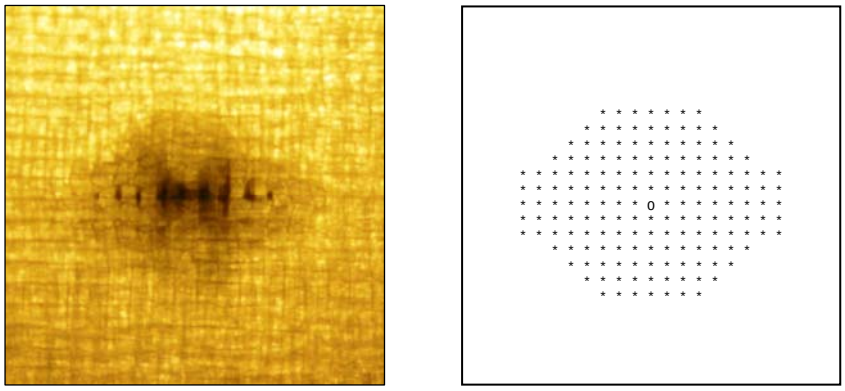

(a) (b)

Figure 5.48 The overall damage zone in $[0°/90°/0°/90°]_S$ stacking sequence for 20 J at 20°C (a) experimental and (b) numerical.

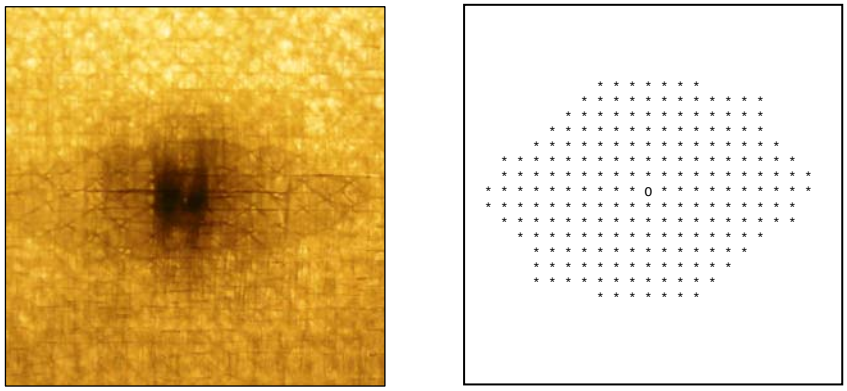

(a) (b)

Figure 5.49 The overall damage zone in $[0°/90°/45°/-45°]_S$ stacking sequence for 20 J at 20°C (a) experimental and (b) numerical.

To investigate the impact energy and temperature effects on the damage area, the biggest damage area which occurs in the lower interface of the specimen are taken into consideration. And, the percentage of damage area (% lower interface damage area/specimen area) which is obtained in experimental and numerical study is given in Figure 5.50. Results from the figures; the percentage of the damage area decreases by increasing temperature in experimental and numerical study for $[0°/90°/0°/90°]_S$ and $[0°/90°/45°/-45°]_S$ stacking sequences. However, it increases with changing energy in both of study for both fiber orientations. The percentage of the damage area

at the same energy level is fairly near in experimental and numerical study for both configurations and for all temperatures. In addition, the gap between experimental and numerical data is opened from 5 J to 40 J for all temperatures. It means, the numerical and experimental data which is obtained at 5 J is nearly same. But, at 40 J, it fairly differs from each other. The reason of this may be fiber fracture criterion is not used in the numerical code.

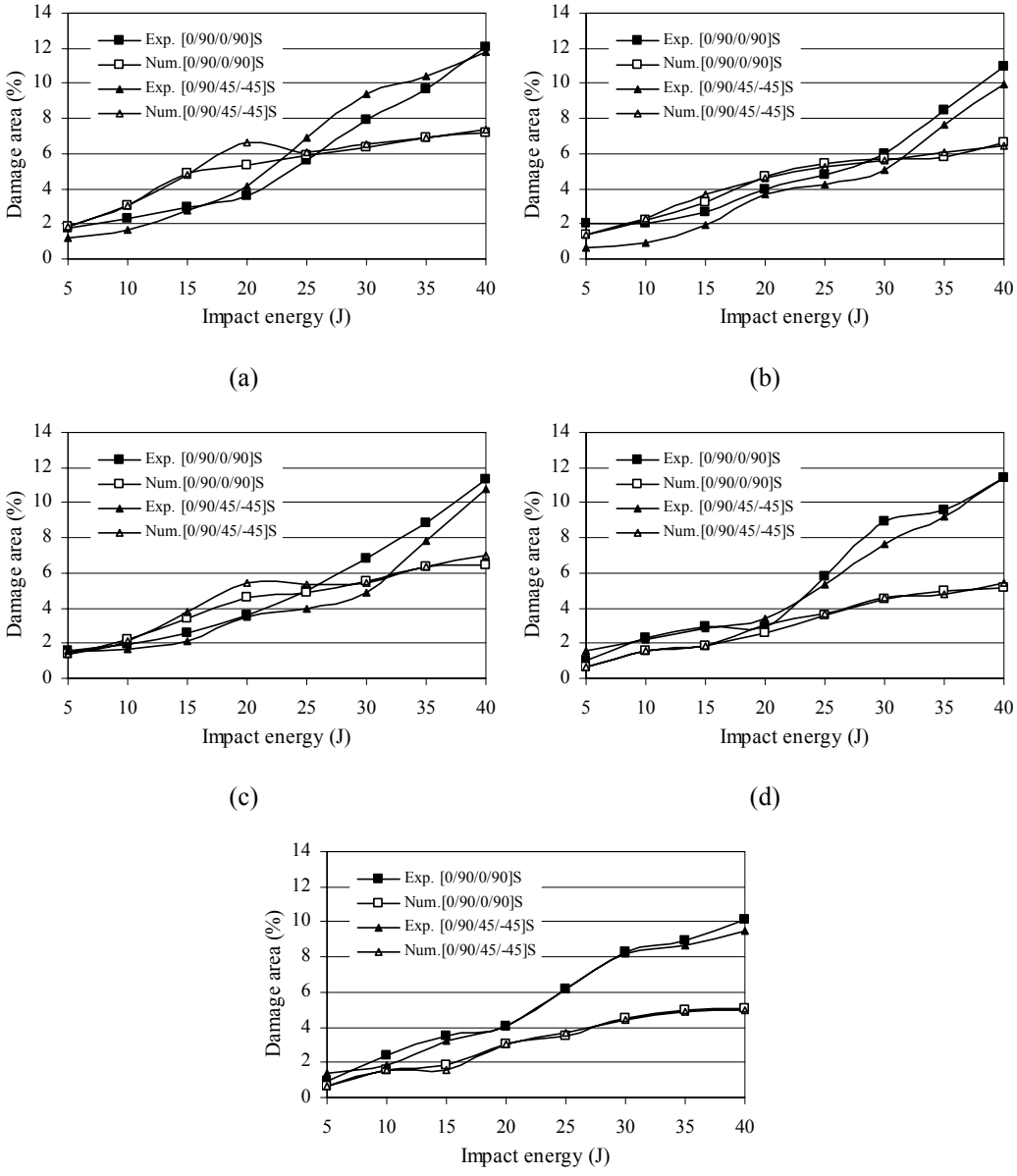


Figure 5.50 The percentage of damage area (% lower interface damage area/specimen area) versus impact energy at (a) 20°C, (b) 40°C, (c) 60°C, (d) 80°C and (e) 100°C.

## 5.4 Compression After Impact (CAI) Strength Test

The compression after impact (CAI) test is an experimental estimation of the degradation of the compressive strength of the composite plate due to impact loading. Under this type of loading, strength reduction is the largest. For this reason, the CAI problem is considered to be one of the most important topics in the design of composite structures (Xilaoquan, Al-Mansour, Zhengneng & Chenghe, 2005).

For determination of the CAI strength of glass/epoxy composite plates, a CAI test fixture is fabricated from Ç-1040 steel according to Boeing CAI test fixture (ASTM D 7137) by KOSMAK Company in Kocaeli-Turkey (Figure 5.51). The CAI fixture is subjected to heat treatment process to increase the corrosion resistance. The fixture is being fully adjustable to accommodate small variations in specimen width and thickness. During CAI tests, the specimens are clamped at the top and bottom edges. To prevent overall buckling of the specimen the lateral support is designed (Figure 5.52.c).

The CAI test consists of two steps: in the first, to obtain the degree of damage inside the laminate, the specimens are subjected to a wide range of impact energy (from 5 J to 70 J) at room (approx. 20°C) and at high temperatures (40°C, 60°C, 80°C and 100°C) by using CEAST Fractovis Plus impact testing machine.

Figure 5.51 Compression after impact (CAI) test fixture

All impacts occurred at the center of the specimen and multiple impacts was prevented by anti-rebounding system Then, the damaged specimens are tested in in-plane compression at room temperature to determine its residual strength for comparing the CAI strength of damaged and undamaged specimens

According to ASTM D 7137 the CAI specimens must be 150 mm long and 100 mm wide and minimum 3 mm thickness. To investigate the damage orientation effects on the CAI strength of the glass/epoxy composites, which have two different fiber orientations as $[0°/90°/0°/90°]_S$ and $[0°/90°/45°/-45°]_S$ specimens having 150x150 mm dimensions are first impacted under room and high temperatures by using Fractovis Plus impact testing machine. Then these impacted plates are trimmed as shown in Figure 5.52.a-b and dimensions of the standard CAI test specimen are obtained. Damage zone are orientated vertically or horizontally according to the loading direction.

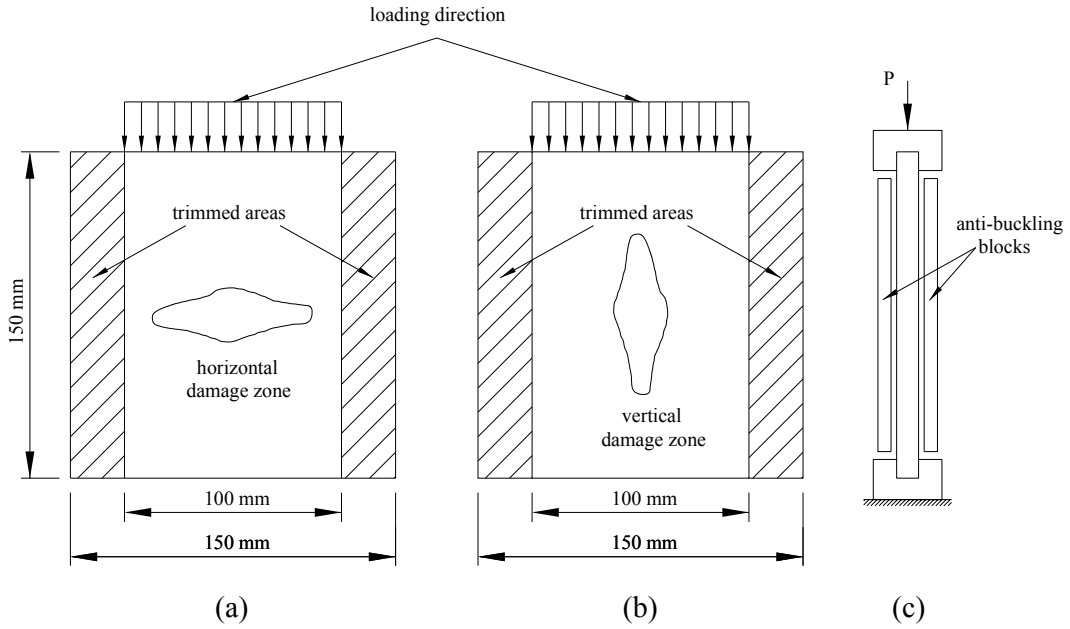


Figure 5.52 (a) Horizontal and (b) vertical damage according to loading direction and (c) anti-buckling blocks at two sides of the specimen.

The CAI tests are done at room temperature, using a Shimadzu AG tensile testing machine with 50 kN load capacity. Compressive load is applied under stroke control at a displacement rate of 1 mm/min. During the CAI test, a data acquisition system is

recorded the force versus displacement history and the force-displacement curve is monitored. The failure force is obtained from the force- displacement curve. Then, the CAI strength ($\sigma_C$) of the specimen is calculated by using equation (5.7),

$$\sigma_C = \frac{F_{\max}}{b.t} \tag{5.7}$$

where $F_{\max}$, $b$ and $t$ denote the maximum force, the width and the thickness of the specimen, respectively.

The CAI strength versus impact energy for $[0°/90°/0°/90°]_S$ and $[0°/90°/45°/-45°]_S$ orientated plate with horizontal and vertical damage are drawn in Figure 5.53-5.56. In the figures, 0 J is expressed the reference specimens which have not any damage on it for both stacking sequences. Given temperatures in all figures are temperatures in which impact tests are done. The results from the figures show that the CAI strength decreases by increasing the impact energy for all temperature case.

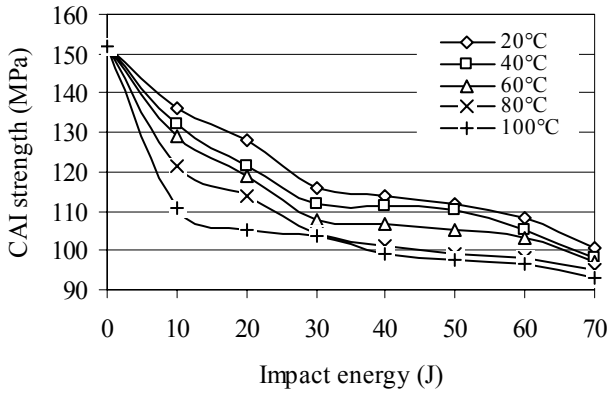


Figure 5.53 The CAI strength versus impact energy for $[0°/90°/0°/90°]_S$ orientated plate with horizontal impact damage.

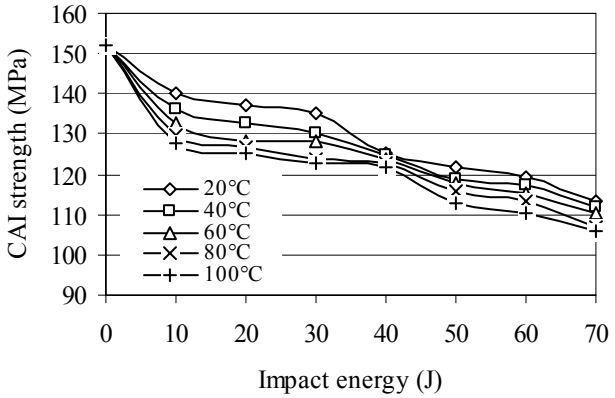


Figure 5.54 The CAI strength versus impact energy for $[0°/90°/0°/90°]_S$ orientated plate with vertical impact damage.

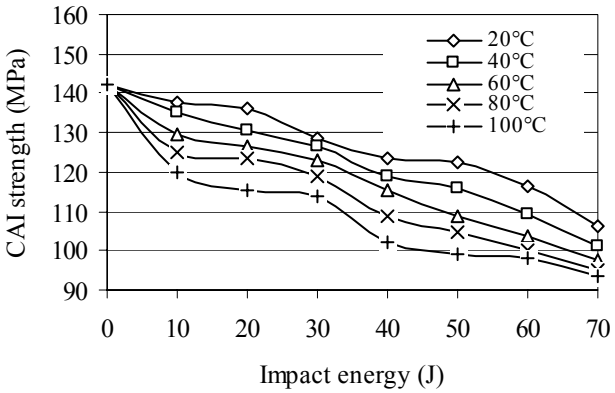


Figure 5.55 The CAI strength versus impact energy for $[0°/90°/45°/-45°]_S$ orientated plate with horizontal impact damage.

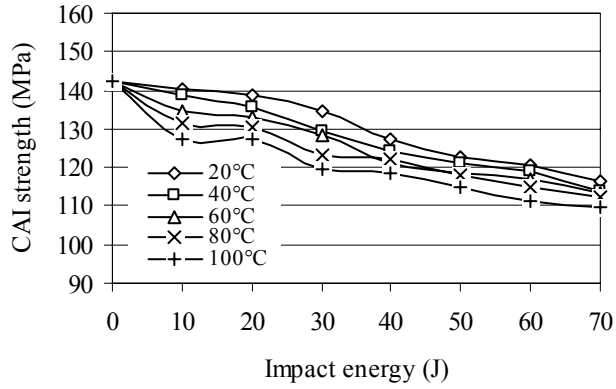


Figure 5.56 The CAI strength versus impact energy for $[0°/90°/45°/-45°]_S$ orientated plate with vertical impact damage.

To show the damage orientation effects on the CAI strength of the glass/epoxy composite plates, Figures 5.57-5.63 are plotted from 10 J to 70 J energy levels. From the results, the CAI strengths of the all damaged specimens are lower than the undamaged specimens (U) for both stacking sequences. This type of result is an expected result. It was noticed that the influence of temperature on the CAI strength of the laminates with $[0°/90/0°/90°]_S$ orientation is larger than that on those with $[0°/90/45°/-45°]_S$ orientation for the same energy level. And also, for both case of stacking sequences, the CAI strength of the specimen with horizontal impact damage (H) is lower than the specimen with vertical impact damage (V) for all energy levels and for all temperatures.

For all energy levels, the CAI strength decreases by increasing temperature from 20°C to 100°C. However, this change is smaller in the range of 20°C and 40°C than the other temperature ranges. The damage orientation as horizontal and vertical not significantly effects the CAI strength for energy levels from 50 J to 70 J (Fig. 5.61-5.63). Because before 50 J energy level (approximately 40J), perforation occurs for glass/epoxy laminated composite specimens. However, little change in the CAI strength occurs after first perforation energy level may be due to splitting, it depends on energy level, in the vicinity of the damage hole. The maximum and minimum differences of the CAI strength are obtained at 100°C and 20°C for all cases, respectively.

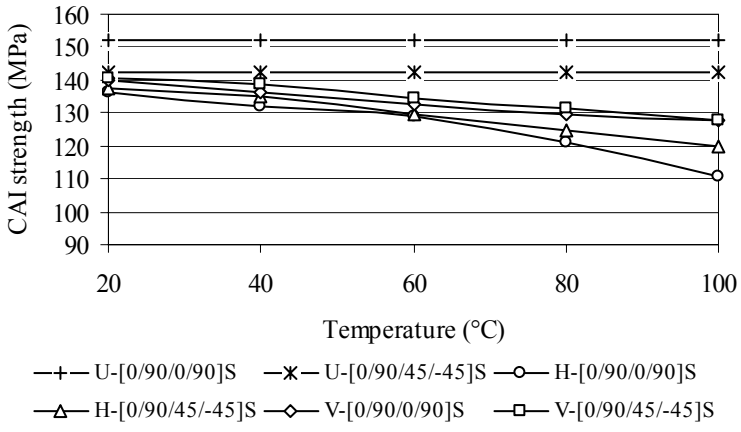


Figure 5.57 The CAI strengths versus temperature for 10J impact energy

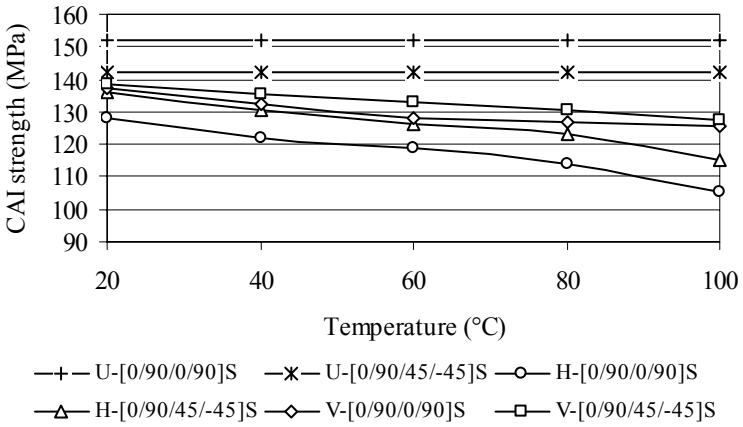


Figure 5.58 The CAI strengths versus temperature for 20J impact energy

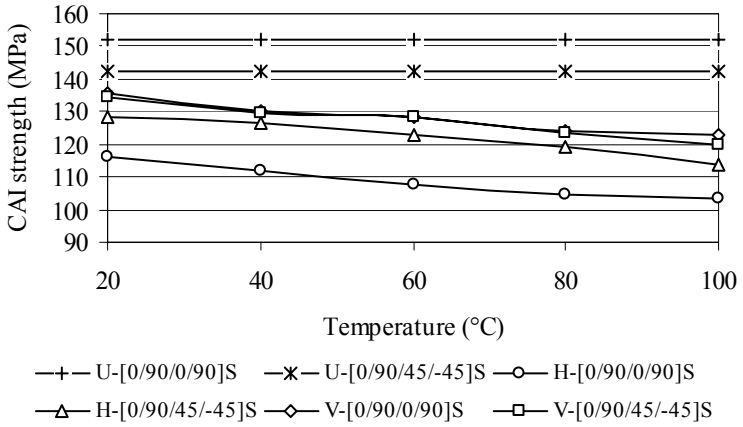


Figure 5.59 The CAI strengths versus temperature for 30J impact energy

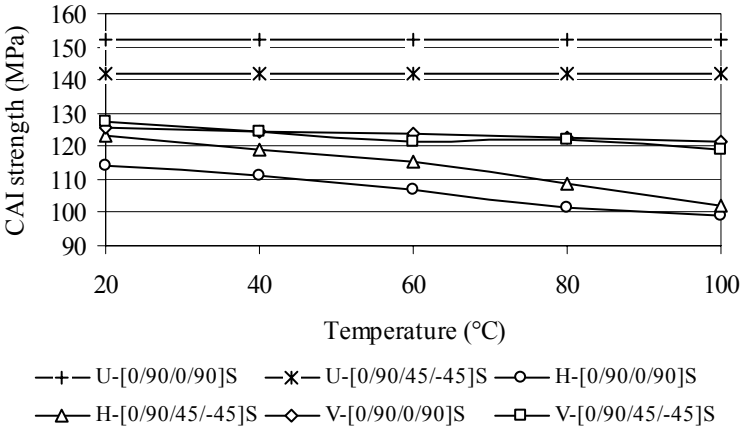


Figure 5.60 The CAI strengths versus temperature for 40J impact energy

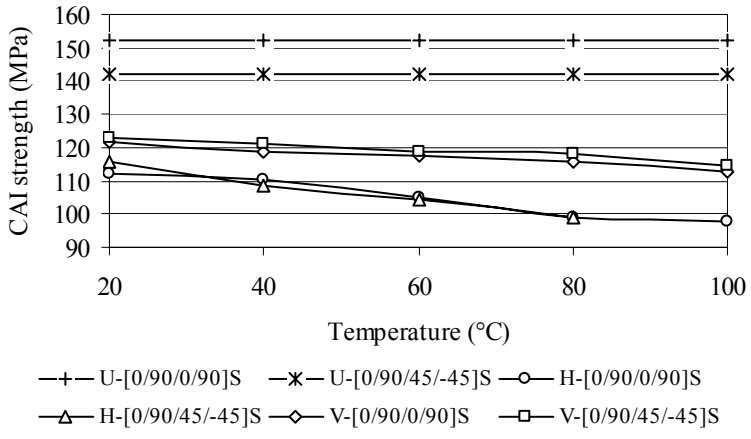


Figure 5.61 The CAI strengths versus temperature for 50J impact energy

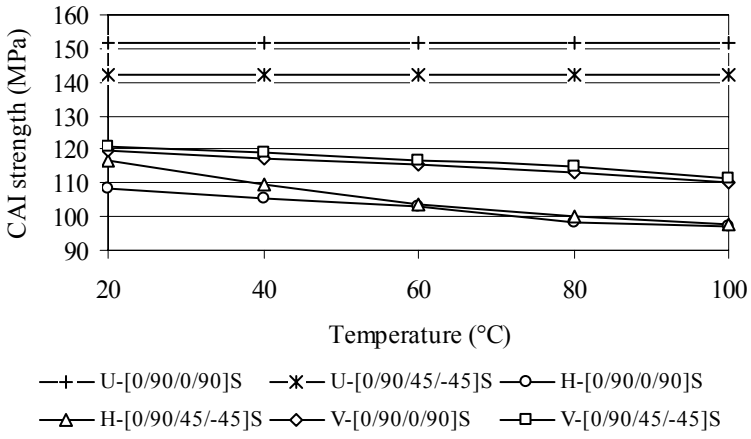


Figure 5.62 The CAI strengths versus temperature for 60J impact energy

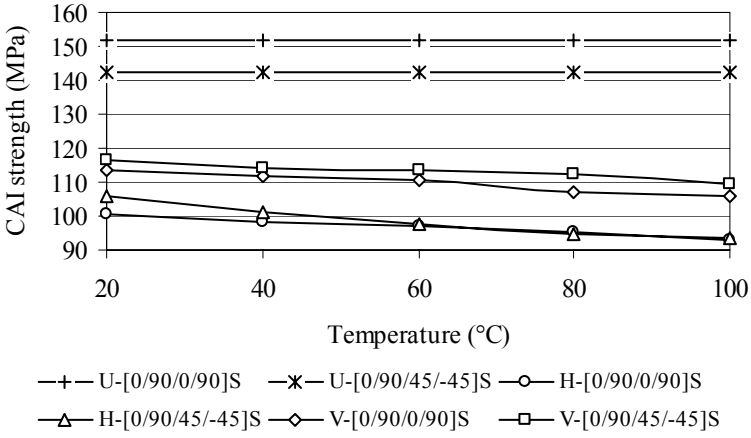


Figure 5.63 The CAI strengths versus temperature for 70J impact energy

To consider the effects of the impact energy on the CAI strength with respect to temperature, Figure 5.64-5.67 are plotted. 0 J denotes the unimpacted specimens for both stacking sequences. It is clear from the figures that the gap between the lines, each of them is explained the variation CAI strength depends on the impact energy, significantly.

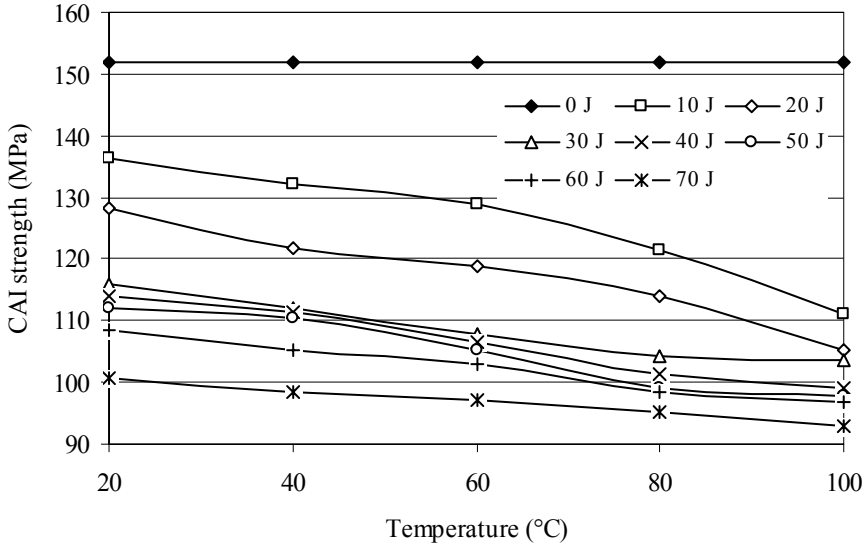


Figure 5.64 The CAI strengths versus temperature for $[0°/90°/0°/90°]_S$ specimen with horizontal impact damage for all impact energies.

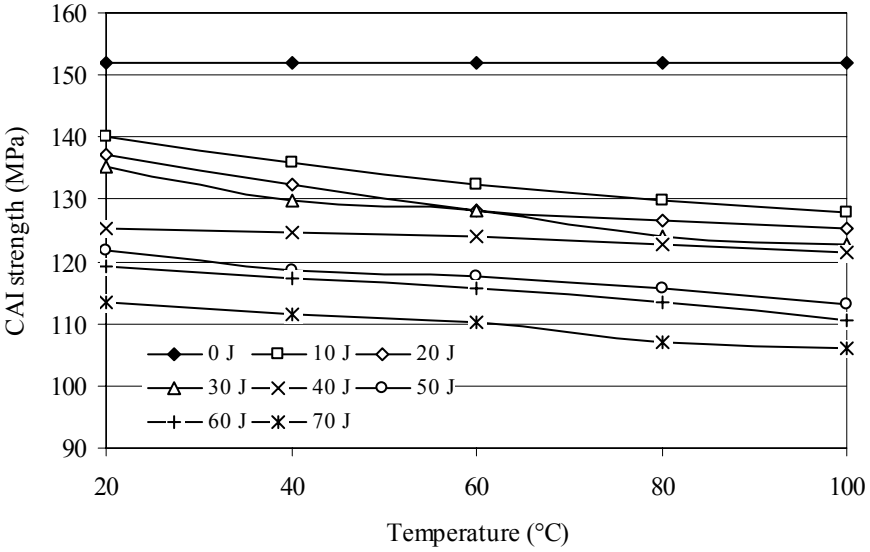


Figure 5.65 The CAI strengths versus temperature for $[0°/90°/0°/90°]_S$ specimen with vertical impact damage for all impact energies.

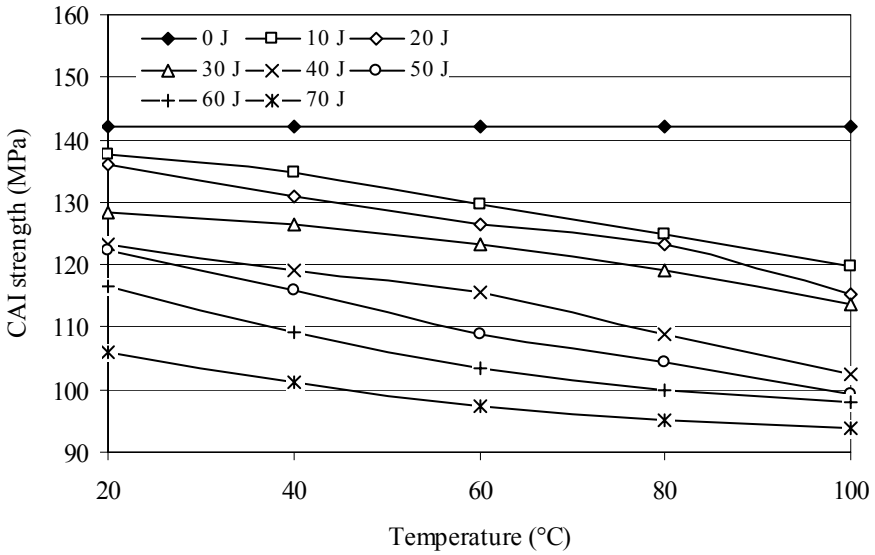


Figure 5.66 The CAI strengths versus temperature for $[0°/90°/45°/-45°]_S$ specimen with horizontal impact damage for all impact energies.

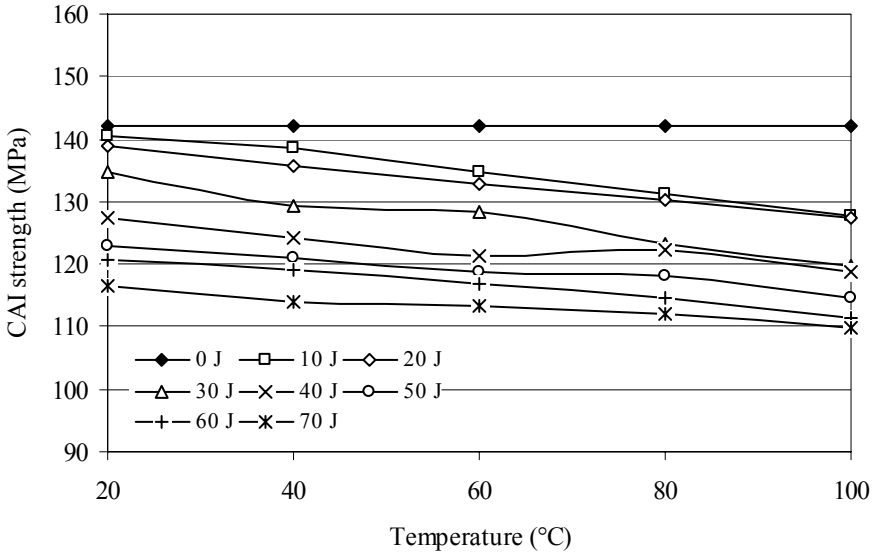


Figure 5.67 The CAI strengths versus temperature for $[0°/90°/45°/-45°]_S$ specimen with vertical impact damage for all impact energies.

The damage propagation of the impacted samples after CAI test for various impact energies and for various temperatures is shown in Figure 5.68-5.75. It is seen from figures;

The CAI damage propagates from the impact damage to the edge of the specimens for the vertical and horizontal damaged specimens and specimen

orientation and for all temperatures (Figure 5.68-5.69). Only impact side of the specimens is given in Figure 5.70 because of the invisible CAI damage occurred in the back side of the specimen. It is clearly seen from the figure, the CAI damage propagates depend on the plate stacking sequences. The smooth lines in Figure 5.70 are drawn to show clearly the CAI damage mechanism. For instance, CAI damage propagates in 0° direction for $[0°/90°/0°/90°]_S$ and in 45° direction for $[0°/90°/45°/-45°]_S$.

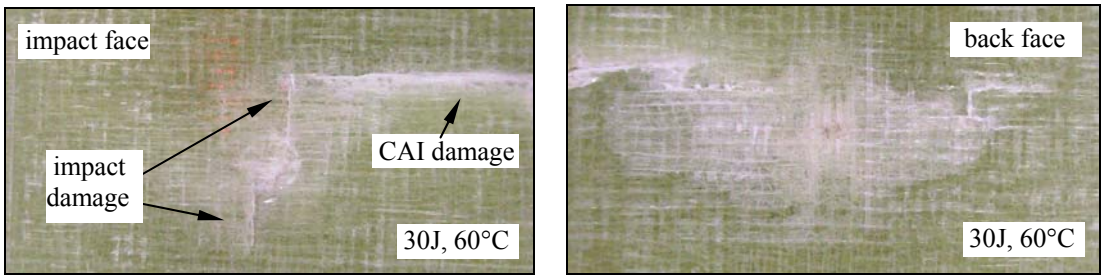


Figure 5.68 The CAI damage propagation of the $[0°/90°/0°/90°]_S$ stacking specimen with horizontal impact damage

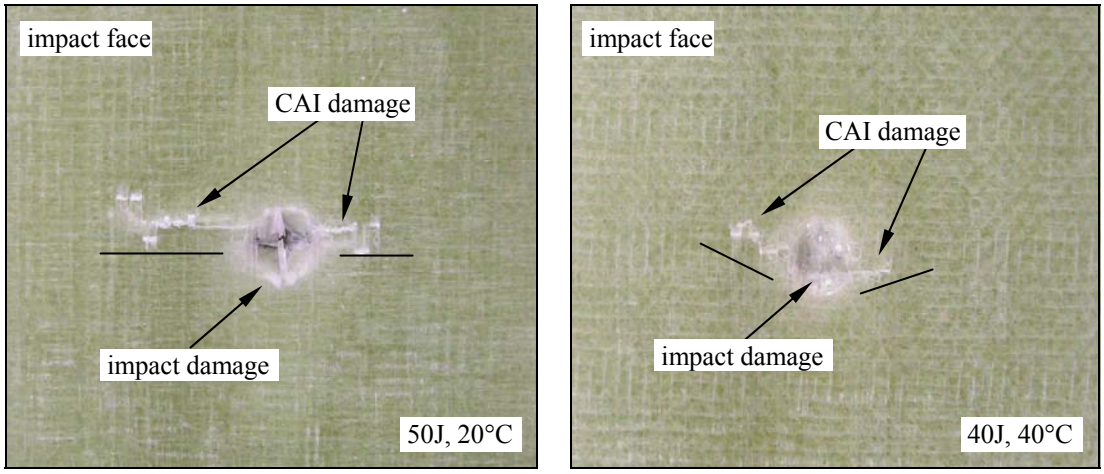


(a) (b)

Figure 5.69 The CAI damage propagation of the (a) $[0°/90°/0°/90°]_S$ and (b) $[0°/90°/45°/-45°]_S$ stacking plate with vertical impact damage

The CAI damage also depends on the orientation of the impact damage as vertical or horizontal (Figure 5.70-5.71). The CAI damage propagates horizontally while the impact damage is horizontal (Figure 5.70) and vertical (Figure 5.71). However, the

CAI damage extents as a certain angle, app. 45°, depend on the stacking sequences (Figure 5.72).

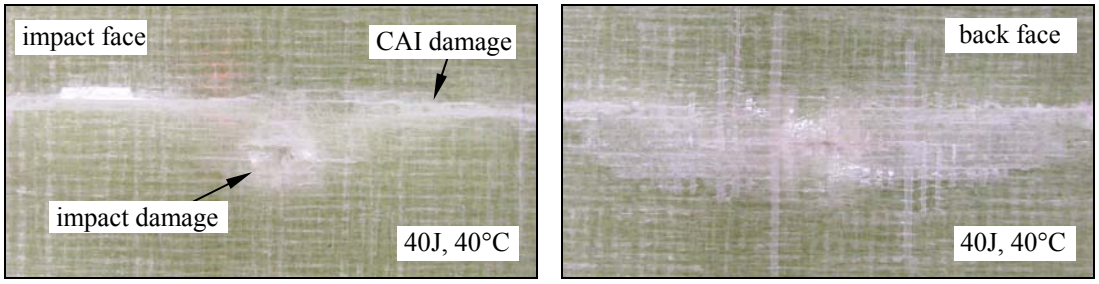


Figure 5.70 The CAI damage propagation of the $[0°/90°/0°/90°]_S$ stacking specimen with horizontal impact damage

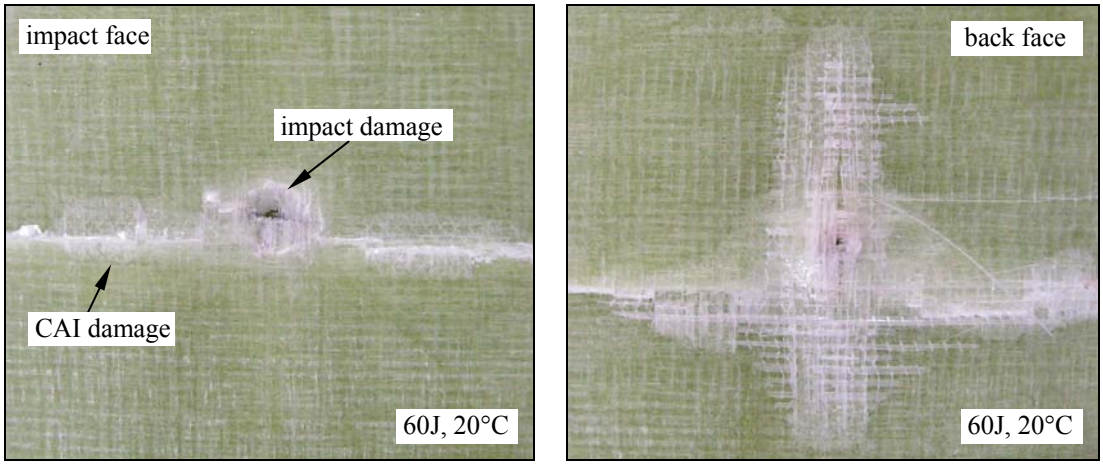


Figure 5.71 The CAI damage propagation of the $[0°/90°/0°/90°]_S$ stacking specimen with vertical impact damage

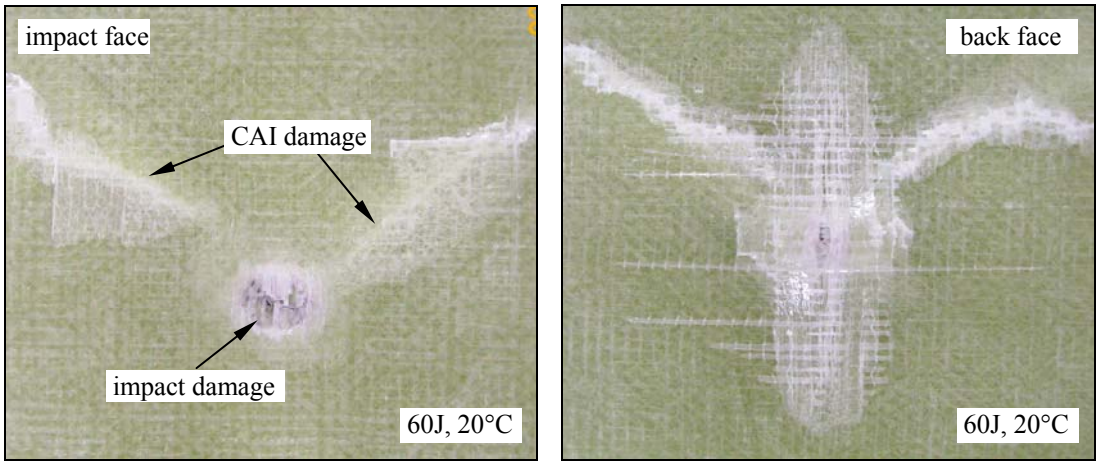


Figure 5.72 The CAI damage propagation of the $[0°/90°/45°/-45°]_S$ stacking specimen with vertical impact damage

The CAI damage initiates at the lateral edge and propagates to the impact damage (Figure 5.73). In the some specimens with vertical impact damage, the CAI damage propagates from the tip of the overall impact damage (Figure 5.74). Particularly for the higher energy level as 70J, the CAI damage extents depending on the specimen orientation. In addition, an area as a delamination occurs due to shear stress (Figure 5.75).

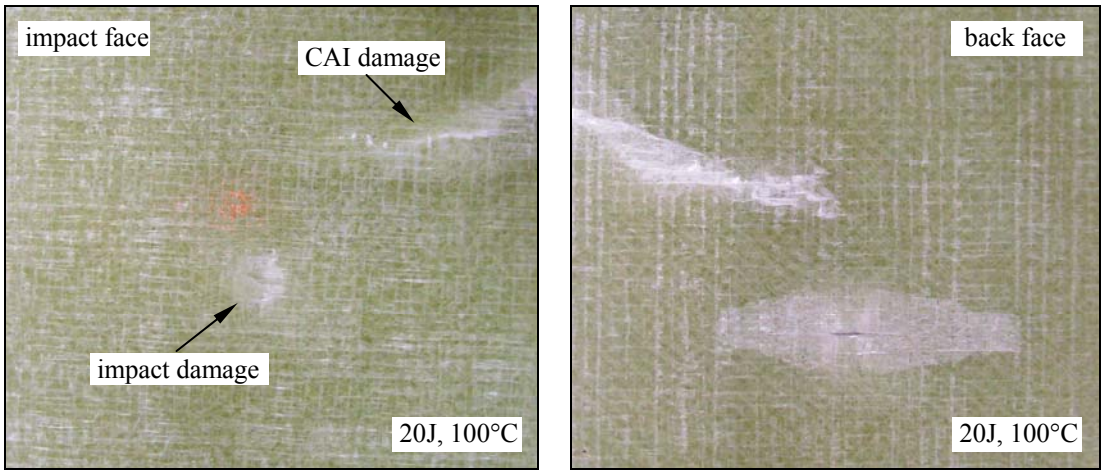


Figure 5.73 The CAI damage propagation of the $[0°/90°/45°/-45°]_S$ stacking specimen with horizontal impact damage

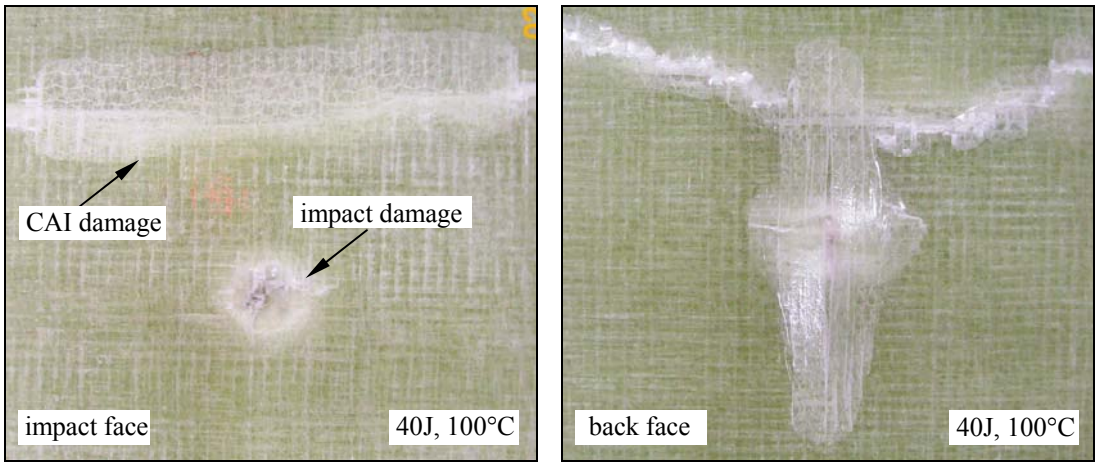


Figure 5.74 The CAI damage propagation of the $[0°/90°/0°/90°]_S$ stacking specimen with vertical impact damage

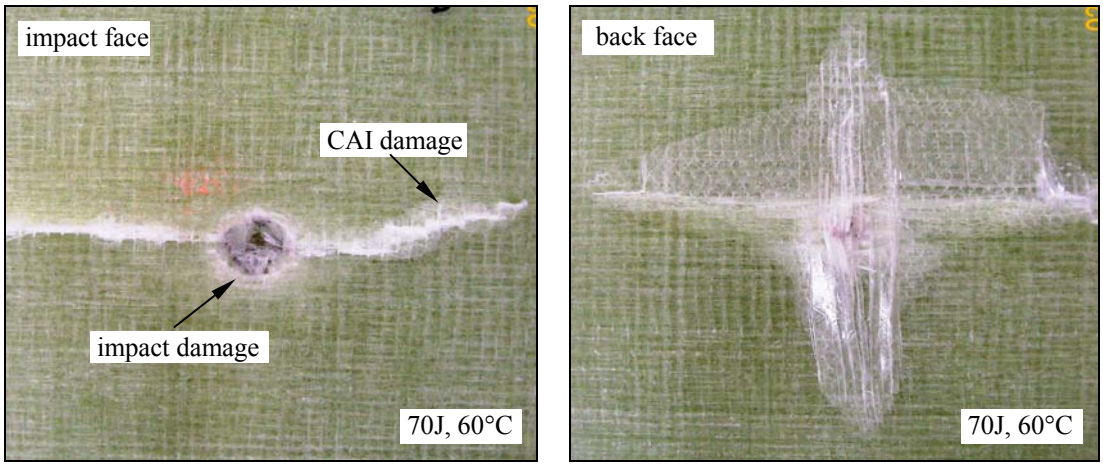


Figure 5.75 The CAI damage propagation of the $[0°/90°/45°/-45°]_S$ stacking specimen with vertical impact damage

# CHAPTER SIX
# CONCLUSIONS

In this study, the thermal impact behavior of glass/epoxy laminated composite plates under room (approx. 20°C) and high (40°C, 60°C, 80°C and 100°C) temperatures are considered experimentally and numerically. Mechanical properties of the composites are obtained under mentioned temperatures. Compression After Impact (CAI) strength of the impacted plates is also investigated under room temperature. In addition, a numerical evaluation is carried out by using 3DIMPACT finite element code. From the results obtained, the following conclusions can be drawn:

- The composites losses their rigidity and their strength with increasing temperature. So, mechanical properties of the composites decrease by increasing temperature.
- The contact force and the deflection of the specimen increase by increasing the impact energy while impact time decreases.
- The contact force increases by increasing the temperature while deflection decreases due to composite specimens which behave more brittle. But it does not exist significant changing in the contact time.
- The contact force for $[0°/90°/45°/-45°]_S$ orientation is obtained greater than for $[0°/90°/0°/90°]_S$ orientation because of the higher bending stiffness. As a result of this, the maximum deflection value for $[0°/90°/0°/90°]_S$ orientation is higher than $[0°/90°/45°/-45°]_S$ orientation for all energy levels and for all temperatures.
- The back face damage area of composites is obtained much bigger than the impacted face due to tensile crack by bending and delamination of back part of the plate.
- The damage area in the impacted face and back face increases by increasing impact energy.
- The excessive energy increases by increasing the temperature, i.e., energy absorbed capability of the specimen reduces with increasing temperature.

- For lower impact energies (less than 25 J), the main damage mode is detected as delamination and matrix cracks rather than fiber fracture. However, for the higher impact energies, splitting between fiber and matrix and fiber fractures are dominant damage modes around point of impact.
- In the lower interface, the delamination seems to have a larger area. However, the result of this appearance is bending of the bottom layer due to the fiber fracture.
- The experimental peak contact force is smaller than the numerical one while the contact time study is larger. However, the absorbed energy is approximately same.
- The numerical damage area shows good agreement with the experimental damage zone.
- The damage area decreases by increasing temperature in experimental and numerical study for $[0°/90°/0°/90°]_S$ and $[0°/90°/45°/-45°]_S$ stacking sequences. However, it increases with changing energy in both of study for both fiber orientations.
- The CAI strength decreases by increasing the impact energy and/or temperature.
- The CAI strengths of the damaged specimens are lower than the undamaged specimens for both stacking sequences.
- The CAI strength of the specimen with horizontal impact damage is lower than the specimen with vertical impact damage for all energy levels and for all temperatures.
- The maximum and minimum differences of the CAI strength are obtained at 100°C and 20°C for all cases, respectively.
- The CAI damage propagates depending on the plate stacking sequences and The CAI damage also depends on the orientation of the impact damage as vertical or horizontal.

# CHAPTER SEVEN
# RECOMMENDATIONS FOR FURTHER RESEARCH

The following recommendations may be listed to shine a light for further research:

*Mechanical properties:*

- The mechanical properties of various composite materials such as carbon/epoxy or kevlar/epoxy may be investigated under high and low temperature.
- Post impact mechanical properties may be investigated.
- Tension after impact properties of composites may be evaluated.

*Impact test:*

- The impact behavior of the various composite materials such as carbon/epoxy or kevlar/epoxy may be tested under high and low temperatures. Also, glass/epoxy may be experienced under low velocity.
- The impact parameters such as laminate orientation and thickness, fiber volume friction, impactor shape (sharp, conical and blind) and mass may be evaluated under high and low temperature.
- The geometry and boundary conditions effects on the impact response may be investigated.
- The environmental such as humidity effects on the impact response may be investigated.
- High velocity impact may be studied under high and low temperature.
- The impact response of delaminated plates may be investigated.
- C-scan photograph may be inspected interface delamination.
- The effects of the residual stresses due to temperature on the impact response may be investigated.
- Thick and thin composite laminate may be tested to investigate the penetration range of them.

- Tension-tension and compression-compression fatigue properties of the impacted and non-impacted composites may be evaluated.
- Quasi-static impact and repeated impact on composite laminates may be evaluated.
- Vibration response of the composite specimen after impact may be investigated.

*CAI test:*

- Compression after impact (CAI) tests may be carried out under low and high temperatures to investigate the temperature effects on the residual compressive stress.
- Buckling strength after impact of the composites may be investigated.
- CAI strength of various composite plates with delamination may be investigated.

**REFERENCES**

Abatan, A., & Hu, H. (2002). Effect of cross section material distribution on impact response of hybrid Composites. *Journal of Thermoplastic Composite Materials, 15,* 375–387.

Abdullah, M. R., & Cantwell, W. J. (2006). The impact resistance of polypropylene-based fibre–metal laminates. *Composites Science and Technology, 66,* 1682–1693.

Abrate, S. (1998). *Impact on composite structures* (1st ed.). Cambridge: Cambridge University Press.

Akimoto, H., Toda, M., Miyashita, J., Shonaike, G. O., Murakami, A., Hogg, P. J., et al. (2000). Impact performance of macro composite laminates—1. Evaluation of energy absorbed in non-penetration impact test. *Journal of Reinforced Plastics and Composites, 19* (17), 1363–1378.

Amid, R. (2001). *Energy absorption of composite materials under high velocity impact*. Msc Thesis, Ryerson University.

Anderson, T.A. (1999). *An analytical and experimental investigation of sandwich composites subjected to low-velocity impact*. Phd Thesis. The University of Arizona.

Aslan, Z. (2002). *Behavior of laminated composite structures subjected to low velocity impact*. Phd Thesis. Dokuz Eylül University.

Aslan, Z., & Karakuzu, R. (2002). Transient dynamic analysis of laminated composite plate subjected to low- velocity impact. *Mathematical & Computational Applications, 7,* (2), 73–82.

Aslan, Z., Karakuzu, R. & Okutan, B. (2003). The response of laminated composite plates under low-velocity impact loading. *Composites Science and Technology, 59,* 119–127.

Aslan, Z., Karakuzu, R. & Sayman, O. (2002). Dynamic characteristics of laminated woven e-glass-epoxy composite plates subjected to low velocity heavy mass imact. *Journal of Composite Materials, 36,* 2421–2442.

ASTM Standards and Literature Referances for Composite Materials, (1990). *Standard Test Method for Tensile Properties of Fiber-Resin Composites D 3039–76,* American Society for Testing and Materials. Philadelphia, PA.

ASTM Standards and Literature Referances for Composite Materials, (1990). *Standard Test Method for Compressive Properties of Unidirection or Cross-Ply Fiber-Resin Composites D 3410–87,* American Society for Testing and Materials. Philadelphia, PA.

ASTM Standards and Literature Referances for Composite Materials, (1990). *D 3846–79,* American Society for Testing and Materials. Philadelphia, PA.

Atas, C. (2004). *Large deformations in composite laminated plates.* PhD Thesis, Dokuz Eylül University.

Atas, C., & Liu, D. (in press). Impact response of woven composites with small weaving angles. *International Journal of Impact Engineering*.

Aydogdu, M. (2006). Thermal buckling analysis of cross-ply laminated composite beams with general boundary conditions. *Composites Science and Technology, 67,* 1096–1104.

Aymerich, F., Pani, C., & Priolo, P. (2007). Effect of stitching on the low-velocity impact response of [03/903]S graphite/epoxy laminates. *Composites: Part A, 38,* 1174–1182.

Baker, P. J. (1994). *Drop-weight impact initiation of ammonium perchlorate composites soid rocket propellants.* PhD Thesis, Vanderbilt University.

Baucom, J. N., & Zikry, M. A. (2005). Low-velocity impact damage progression in woven E-glass composite systems. *Composites: Part A, 36,* 658–664.

Baucom, J. N., Zikry, M. A., & Rajendran, A. M. (2006). Low-velocity impact damage accumulation in woven S2-glass composite systems. *Composites Science and Technology, 66,* 1229–1238.

Belingardi, G., & Vadori, R. (2002). Low velocity impact tests of laminate glass-fiber-epoxy matrix composite material plates. International *Journal of Impact Engineering, 27,* 213–229.

Bonollo, F., Ceschini, L., & Garagnani, G. L. (1997). Mechanical and impact behaviour of (Al2O3)p/2014 and (Al2O3)p/6061 Al metal matrix composites in the 25–200°C range. *Applied Composite Materials, 4,* 173–185.

Breen, C., Guild, F., & Pavier, M. (2005). Impact of thick CFRP laminates: the effect of impact velocity. *Composites: Part A, 36,* 205–211.

Bull, P. H., & Edgren, F. (2004). Compressive strength after impact of CFRP-foam core sandwich panels in marine applications. *Composite: Part B, 35,* 535–541.

Cantwell, W. J. (2007). Geometrical effects in the low velocity impact response of GFRP. *Composites Science and Technology, 67* (9), 1900–1908.

Caprino, G., Langella, A., & Lopresto, V. (2003). Indentation and penetration of carbon fibre reinforced plastic laminates. *Composite: Part B, 32,* 319–325.

Caprino, G., Lopresto, V., & Iaccarino, P. (2007). A simple mechanistic model to predict the macroscopic response of fibreglass–aluminium laminates under low-velocity impact. *Composites: Part A, 38,* 290–300.

Caprino, G., Lopresto, V., Scarponi, C., & Briotti, G. (1999). Influence of material thickness on the response of carbon-fabric/epoxy panels to low velocity impact. *Composites Science and Technology, 59,* 2279–2286.

Caprino, G., Spataro, G., & Luongo, S. D. (2004). Low-velocity impact behavior of fiberglass-aluminum laminates. *Composites: Part A, 35,* 605–616.

Carlsson, L. A., & Pipes, R. B. (1997). *Experimental Characterization of Advanced Composite Materials* (2nd ed.). USA: Technomic Publishing Company.

Cartie, D. D. R., & Irving, P. E. (2002). Effect of resin and fibre properties on impact and compression after impact performance of CFRP. *Composites: Part A, 33,* 483–493.

Cesari, F., Re, V. D., Minak, G., & Zucchelli, A. (2007). Damage and residual strength of laminated carbon–epoxy composite circular plates loaded at the centre. *Composites: Part A, 38,* 1163–1173.

Chakraborty D. (2007). Delamination of laminated fiber reinforced plastic composites under multiple cylindrical impact. *Materials and Design, 28,* 1142–1153.

Chakraborty, D., & Kumar, M. (2005). Response of laminated FRP composites under multiple impact loading. *Journal of Reinforced Plastics and Composites, 24* (14), 1457–1477.

Chandrashekhara, K., & Schroeder, T. (1995). Nonlinear impact analysis of laminated cylindrical and doubly curved shells. *Journal of Composite Materials, 29,* 2160–2179.

Chang, L., Zhang, Z., & Breidt, C. (2004). Impact resistance of short fibre/particle reinforced epoxy. *Applied Composite Materials, 11,* 1–15.

Changliang, Z., Mingfa, R., Wei, Z., & Haoran, C. (2006). Delamination prediction of composite filament wound vessel with metal liner under low velocity impact. *Composite Structures, 75* (1–4), 387–392.

Chen, G., Li, Z., Kou, C., & Gui, L. (2004). Finite element analysis of low-velocity impact damage of stitched laminates. *Journal of Reinforced Plastics and Composites, 23* (9), 987–995.

Cho, C., & Zhao, G. (2002). Effects of geometric and material factors on mechanical response of laminated composites due to low velocity impact. *Journal of Composite Materials, 36* (12), 1403–1428.

Choi, I.H. (2006). Contact force history analysis of composite sandwich plates subjected to low-velocity impact. *Composite Structures, 75* (1–4), 582–586.

Choi, H. Y. (1990). *Damage in graphite/epoxy laminated composites due to low velocity impact*. Phd Thesis. Stanford University.

Choi, H. Y., & Chang, F. K. (1992). A model for predicting damage in graphite/epoxy laminated composites resulting from low-velocity point impact. *Journal of Composite Materials, 26,* 2134–2169.

Choi, H. Y., Wu, H. Y. T., & Chang, F. K. (1991). A new approach toward understanding damage mechanisms and mechanics of laminated composites due to low-velocity impact: Part II- Analysis. *Journal of Composite Materials, 25,* 1012–1038.

Chotard, T. J., & Benzeggagh, M. L. (1999). On the mechanical Behaviour of pultruded sections Submitted to low-velocity impact. *Composites Science and Technology, 58,* 839–854.

Chotard, T. J., Pasquiet, J., & Benzeggagh, M. L. (2000). Impact response and residual performance of GRP pultruded shapes under static and fatigue loading. *Composites Science and Technology, 60,* 895–912.

Christopherson, J., Mahinfalah, M., Jazar, G. N., & Aagaah, M. R. (2005). An investigation on the effect of a small mass impact on sandwich composite plates. *Composite Structures, 67* (3), 299–306.

Corte´s, P., & Cantwell, W. J. (2007). The impact properties of high-temperature fiber-metal laminates. *Journal of Composite Materials, 41* (5), 613–632.

Dang, X. (2000). *Testing and simulation of composite laminates under impact loading.* PhD Thesis, Michigan State University.

Daniel, I. M., & Ishai, O. (1994). *Engineering Mechanics of Composite Materials* (1st ed.). New York: Oxford University Press.

Datta, S., Krishna, A. V., & Rao, R. M. V. G. K. (2004). Low velocity impact damage tolerance studies on glass/epoxy laminates – effects of material, process and test parameters. *Journal of Reinforced Plastics and Composites, 23* (3), 327–345.

Deng, S., & Ye, L. (2000). Influence of fibre-matrix adhesion on mechanical properties of graphite/epoxy composites: III. Impact and dynamic mechanical properties. *Journal of Reinforced Plastics and Composites, 19* (9), 689–703.

Dvorak, G. J., & Suvorov, A. P. (2006). Protection of sandwich plates from low-velocity impact. *Journal of Composite Materials, 40* (15), 1317–1331.

Ellis, R. L. (1996). *Ballistic impact resistance of graphite epoxy composites with shape memory alloy and extended chain polyethylene spectra™ hybrid components.* Msc Thesis, Virginia Polytechnic Institute and State University.

Erickson, M. D., Kallmeyer, A. R., & Kellogg, K. G. (2005). Effect of temperature on the low-velocity impact behavior of composite sandwich panels. *Journal of Sandwich Structures and Materials, 7,* 245–264.

Finn, S. R. (1991). *Delamination in composite plates under transverse static or impact loads.* PhD Thesis, Stanford University.

Floyd, A. M. (1994). *An engineering approach to the simulation of gross damage development in composite laminates.* PhD Thesis, The University of British Columbia.

Freitas, M., Silva, A., & Reis, L. (2000). Numerical evaluation of failure mechanisms on composite specimens subjected to impact loading. *Composites: Part B, 31,* 199- 207.

Fuoss, E. (1996). *Effects of stacking sequence on the impact damage resistance of composite laminates.* Msc Thesis, Carleton University.

Ganapathy, S., & Rao, K. P. (1997). Interlaminar stresses in laminated composite plates, cylindrical/ spherical shell panels damaged by low-velocity impact. *Composite Structures, 38* (1–4), 157–168.

Ganapathy, S., Rao, K. P. (1998). Failure analysis of laminated composite cylindrical/spherical shell panels subjected to low-velocity impact. *Computers and Structures, 68,* 627–641.

Gao, S. L., & Kim, J. K. (2001). Cooling rate infuences in carbon fibre/PEEK composites. Part III: impact damage performance. *Composites: Part A, 32,* 775–785.

Gning, P. B., Tarfaoui, M., Collombet, F., & Davies, P. (2005). Prediction of damage in composite cylinders after impact. *Journal of Composite Materials, 39* (10), 917–928.

Gong, S. W., Lam, K. Y., & Reddy, J. N. (1999). The elastic response of functionally graded cylindrical shells to low-velocity impact. *International Journal of Impact Engineering, 22,* 397–417.

Groves, S. E. (1986). *A study of damage mechanics in continuous fiber composite laminates with matrix cracking and internal delaminations.* PhD Thesis, Texas A & M University.

Guan, Z., & Yang, C. (2002). Low-velocity impact and damage process of composite laminates. *Journal of Composite Materials, 36* (7), 851–871.

Gustin, J., Joneson, A., Mahinfalah, M., & Stone, J. (2005). Low velocity impact of combination kevlar/carbon fiber sandwich composites. *Composite Structures, 69* (4), 396–406.

Habib, F. A. (2001). A new method for evaluating the residual compression strength of composites after impact. *Composite Structures, 53,* 309–316.

Halvorsen, A., Khojn, A. S., Mahinfalah, M., & Jazar, R. N. (2006). Temperature effects on the impact behavior of fiberglass and fiberglass/kevlar sandwich composites. *Applied Composite Materials, 13,* 369–383.

Hazizan, M. A., & Cantwell, W. J. (2003). The low velocity impact response of an aluminium honeycomb sandwich structure. *Composites: Part B, 34,* 679–687.

Her, S. C., & Liang, Y. C. (2004). The finite element analysis of composite laminates and shell structures subjected to low velocity impact. *Composite Structures, 66,* 277–285.

Herup, E. J. (1996). *Low-velocity impact on composite sandwich plates.* PhD Thesis, Air University.

Hosseinzadeh, R., Shokrieh, M. M., & Lessard, L. (2006). Damage behavior of fiber reinforced composite plates subjected to drop weight impacts. *Composites Science and Technology, 66,* 61–68.

Hosur, M. V., Abdullah, M., & Jeelani, S. (2005). Studies on the low-velocity impact response of woven hybrid composites. *Composite Structures, 67* (3), 253–262.

Hosur, M. V., Adya, M., Alexander, J., Jeelani, S., Vaidya, U., & Mayer, A. (2003). Studies on impact damage resistance of affordable stitched woven carbon/epoxy composite laminates. *Journal of Reinforced Plastics and Composites, 22* (10), 927–952.

Hosur, M. V., Karim, M. R., & Jeelani, S. (2003). Experimental investigations on the response of stitched/unstitched woven S2-glass/SC15 epoxy composites under single and repeated low velocity impact loading. *Composite Structures, 61,* 89–102.

Hou, J. P., Petrinic, N., Ruiz, C., & Hallett, S. R. (2000). Prediction of impact damage in composite plates. *Composites Science and Technology, 60,* 273–281.

Houde, M. (1990). *Impact force model for composite materials.* Msc Thesis, University of Toronto.

Hu, N., Sekine, H., Fukunaga, H., & Yao, Z. H. (1999). Impact analysis composite laminates with multiple delaminations. *International Journal of Impact Engineering, 22,* 633–648.

Huang, C. H., & Lee, Y. J. (2005). Quasi-static simulation of composite-laminated shells subjected to low-velocity impact. *Journal of Reinforced Plastics and Composites, 24* (7), 763–774.

Hwang, S. F., & Liu, G. H. (2002). Experimental study for buckling and post buckling behaviors of composite laminates with multiple delaminations. *Journal of Reinforced Plastics and Composites, 21* (4), 333–349.

Iannucci, L., & Ankersen, J. (2006). An energy based damage model for thin laminated composites. *Composites Science and Technology, 66,* 934–951.

Iannucci, L., & Willows, M. L. (2007). An energy based damage mechanics approach to modeling impact onto woven composite materials: Part II experimental and numerical results. *Composites: Part A, 38* (2), 827–837.

Ibekwe, S. I., Mensah, P. F., Li, G., Pang, S. S., & Stubblefield, M. A. (2006). Impact and post impact response of laminated beams at low temperatures. *Composite Structures, 79* (1), 12–17.

Içten, B. M. (2006). *Damage in laminated composite plates subjected to low-velocity impact.* PhD Thesis, Dokuz Eylül University.

Im, K. H., Cha, C. S., Kim, S. K., & Yang, I. Y. (2001). Effects of temperature on impact damages in CFRP composite laminates. *Composite: Part B, 32,* 669–682.

Jones, R. M. (1998). *Mechanics of Composite Materials* (2nd ed.). Tokyo: McGraw-Hill.

Kabir, H. R. H., Hamad, M. A. M., Duaij, J. A., & John, M. J. (2007). Thermal buckling response of all-edge clamped rectangular plates with symmetric angle-ply lamination. *Composite Structures, 79,* 148–155.

Kalyan, J. B., & Bhaskar, K. (in press). An analytical parametric study on buckling of non-uniformly compressed orthotropic rectangular plates. *Composite Structures*.

Kang, T. J., & Kim, C. (2000). Impact energy absorption mechanism of largely deformable composites with different reinforcing structures. *Fibers and Polymers, 1* (1), 45–54.

Kepler, J. (2004a). Impact penetration of sandwich panels at different velocities – an experimental parameter study: Part I – parameters and results. *Journal of Sandwich Structures and Materials, 6,* 357–374.

Kepler, J. (2004b). Impact penetration of sandwich panels at different velocities – an experimental parameter study: Part II – interpretation of results and modeling. *Journal of Sandwich Structures and Materials, 6,* 379–397.

Khalili, M. R., Malekzadeh, K., & Mittal, R. K. (2007a). Effect of physical and geometrical parameters on transverse low-velocity impact response of sandwich panels with a transversely flexible core. *Composite Structures, 77,* 430–443.

Khalili, S. M. R., Mittal, R.K., & Panah, N. M. (2007b). Analysis of fiber reinforced composite plates subjected to transverse impact in the presence of initial stresses. *Composite Structures, 77,* 263–268.

Khojin, A. S., Bashirzadeh, R., Mahinfalah, M., & Jazar, R. K. (2006a). The role of temperature on impact properties of Kevlar/fiberglass composite laminates, *Composites: Part B, 37* (7–8), 593–602.

Khondker, O. A., Herszberg, I., & Hamad, H. (2004). Measurements and prediction of the compression-after-impact strength of glass knitted textile composites. *Composites: Part A, 35,*145–157.

Khondker, O. A., Leong, K. H., Herszberg, I., & Hamada, H. (2005). Impact and compression-after-impact performance of weft-knitted glass textile composites. *Composites: Part A, 36,* 638–648.

Kim, H., Kayır, T., & Mousseau, S. L. (2005). Mechanisms of damage formation in transversely impacted glass-epoxy bonded lap joints. *Journal of Composite Materials, 39* (22), 2039–2052.

Kim, J. K., & Sham, M. L. (2000). Impact and delamination failure of woven-fabric composites. *Composites Science and Technology, 60,* 745–761.

Kim, J. S., & Chung, S. K. (2007). A study on the low-velocity impact response of laminates for omposite railway bodyshells. *Composite Structures, 77,* 484–492.

Kim, R. Y., & Donaldson, S. L. (2006). Experimental and analytical studies on the damage initiation in composite laminates at cryogenic temperatures. *Composite Structures, 76,* 62–66.

Kiratisaevee, H., & Cantwell, W. J. (2005). Low-velocity impact response of high-performance aluminum foam sandwich structures. *Journal of Reinforced Plastics and Composites, 24* (10), 1057–1072.

Kistler, L. S., Waas, A. M. (1998). Experiment and analysis on the response of curved laminated composite panels subjected to low velocity impact. *International journal of Impact Engineering, 21* (9), 711–736.

Kowsika, M. V. S. L. N. (1997). *Impact performance characteristics and modeling failure mechanisms of pultruded glass-graphite/epoxy hybrid composite beams.* PhD Thesis, University of Mississippi.

Krishnamurthy, K. S., Mahajan, P., & Mittal, R. K. (2003). Impact response and damage in laminated composite cylindrical shells. *Composite Structures, 59,* 15–36.

Kumar, C. R., Radhakrishna, K., & Rao, R. M. V. G. K. (2005). Postcuring effects on impact behavior of glass/epoxy composite laminates. *Journal of Reinforced Plastics and Composites, 24* (9), 949–960.

Lam, K. Y., Sathiyamoorthy, T. S. (1999). Response of composite beam under low-velocity impact of multiple masses. *Composite Structures, 44,* 205–220.

Laurin, F., Carrere, N., & Maire, J. F. (2007). Laminated composite structures subjected to compressive loading: A material and structural buckling analysis. *Composite Structures, 80* (2), 172–182.

Lee, D. G., & Cheon, S. S. (2001). Impact characteristics of glass fiber composites with respect to fiber volume fraction. *Journal of Composite Materials, 35* (1), 27–56.

Lee, J. D., Du, S., & Liebowitz, H. (1984). Three dimensional finite element and dynamic analysis of composite laminate subjected to impact. *Computers & Structures, 19,* 807–813.

Lee, Y. J., & Huang, C. H. (2003). Ultimate strength and failure process of composite laminated plates subjected to low-velocity impact. *Journal of Reinforced Plastics and Composites, 22* (12), 1059–1081.

Lee, J., & Soutis, C. (2005). Prediction of impact-induced fibre damage in circular composite plates. *Applied Composite Materials, 12,* 109–131.

Li, C. F., Hu, N., Yin, Y. J., Sekine, H., & Fukunaga, H. (2002). Low-velocity impact-induced damage of continuous fiber-reinforced composite laminates. Part I. a fem numerical model. *Composites: Part A, 33,* 1055–1062.

Li, C. F., Hu, N., Cheng, J. G., Fukunaga, H., & Sekine, H. (2002). Low-velocity impact-induced damage of continuous fiber-reinforced composite laminates. Part II. Verification and numerical investigation. *Composites: Part A, 33,* 1063–1072.

Li, G., Pang, S. S., Helms, J. E., & Ibekwe, S. I. (2000). Low velocity impact response of GFRP laminates subjected to cycling moistures. *Polymer Composites, 21* (5), 686–695.

Li, G., Pang, S. S., Zhao, Y., & Ibekwe, S. I. (1999). Local buckling analysis of composite laminate with large delaminations induced by low velocity impact. *Polymer Composites, 20* (5), 634–642.

Li, Q. M., Ma, G. W., & Ye, Z. Q. (2006). An elastic–plastic model on the dynamic response of composite sandwich beams subjected to mass impact. *Composite Structures, 72,* 1–9.

Lim, C. T., Tan, V. B. C., Ramakrishna, S., & Lee, J. B. K. (2002). Low velocity impact studies on a 4-ply knitted kevlar fabric reinforced epoxy composite. *Journal of Reinforced Plastics and Composites, 21* (2), 121–138.

Liu, D. (1988). Impact induced delamination-a view of bending stiffness mismatching. *Journal of Composite Materials, 22,* 674–692.

Liu, D., Raju, B. B., & Dang, X. (1998). Size effects on impact response of Composite laminates. *International Journal of Impact Engineering, 21* (10), 837–852.

Lopresto, V., Melito, V., Leone, C., & Caprino, G. (2006). Effect of stitches on the impact behaviour of graphite/epoxy composites. *Composites Science and Technology, 66,* 206–214.

Luo, C., & DesJardin, P. E. (2007). Thermo-mechanical damage modeling of a glass–phenolic composite material. *Composites Science and Technology, 67* (7–8), 1475–1488.

Luo, R. K., Green, E. R., & Morrison, C. J. (2001). An approach to evaluate the impact damage initiation and propagation in composite plates. *Composite: Part B, 32,* 513–520.

Mahfuz, H., Thomas, T., Rangari, V., & Jeelani, S. (2006). On the dynamic response of sandwich composites and their core materials. *Composites Science and Technology, 66,* 2465–2472.

Majeed, O. (1995). *Numerical modelling of transverse impact on composite coupons.* Msc Thesis, Carleton University.

Malekzadeh, K., Khalili, M. R., & Mittal, R. K. (2006). Analytical prediction of low-velocity impact response of composite sandwich panels using new TDOF spring–mass–damper model. *Journal of Composite Materials, 40* (9), 1671–1689.

Margueres, P., Meraghni, F., & Benzeggagh, M. L. (2000). Comparison of stiffness measurements and damage investigation techniques for a fatigued and post-impact fatigued GFRP composite obtained by RTM process. *Composites Part A, 31,* 151–163.

Meo, M., Morris, A. J., Vignjevic, R., & Marengo, G. (2003). Numerical simulations of low-velocity impact on an aircraft sandwich panel. *Composite Structures, 62,* 353–360.

Mitrevski, T., Marshall, I.H., & Thomson, R. (2006). The influence of impactor shape on the damage to composite laminates. *Composite Structures, 76,* 116–122.

Mitrevski, T., Marshall, I. H., Thomson, R. S., & Jones, R. (2006). Low-velocity impacts on preloaded GFRP specimens with various impactor shapes. *Composite Structures, 76,* 209–217.

Moody, R. C., Harris, J. S., & Vizzini, A. J. (2002). Scaling and curvature effects on the damage tolerance of impacted composite sandwich panels. *Journal of Sandwich Structures and Materials, 4,* 71–82.

Morais, W. A., Monteiro, S. N., & d'Almeida, J. R. M. (2005). Evaluation of repeated low energy impact damage in carbon–epoxy composite materials. *Composite Structures, 67* (3), 307–315.

Moura, M. F. S. F., & Goncalves, J. P. M. (2004). Modelling the interaction between matrix cracking and delamination in carbon–epoxy laminates under low velocity impact. *Composites Science and Technology, 64,* 1021–1027.

Moura, M. F. S. F., Goncalves, J. P. M., Marques, A. T., & Castro P. M. S. T. (1997). Modelling compression failure after low velocity impact on laminated composites using interface elements. *Journal of Composite Materials, 31,* 1462–1479.

Moura, M. F. S. F., & Marques, A. T. (2002). Prediction of low velocity impact damage in carbon-epoxy laminates. *Composites: Part A, 33,* 361–368.

Naik, N. K., Borade, S. V., Arya, H., Sailendra, M., & Prabhu, S. V. (2002). Experimental studies on impact behaviour of woven fabric composites: Effect of impact parameters. *Journal of Reinforced Plastics and Composites, 21* (15), 1347–1362.

Naik, N. K., Meduri, S., & Sekher, Y. C. (2000). Polymer matrix woven fabric composites subjected to low velocity impact: Part II-Effect of plate thickness. *Journal of Reinforced Plastics and Composites, 19* (13), 1031–1055.

Naik, N. K., Meduri, S., & Sekher, Y. C. (2001). Polymer matrix woven fabric composites subjected to low velocity impact: Part III-Effect of incident impact velocity and impactor mass. *Journal of Reinforced Plastics and Composites, 20* (9), 720–743.

Naik, N. K., Ramasimha, R., Arya, H., Prabhu, S. V., & Rao, N. S. (2001). Impact response and damage tolerance characteristics of glass-carbon/epoxy hybrid composite plates. *Composite: Part B, 32,* 565–574.

Naik, N. K., Sekher, Y. C., & Meduri, S. (2000). Damage in woven-fabric composites subjected to low-velocity impact. *Composites Science and Technology, 60,* 731–744.

Odegard, G., & Kumosa, M. (2000). *Elastic-plastic and failure properties of a unidirectional carbon/PMR–15 composite at room and elevated temperatures. Composites Science and Technology, 60,* 2979–2988.

Papanicolaou, G. C., Blanas, A. M., Pournaras, A. V., & Stavropoulos, C. D. (1998). Impact damage and residual strength of FRP composites. *Key Engineering Materials, 141–143,* 127–148.

Parhi, P. K., Sinha, P. K., & Bhattacharyya, S. K. (2001). Dynamic behavior and impact induced first ply failure of multiple delaminated composite shells. *Journal of Reinforced Plastics and Composites, 20* (15), 1276–1300.

Park, S. W., Zhou, M., & Veazire, D. R. (2000). Time- resolved impact response and damage of fiber-reinforced composite laminates. *Journal of Composite Materials, 34,* 879–904.

Potti, S. V., & Sun, C. T. (1997). Predıctıon of impact induced penetration and delamination in thick composite laminates. *International Journal of Impact Engineering, 19* (1), 485–509.

Pradhan, B., & Kumar, S. (2000). Finite element analysis of low-velocity impact damage in composite laminates. *Journal of Reinforced Plastics and Composites, 19* (4), 322–339.

Puhui, C., Zhen, S., & Junyang, W. (2002). A new method for compression after impact strength prediction of composite laminates. *Journal of Composite Materials, 36* (5), 589–610.

Razi, H., & Kobayashi, A. S. (1993). Delamination in cross-ply laminated composite subjected to low-velocity impact. *AIAA Journal, 31,* 1498–1502.

Reid, S. R., & Zhou, G. (Eds.) (2000). *Impact behaviour of fibre-reinforced composite materials and structures.* USA: CRC press.

Reis, L., & Freitas, M. (1997). Damage growth analysis of low velocity impacted composite panels. *Composite Structures, 38* (l–4), 509–515.

Rio, T. G., Zaera, R., Barbero, E., & Navarro, C. (2005). Damage in CFRPs due to low velocity impact at low temperature. *Composite: Part B, 36,* 41–50.

Roeder, B. A., & Sun, C. T. (2001). Dynamic penetration of alumina/aluminum laminates: experiments and modeling. *International Journal of Impact Engineering, 25,* 169–185.

Roy, T., & Chakraborty, D. (2006). Delamination in hybrid FRP laminates under low velocity impact. *Journal of Reinforced Plastics and Composites, 25* (18), 1939–1956.

Roy, T., & Chakraborty, D. (in press). Delamination in FRP laminates with holes under transverse impact. *Materials and Design*.

Ruhala, L. A., & Engel, R. S. (2000). An investigation of the effects of fiber volume fraction on the impact properties of fiber reinforced composite laminated plates. *Journal of Reinforced Plastics and Composites, 19* (6), 449–464.

Rydin, R. W. (1996). *Using the drop weight impact tower to assess impact resistance of FRP composite plates.* PhD Thesis, University of Delaware.

Sadasivam, B., Cherng, J. G., & Mallick, P.K. (2000). Dynamic response of impact damaged random fiber automotive composites. *Journal of Reinforced Plastics and Composites, 19* (2), 124–136.

Sadasivam, B., & Mallick, P. K. (2002). Impact damage resistance of random fiber reinforced automotive Composites. *Journal of Thermoplastic Composite Materials, 15,* 181–191.

Saito, E. H., & Kimpara, I. (2006). Evaluation of impact damage mechanism of multi-axial stitched CFRP laminate. *Composites: Part A, 37* (12), 2226–2235.

Sala, G. (1997). Post-impact behaviour of aerospace composites for high-temperature applications: experiments and simulations. *Composite: Part B, 28* (5–6), 651–665.

Salehi, F. A. R., Hassani, S. T. S., Haftchenari, H., & Hinton, M. J. (2001). Temperature and rate effects on GRP tubes under tensile hoop loading. *Applied Composite Materials, 8,* 1–24.

Sankar, B. V., & Sun, C. T. (1985). Low-velocity impact response of laminated beams subjected to initial stresses. *AIAA Journal, 23,* 1962–1969.

Sankar, B. V., & Zhu, H. (2000). The effect of stitching on the low-velocity impact response of delaminated composite beams. *Composites Science and Technology, 60,* 2681–2691.

Sburlati, R. (2002a). The contact behavior between a foam core sandwich plate and a rigid indentor. *Composite: Part B, 33,* 325–332.

Sburlati, R. (2002b). The effect of a slow impact on sandwich plates. *Journal of Composite Materials, 36* (9), 1079–1092.

Schrauwen, B., & Peijs, T. (2002). Influence of matrix ductility and fibre architecture on the repeated impact response of glass-fibre-reinforced laminated Composites. *Applied Composite Materials, 9,* 331–352.

Schubel, P. M., Luo, J. J., & Daniel, I. M. (2007). Impact and post impact behavior of composite sandwich panels. *Composites: Part A, 38,* 1051–1057.

Shariat, B. A. S., & Eslami, M. R. (2007). Buckling of thick functionally graded plates under mechanical and thermal loads. *Composite Structures, 78,* 433–439.

Sharma, S. C., Murty, H. N. N., & Krishna, M. (2004). Low-velocity impact response of polyurethane foam composite sandwich structures. *Journal of Reinforced Plastics and Composites, 23* (17), 1869–1882.

Shipsha, A., & Zenkert, D. (2005). Compression-after-impact strength of sandwich panels with core crushing damage. *Applied Composite Materials, 12,* 149–164.

Short, G. J., Guild, F. J., & Pavier, M. J. (2002). Post-impact compressive strength of curved GFRP laminates. *Composites: Part A, 33,* 1487–1495.

Soutis, C., & Turkmen, D. (1993, July). High temperature effects on the compressive strength of glass fibre reinforced composites. Proceedings 9th International Conference on Composite Materials, 581–587.

Sugun, B. S., & Rao, R. M. V. G. K. (2004). Low-velocity impact characterization of glass, carbon and kevlar composites using repeated drop tests. *Journal of Reinforced Plastics and Composites, 23* (15), 1583–1599.

Sutherland, L. S., & Soares, C. G. (2005). Impact charactersation of low fibre-volume glass reinforced polyester circular laminated plates. *International Journal of Impact Engineering, 31* (1), 1–23.

Sutherland, L. S., & Soares, C. G. (2006). Impact behaviour of typical marine composite laminates. *Composites: Part B, 37,* 89–100.

Tay, T. E., & Shen, F. (2002). Analysis of delamination growth in laminated composites with consideration for residual thermal stress effects. *Journal of Composite Materials, 36* (11), 1299–1320.

Uyaner, M., & Kara, M. (in press). Dynamic response of laminated composites subjected to low-velocity impact. *Journal of Composite Materials.*

Xiaoquan, C., Mansour, A. M., Zhengneng, Li, & Chenghe, K. (2005). Compression strength of stitched laminates after low-velocity impact. *Journal of Reinforced Plastics and Composites, 24* (9), 935–947.

Xie, Z., & Vizzini, A. J. (2005). Damage propagation in a composite sandwich panel subjected to increasing uniaxial compression after low-velocity impact. *Journal of Sandwich Structures and Materials, 7,* 269–288.

Xilaoquan, C., Al-Mansour, A. M., Zhengneng, L., & Chenghe, K. (2005). Compression strength of stitched laminates after low-velocity impact. *Journal of Reinforced Plastics and Composites, 24,* (9), 935–947.

Vaidya, U. K., Gautam, A. R. S., Hosur, M., & Dutta, P. (2006). Experimental–numerical studies of transverse impact response of adhesively bonded lap joints in composite structures. *International Journal of Adhesion & Adhesives, 26,* 184–198.

Vaidya, U. K., & Hosur, M. V. (2003). High strain rate impact response of graphite/epoxy composites with polycarbonate facing. *Journal of Thermoplastic Composite Materials, 16,* 75–95.

Wee, Y. C., & Boay, C. G. (2007). Analytical and numerical studies on the buckling of delaminated composite beams. *Composite Structures, 80* (2), 307–319.

Whittingham, B., Marshall, I. H., Mitrevski, T., & Jones, R. (2004). The response of composite structures with pre-stress subject to low velocity impact damage. *Composite Structures, 66,* 685–698.

Wu, H. Y. T., & Chang, F. K. (1989). Transient dynamic analysis of laminated composite plates subjected to transverse impact. *Computers & Structures, 31,* 453–466.

Zhang, X., Davies, G. A. O., & Hitchings, D. (1999). Impact damage with compressive preload and post-impact compression of carbon composite plates. *International Journal of Impact Engineering, 22,* 485–509.

Zhang, X., Hounslow, L., & Grassi, M. (2006). Improvement of low-velocity impact and compression-after-impact performance by z-fibre pinning. *Composites Science and Technology, 66* (15), 2785–2794.

Zhang, Y., Zhu, P., & Lai, X. (2006). Finite element analysis of low-velocity impact damage in composite laminated plates. *Materials and Design, 27,* 513–519.

Zhao, G., & Cho, C. (2004). On impact damage of composite shells by a low-velocity projectile. *Journal of Composite Materials, 38* (14), 1231–1254.

Zhao, G. P., & Cho, C. D. (2007). Damage initiation and propagation in composite shells subjected to impact. *Composite Structures, 78,* 91–100.